ISSN: 2146-1414

MIRT

Molecular Imaging and Radionuclide Therapy

October 2020 Volume 29 Issue 3 www.tsnm.org

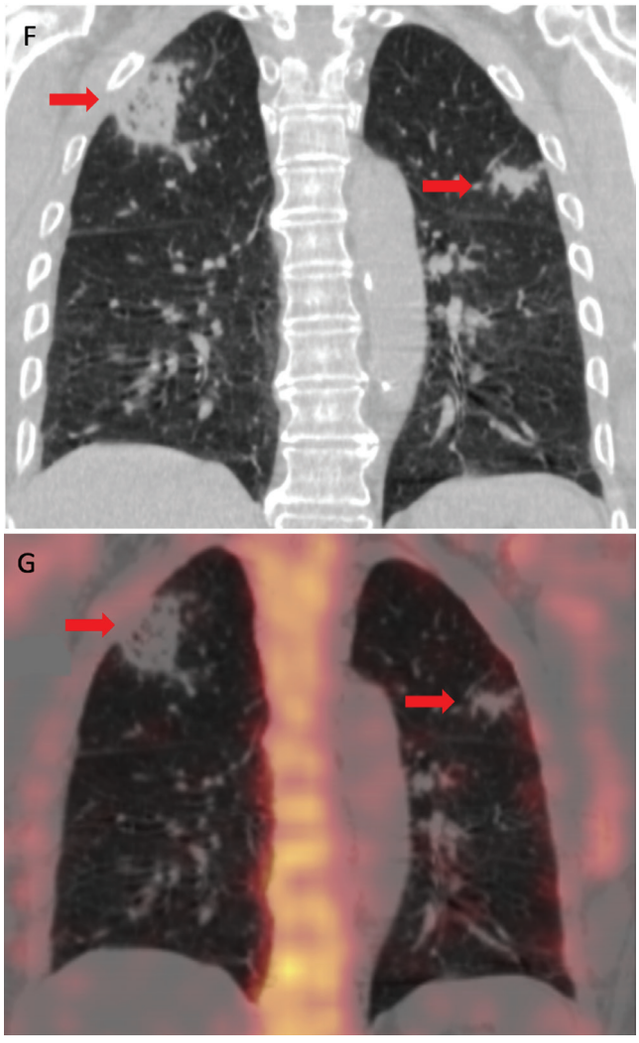

Molecular Imaging and Radionuclide Therapy

Volume: 29 Issue:3 October 2020 Page: 88-149

"Official Journal of the Turkish Society of Nuclear Medicine"

galenos yayinevi

TURKISH SOCIETY OF NUCLEAR MEDICINE 1975

MIRT

Molecular Imaging and Radionuclide Therapy

Scientific Advisory Board

MIRT

Molecular Imaging and Radionuclide Therapy

Turkish Society of Nuclear Medicine
Cinnah Caddesi Pilot Sokak No: 10/12 Çankaya 06650 Ankara, Turkey **Phone:** +90 312 441 00 45 **Fax:** +90 312 441 12 95 **Web:** www.tsnm.org **E-mail:** dernekmerkezi@tsnm.org
"Formerly Turkish Journal of Nuclear Medicine"

Reviewing the articles' conformity to the publishing standards of the Journal, typesetting, reviewing and editing the manuscripts and abstracts in English, creating links to source data, and publishing process are realized by Galenos.

Galenos Publishing House
Owner and Publisher
Derya Mor
Erkan Mor

Publication Coordinator
Burak Sever

Web Coordinators
Fuat Hocalar
Turgay Akpınar

Graphics Department
Ayda Alaca
Çiğdem Birinci
Gülşah Özgül

Finance Coordinator
Sevinç Çakmak

Project Coordinators
Proje Koordinatörü
Duygu Yıldırm
Gamze Aksoy
Gülay Akın
Hatice Sever
Melike Eren
Özlem Çelik
Pınar Akpınar
Rabia Palazoğlu
Saliha Tuğçe Evin

Research&Development
Mert Can Köse
Mevlüde Özlem Akgüney

Publisher Contact
Address: Molla Gürani Mah. Kaçamak Sk. No: 21/1
34093 İstanbul, Turkey
Phone: +90 (212) 621 99 25 **Fax:** +90 (212) 621 99 27
E-mail: info@galenos.com.tr/yayin@galenos.com.tr
Web: www.galenos.com.tr
Publisher Certificate Number: 14521

Publication Date: October 2020
ISSN: 2146-1414 **E-ISSN:** 2147-1959
International scientific journal published quarterly.

MIRT

Molecular Imaging and Radionuclide Therapy

ABOUT US

Molecular Imaging and Radionuclide Therapy (formerly Turkish Journal of Nuclear Medicine) is the official publication of Turkish Society of Nuclear Medicine.

Focus and Scope

Molecular Imaging and Radionuclide Therapy (Mol Imaging Radionucl Ther, MIRT) is a double-blind peer-review journal published in English language. It publishes original research articles, invited reviews, editorials, short communications, letters, consensus statements, guidelines and case reports with a literature review on the topic, in the field of molecular imaging, multimodality imaging, nuclear medicine, radionuclide therapy, radiopharmacy, medical physics, dosimetry and radiobiology. MIRT is published three times a year (February, June, October). Audience: Nuclear medicine physicians, medical physicists, radiopharmaceutical scientists, radiobiologists.

The editorial policies are based on the "Recommendations for the Conduct, Reporting, Editing, and Publication of Scholarly Work in Medical Journals (ICMJE Recommendations)" by the International Committee of Medical Journal Editors (2016, archived at http://www.icmje.org/) rules.

Molecular Imaging and Radionuclide Therapy is indexed in **Pubmed, Pubmed Central (PMC), Emerging Sources Citation Index (ESCI), TUBITAK-ULAKBIM, Scopus, Gale/Cengage Learning, EBSCO databases, ProQuest Health & Medical Complete, CINAHL, DOAJ, Index Copernicus, J-Gate, IdealOnline, ROOT INDEXING, Türkiye Atıf Dizini-Turkiye Citation Index, Turk Medline, EuroPub, Hinari, GOALI, ARDI, OARE** and **AGORA**.

Open Access Policy

This journal provides immediate open access to its content on the principle that making research freely available to the public supports a greater global exchange of knowledge.

Open Access Policy is based on rules of Budapest Open Access Initiative (BOAI) (http://www.budapestopenaccessinitiative.org/). By "open access" to [peer-reviewed research literature], we mean its free availability on the public internet, permitting any users to read, download, copy, distribute, print, search, or link to the full texts of these articles, crawl them for indexing, pass them as data to software, or use them for any other lawful purpose, without financial, legal, or technical barriers other than those inseparable from gaining access to the internet itself. The only constraint on reproduction and distribution, and the only role for copyright in this domain, should be to give authors control over the integrity of their work and the right to be properly acknowledged and cited.

Subscription Information

Manuscripts can only be submitted electronically through the Journal Agent website (http://www.journalagent.com/mirt/?plng=eng) after creating an account. This system allows online submission and review.

All published volumes in full text can be reached free of charge through the website http://mirt.tsnmjournals.org

Copyright Statement

Instructions for Authors

Instructions for authors are published in the journal and on the website http://mirt.tsnmjournals.org

Material Disclaimer

Scientific and legal responsibilities pertaining to the papers belong to the authors. Contents of the manuscripts and accuracy of references are also the author's responsibility. The Turkish Society of Nuclear Medicine, the Editor, the Editorial Board or the publisher do not accept any responsibility for opinions expressed in articles.

Financial expenses of the journal are covered by Turkish Society of Nuclear Medicine.

Correspondence Address

Editor in Chief Prof. Dr. Zehra Özcan, Ege University, Medical School, Department of Nuclear Medicine, İzmir, Turkey

E-mail: zehra.ozcan@yahoo.com

Web page: http://mirt.tsnmjournals.org/

Publisher Corresponding Address

Galenos Yayınevi Tic. Ltd. Şti.
Address: Molla Gürani Mah. Kaçamak Sk. No: 21/1 34093 Fındıkzade, İstanbul, Turkey
Phone: +90 212 621 99 25
Fax: +90 212 621 99 27
E-mail: info@galenos.com.tr

MIRT

Molecular Imaging and Radionuclide Therapy

INSTRUCTIONS TO AUTHORS

Molecular Imaging and Radionuclide Therapy (Mol Imaging Radionucl Ther, MIRT) publishes original research articles, short communications, invited reviews, editorials, case reports with a literature review on the topic, interesting images, consensus statements, guidelines, letters in the field of molecular imaging, multimodality imaging, nuclear medicine, radionuclide therapy, radiopharmacy, medical physics, dosimetry and radiobiology. MIRT is published by the Turkish Society of Nuclear Medicine three times a year (February, June, October).

Molecular Imaging and Radionuclide Therapy does not charge any article submission or processing fees.

GENERAL INFORMATION

MIRT commits to rigorous peer review, and stipulates freedom from commercial influence, and promotion of the highest ethical and scientific standards in published articles. Neither the Editor(s) nor the publisher guarantees, warrants or endorses any product or service advertised in this publication. All articles are subject to review by the editors and peer reviewers. If the article is accepted for publication, it may be subjected to editorial revisions to aid clarity and understanding without changing the data presented.

Manuscripts must be written in English and must meet the requirements of the journal. The journal is in compliance with the uniform requirements for manuscripts submitted to biomedical journals published by the International Committee of Medical Journal Editors (NEJM 1997; 336:309-315, updated 2016). Manuscripts that do not meet these requirements will be returned to the author for necessary revision before the review. Authors of manuscripts requiring modifications have a maximum of two months to resubmit the revised text. Manuscripts returned after this deadline will be treated as new submissions.

It is the authors' responsibility to prepare a manuscript that meets ethical criteria. The Journal adheres to the principles set forth in the Helsinki Declaration October 2013 (https://www.wma.net/policies-post/wma-declaration-of-helsinki-ethical-principles-for-medical-research-involving-human-subjects/) and holds that all reported research involving "Human beings" conducted in accordance with such principles.

Reports describing data obtained from research conducted in human participants must contain a statement in the MATERIALS AND METHODS section indicating approval by the ethical review board (including the approval number) and affirmation that INFORMED CONSENT was obtained from each participant.

All manuscripts reporting experiments using animals must include a statement in the MATERIALS AND METHODS section giving assurance that all animals have received humane care in compliance with the Guide for the Care and Use of Laboratory Animals (www.nap.edu) and indicating approval by the ethical review board.

If the study should have ethical approval, authors asked to provide ethical approval in order to proceed the review process. If they provide approval, review of the manuscript will continue.

In case report(s) and interesting image(s) a statement regarding the informed consent of the patients should be included in the manuscript and the identity of the patient(s) should be hidden.

Subjects must be identified only by number or letter, not by initials or names. Photographs of patients' faces should be included only if scientifically relevant. Authors must obtain written consent from the patient for use of such photographs. In cases of image media usage that potentially expose patients' identity requires obtaining permission for publication from the patients or their parents/guardians.

If the proposed publication concerns any commercial product, the author must include in the cover letter a statement indicating that the author(s) has (have) no financial or other interest with the product or explaining the nature of any relations (including consultancies) between the author(s) and editor the manufacturer or distributor of the product.

All submissions will be screened by Crossref Smilarity Check powered by "iThenticate". Manuscripts with an overall similarity index of greater than 25%, or duplication rate at or higher than 5% with a single source will be returned back to authors.

MANUSCRIPT CATEGORIES

1. Original Articles

2. Short Communications are short descriptions of focused studies with important, but very straightforward results.

3. Reviews address important topics in the field. Authors considering the submission of uninvited reviews should contact the editor in advance to determine if the topic that they propose is of current potential interest to the Journal. Reviews will be considered for publication only if they are written by authors who have at least three published manuscripts in the international peer reviewed journals and these studies should be cited in the review. Otherwise only invited reviews will be considered for peer review from qualified experts in the area.

4. Editorials are usually written by invitation of the editor by the editors on current topics or by the reviewers involved in the evaluation of a submitted manuscript and published concurrently with that manuscript.

5. Case Report and Literature Reviews are descriptions of a case or small number of cases revealing a previously undocumented disease process, a unique unreported manifestation or treatment of a known disease process, unique unreported complications of treatment regimens or novel and important insights into a condition's pathogenesis, presentation, and/or management. The journal's policy is to accept case reports only if it is accompanied by a review of the literature on the related topic. They should include an adequate number of images and figures.

6. Interesting Image

One of the regular parts of Molecular Imaging and Radionuclide Therapy is a section devoted to interesting images. Interesting image(s) should describe case(s) which are unique and include interesting findings adding insights into the interpretation of patient images, a condition's pathogenesis, presentation, and/or management.

7. Consensus Statements or Guidelines may be submitted by professional societies. All such submissions will be subjected to peer review, must be modifiable in response to criticisms, and will be published only if they meet the Journal's usual editorial standards.

8. Letters to the Editor may be submitted in response to work that has been published in the Journal. Letters should be short commentaries related to specific points of agreement or disagreement with the published work.

Note on Prior Publication

Articles are accepted for publication on the condition that they are original, are not under consideration by another journal, or have not been previously published. Direct quotations, tables, or illustrations that have appeared in

MIRT

Molecular Imaging and Radionuclide Therapy

copyrighted material must be accompanied by written permission for their use from the copyright owner and authors. Materials previously published in whole or in part shall not be considered for publication. At the time of submission, authors must report that the manuscript has not been published elsewhere. Abstracts or posters displayed at scientific meetings need not be reported.

MANUSCRIPT SUBMISSION PROCEDURES

MIRT only accepts electronic manuscript submission at the web site http://www.journalagent.com/mirt/. After logging on to the website Click the 'online manuscript submission' icon. All corresponding authors should be provided with a password and a username after entering the information required. If you already have an account from a previous submission, enter your username and password to submit a new or revised manuscript. If you have forgotten your username and/or password, please send an e-mail to the editorial office for assistance. After logging on to the article submission system please read carefully the directions of the system to give all needed information and attach the manuscript, tables and figures and additional documents.

All Submissions Must Include:

1. Completed Copyright Assignment & Disclosure of Potential Conflict of Interest Form; This form should be downloaded from the website (provided in the author section), filled in thoroughly and uploaded to the website during the submission.
2. All manuscripts describing data obtained from research conducted in human participants must be accompanied with an approval document by the ethical review board.
3. All manuscripts reporting experiments using animals must include approval document by the animal ethical review board.
4. All submissions must include the authorship contribution form which is signed by all authors.

Authors must complete all online submission forms. If you are unable to successfully upload the files please contact the editorial office by e-mail.

MANUSCRIPT PREPARATION

General Format

The Journal requires that all submissions be submitted according to these guidelines:

- Text should be double spaced with 2.5 cm margins on both sides using 12-point type in Times Roman font.
- All tables and figures must be placed after the text and must be labeled.
- Each section (abstract, text, references, tables, figures) should start on a separate page.
- Manuscripts should be prepared as a word document (*.doc) or rich text format (*.rtf).
- Please make the tables using the table function in Word.
- Abbreviations should be defined in parenthesis where the word is first mentioned and used consistently thereafter.
- Results should be expressed in metric units. Statistical analysis should be done accurately and with precision. Please consult a statistician if necessary.
- Authors' names and institutions should not be included in the manuscript text and should be written only in the title page.

Title Page

The title page should be a separate form from the main text and should include the following:

- Full title (in English and in Turkish). Turkish title will be provided by the editorial office for the authors who are not Turkish speakers.
- Authors' names and institutions.
- Short title of not more than 40 characters for page headings.
- At least three and maximum eight keywords. (in English and in Turkish). Do not use abbreviations in the keywords. Turkish keywords will be provided by the editorial office for the authors who are not Turkish speakers. If you are not a native Turkish speaker, please reenter your English keywords to the area provided for the Turkish keywords. English keywords should be provided from http://www.nlm.nih.gov/mesh (Medical Subject Headings) while Turkish keywords should be provided from http://www.bilimterimleri.com.
- Word count (excluding abstract, figure legends and references).
- Corresponding author's e-mail and address, telephone and fax numbers.
- Name and address of person to whom reprint requests should be addressed.

Original Articles

Authors are required to state in their manuscripts that ethical approval from an appropriate committee and informed consents of the patients were obtained.

Original Articles should be submitted with a structured abstract of no more than 250 words. All information reported in the abstract must appear in the manuscript. The abstract should not include references. Please use complete sentences for all sections of the abstract. Structured abstract should include background, objective, methods, results and conclusions. Turkish abstract will be provided by the editorial office for the authors who are not Turkish speakers. If you are not a native Turkish speaker, please reenter your English abstract to the area provided for the Turkish abstract.

- Introduction
- Materials and Methods
- Results
- Discussion
- Study Limitations
- Conclusion

May be given for contributors who are not listed as authors, or for grant support of the research.

References should be cited in numerical order (in parentheses) in the text and listed in the same numerical order at the end of the manuscript on a separate page or pages. The author is responsible for the accuracy of references. Examples of the reference style are given below. Further examples will be found in the articles describing the Uniform Requirements for Manuscripts Submitted to Biomedical Journals (Ann Intern Med.1988; 208:258-265, Br Med J. 1988; 296:401-405). The titles of journals should be abbreviated according to the style used in the Index Medicus. Journal Articles and Abstracts: Surnames and initials of author's name, title of the article, journal name, date, volume number, and pages. All authors should be listed regardless of number. The citation of unpublished papers, observations or personal communications is not permitted. Citing an abstract is not recommended. Books: Surnames and initials of author's names, chapter title, editor's name, book title, edition, city, publisher, date and pages.

MIRT
Molecular Imaging and Radionuclide Therapy

Sample References

Journal Article: Sayit E, Söylev M, Capa G, Durak I, Ada E, Yilmaz M. The role of technetium-99m-HMPAO-labeled WBC scintigraphy in the diagnosis of orbital cellulitis. Ann Nucl Med 2001;15:41-44.

Erselcan T, Hasbek Z, Tandogan I, Gumus C, Akkurt I. Modification of Diet in Renal Disease equation in the risk stratification of contrast induced acute kidney injury in hospital inpatients. Nefrologia 2009 doi: 10.3265/Nefrologia.2009.29.5.5449.en.full.

Article in a journal published ahead of print: Ludbrook J. Musculovenous pumps in the human lower limb. Am Heart J 2009;00:1-6. (accessed 20 February 2009).

Lang TF, Duryea J. Peripheral Bone Mineral Assessment of the Axial Skeleton: Technical Aspects. In: Orwoll ES, Bliziotes M (eds). Osteoporosis: Pathophsiology and Clinical Management. New Jersey, Humana Pres Inc, 2003;83-104.

Books: Greenspan A. Orthopaedic Radiology a Pratical Approach. 3th ed. Philadelphia, Lippincott Williams Wilkins 2000, 295-330.

Website: Smith JR. 'Choosing Your Reference Style', Online Referencing 2(3), http://orj.sagepub.com (2003, accessed October 2008).

- Tables

Tables must be constructed as simply as possible. Each table must have a concise heading and should be submitted on a separate page. Tables must not simply duplicate the text or figures. Number all tables in the order of their citation in the text. Include a title for each table (a brief phrase, preferably no longer than 10 to 15 words). Include all tables in a single file following the manuscript.

– Figure Legends

Figure legends should be submitted on a separate page and should be clear and informative.

– Figures

Number all figures (graphs, charts, photographs, and illustrations) in the order of their citation in the text. At submission, the following file formats are acceptable: AI, EMF, EPS, JPG, PDF, PPT, PSD, TIF. Figures may be embedded at the end of the manuscript text file or loaded as separate files for submission. All images MUST be at or above intended display size, with the following image resolutions: Line Art 800 dpi, Combination (Line Art + Halftone) 600 dpi, Halftone 300 dpi. Image files also must be cropped as close to the actual image as possible.

Short Communications:

Short communications should be submitted with a structured abstract of no more than 200 words. These manuscripts should be no longer than 2000 words, and include no more than two figures and tables and 20 references. Other rules which the authors are required to prepare and submit their manuscripts are the same as described above for the original articles.

Invited Review Articles:

- Title page (see above)
- Abstract: Maximum 250 words; without structural divisions; in English and in Turkish . Turkish abstract will be provided by the editorial office for the authors who are not Turkish speakers. If you are not a native Turkish speaker, please reenter your English abstract to the area provided for the Turkish abstract.
- Text
- Conclusion
- Acknowledgements (if any)
- References

Editorial:

- Title page (see above)
- Abstract: Maximum 250 words; without structural divisions; in English and in Turkish. Turkish abstract will be provided by the editorial office for the authors who are not Turkish speakers. If you are not a native Turkish speaker, please re enter your English abstract to the area provided for the Turkish abstract.
- Text
- References

Case Report and Literature Review

- Title page (see above)
- Abstract: Approximately 100-150 words; without structural divisions; in English and in Turkish. Turkish abstract will be provided by the editorial office for the authors who are not Turkish speakers. If you are not a native Turkish speaker, please re-enter your English abstract to the area provided for the Turkish abstract.
- Introduction
- Case report
- Literature Review and Discussion
- References

Interesting Image:

No manuscript text is required. Interesting Image submissions must include the following:

Title Page: (see Original article section)

Abstract: Approximately 100-150 words; without structural divisions; in English and in Turkish. Turkish abstract will be provided by the editorial office for the authors who are not Turkish speakers. If you are not a native Turkish speaker, please re-enter your English abstract to the area provided for the Turkish abstract.

Image(s): The number of images is left to the discretion of the author. (See Original article section)

Figure Legend: Reference citations should appear in the legends, not in the abstract. Since there is no manuscript text, the legends for illustrations should be prepared in considerable detail but should be no more than 500 words total. The case should be presented and discussed in the Figure legend section.

References: Maximum eight references (see original article section).

Letters to the Editor:

- Title page (see above)
- Short comment to a published work, no longer than 500 words, no figures or tables.
- References no more than five.

Consensus Statements or Guidelines: These manuscripts should typically be no longer than 4000 words and include no more than six figures and tables and 120 references.

Proofs and Reprints

Proofs and a reprint orders are sent to the corresponding author. The author should designate by footnote on the title page of the manuscript the name and

MIRT
Molecular Imaging and Radionuclide Therapy

address of the person to whom reprint requests should be directed. The manuscript when published will become the property of the journal.

Archiving

The editorial office will retain all manuscripts and related documentation (correspondence, reviews, etc.) for 12 months following the date of publication or rejection.

Submission Preparation Checklist

As part of the submission process, authors are required to check off their submission's compliance with all of the following items, and submissions may be returned to authors that do not adhere to these guidelines.

1. The submission has not been previously published, nor is it before another journal for consideration (or an explanation has been provided in Comments to the Editor).
2. The submission file is in Microsoft Word, RTF, or WordPerfect document file format. The text is double-spaced; uses a 12-point font; employs italics, rather than underlining (except with URL addresses); and the location for all illustrations, figures, and tables should be marked within the text at the appropriate points.
3. Where available, URLs for the references will be provided.
4. All authors should be listed in the references, regardless of the number.
5. The text adheres to the stylistic and bibliographic requirements outlined in the Author Guidelines, which is found in About the Journal.
6. English keywords should be provided from http://www.nlm.nih.gov/mesh(Medical Subject Headings), while Turkish keywords should be provided fromhttp://www.bilimterimleri.com
7. The title page should be a separate document from the main text and should be uploaded separately.
8. The "Affirmation of Originality and Assignment of Copyright/The Disclosure Form for Potential Conflicts of Interest Form" and Authorship Contribution Form should be downloaded from the website, filled thoroughly and uploaded during the submission of the manuscript.

TO AUTHORS

Copyright Notice

The author(s) hereby affirms that the manuscript submitted is original, that all statement asserted as facts are based on author(s) careful investigation and research for accuracy, that the manuscript does not, in whole or part, infringe any copyright, that it has not been published in total or in part and is not being submitted or considered for publication in total or in part elsewhere. Completed Copyright Assignment & Affirmation of Originality Form will be uploaded during submission. By signing this form;

1. Each author acknowledges that he/she participated in the work in a substantive way and is prepared to take public responsibility for the work.
2. Each author further affirms that he or she has read and understands the "Ethical Guidelines for Publication of Research".
3. The author(s), in consideration of the acceptance of the manuscript for publication, does hereby assign and transfer to the Molecular Imaging and Radionuclide Therapy all of the rights and interest in and the copyright of the work in its current form and in any form subsequently revised for publication and/or electronic dissemination.

Privacy Statement

The names and email addresses entered in this journal site will be used exclusively for the stated purposes of this journal and will not be made available for any other purpose or to any other party.

Peer Review Process

1. The manuscript is assigned to an editor, who reviews the manuscript and makes an initial decision based on manuscript quality and editorial priorities.
2. For those manuscripts sent for external peer review, the editor assigns at least two reviewers to the manuscript.
3. The reviewers review the manuscript.
4. The editor makes a final decision based on editorial priorities, manuscript quality, and reviewer recommendations.
5. The decision letter is sent to the author.

Contact Address

All correspondence should be directed to the Editorial Office:
Cinnah Caddesi Pilot Sokak No:10/12 06650 Çankaya / Ankara, Turkey
Phone: +90 312 441 00 45
Fax: +90 312 441 12 97
E-mail: info@tsnmjournals.org

MIRT
Molecular Imaging and Radionuclide Therapy

CONTENTS

Review

88 A Review of the History of Radioactive Iodine Theranostics: The Origin of Nuclear Ontology
Radyoaktif İyot Teranostiğinin Kısa Hikayesi: Nükleer Ontolojinin Kökenleri
John Dennis Ehrhardt, Seza Güleç; Miami, USA

Original Articles

98 The Role of Ga-68 PSMA PET/CT Scan on Differentiating of Oligometastatic and High Risk Prostate Cancer
Oligometastatik ve Yüksek Riskli Prostat Kanserinin Ayrımında Ga-68 PSMA PET/BT Taramasının Rolü
Mehmet Erdoğan, Emine Elif Özkan, Sefa Alperen Öztürk, Mustafa Yıldız, Sevim Süreyya Şengül; Isparta, Turkey

105 Metabolic Characterization of Anterior Mediastinal Masses by ^{18}F-FDG PET/CT
^{18}F-FDG PET/BT ile Anterior Mediastinal Kitlelerin Metabolik Karakterizasyonu
Zehra Pınar Koç, Pınar Pelin Özcan, Erhan Ayan, Rabia Bozdoğan Arpacı; Mersin, Turkey

112 Value of C-reactive Protein/Albumin Ratio for Predicting Ischemia in Myocardial Perfusion Scintigraphy
C-reaktif Protein/Albumin Oranının Miyokardiyal Perfüzyon Sintigrafisinde İskemi Öngörmedeki Rolü
Süleyman Çağan Efe, Özlem Özdemir Candan, Cihan Gündoğan, Ahmet Öz, Yasin Yüksel, Burak Ayca, Tevfik Fikret Çermik; İstanbul, Turkey

118 Collimator and Energy Window Evaluation in Ga-67 Imaging by Monte Carlo Simulation
Ga-67 Görüntülemede Monte Carlo Simulasyonu Kullanılarak Kolimatör ve Enerji Penceresi Değerlendirmesi
Mina Ouahman, Rachid Errifai, Hicham Asmi, Youssef Bouzekraoui, Sanae Douama, Farida Bentayeb, Faustino Bonutti; Rabat, Udine, Morocco, Italy

124 Red Marrow Absorbed Dose Calculation in Thyroid Cancer Patient Using a Simplified Excel Spreadsheet
Tiroid Kanseri Hastasında Basitleştirilmiş Bir Excel Elektronik Tablosu Kullanılarak Kırmızı İliğin Absorbe Ettiği Dozun Hesaplaması
Rangsee Songprakhon, Krisana Roysri, Putthiporn Charoenphun, Krisanat Chuamsaamarkkee; Surin, Bangkok, Thailand

Interesting Images

132 Mickey Mouse Sign on Bone Scan in the Monostotic Form of Paget's Disease Mimicking Osseous Metastasis
Metastazı Taklit Eden Monostotik Tip Paget Hastalığı'nda Mickey Mouse İşareti
Selin Kesim, Halil Turgut Turoğlu, Salih Özgüven, Tunç Öneş, Tanju Yusuf Erdil; İstanbul, Turkey

135 Comparative Findings Between ^{68}Ga-PSMA and ^{18}F-FDG PET/CT for Hepatocellular Carcinoma
Hepatoselüler Karsinomda ^{68}Ga-PSMA ve ^{18}F-FDG PET/BT ile Karşılaştırmalı Bulgular
Seval Erhamamcı, Nesrin Aslan; İstanbul, Turkey

MIRT
Molecular Imaging and Radionuclide Therapy

CONTENTS

139 Unforeseen COVID-19 on Oncologic Bone Scan with SPECT/CT in a High Prevalence Area

COVID-19'un Yaygın Görüldüğü Bir Bölgede SPECT/BT ile Onkolojik Kemik Taramasında Beklenmedik Şekilde COVID-19 Bulguları

Sana Munir Gill, Aamna Hassan, Humayun Bashir; Lahore, Pakistan

Letter to the Editor

143 Lung Perfusion Imaging with Technetium-99m Macroaggregated Albumin should be Combined with Contrast-enhanced Echocardiography for the Diagnosis of Hepatopulmonary Syndrome

Hepatopulmoner Sendrom Tanısı için Teknesyum-99m Makroagregasyonlu Albümin ile Akciğer Perfüzyon Görüntülemesi Kontrastlı Ekokardiyografi ile Birleştirilmelidir

Georgios Meristoudis, Georgia Keramida, Ioannis Ilias; Thessaloniki, London, Athens, Greece, United Kingdom

Index

2020 Referee Index / *2019 Hakem Dizini*

2020 Author Index / *2019 Yazar Dizini*

2020 Subject Index / *2019 Konu Dizini*

Review
Mol Imaging Radionucl Ther 2020;29:88-97 DOI:10.4274/mirt.galenos.2020.83703

A Review of the History of Radioactive Iodine Theranostics: The Origin of Nuclear Ontology

Radyoaktif İyot Teranostiğinin Kısa Hikayesi: Nükleer Ontolojinin Kökenleri

John Dennis Ehrhardt Jr[1,2], Seza Güleç[1,2,3]
[1]*Miami Cancer Research Center, Miami, USA*
[2]*Aventura Hospital and Medical Center, Miami, USA*
[3]*Florida International University Herbert Wertheim College of Medicine, Miami, USA*

Abstract

Studies on the first years of radioactive iodine (RAI) use in thyroid diseases have focused on hyperthyroidism. Saul Hertz's success with RAI in thyrotoxicosis fueled a seamless transition to Samuel Seidlin's investigations with RAI in thyroid cancer. These landmark events embody nuclear ontology, a philosophical foundation for the creation and existence of radio-therapeutic principles that continue to influence clinical practices today. Laying this ontological foundation, Dr. Saul Hertz who is the founding director of Massachusetts General Hospital Thyroid Clinic, affiliated with Harvard University created a framework for RAI theranostics with preclinical experiments and clinical cases from 1937 to 1942. The first thyroid cancer treatment with RAI was applied in 1942 by Samuel Seidlin. The sensational effect of the first application was interestingly powerful enough to overshadow scientific data. Seidlin and colleagues assembled a sixteen-patient series showcasing a unique entity: functional thyroid metastases that respond to RAI. Other investigations at the time demonstrated that RAI had little efficacy as a therapeutic agent, mainly because most thyroid tumors do not form colloid, and therefore cannot concentrate RAI. These findings were soon overshadowed by a mainstream article in the October 1949 issue of Life that portrayed RAI as a lifesaving therapy for thyroid cancer. The paradigm was set, and later writings by William H. Beierwaltes and other prominent nuclear medicine physicians established the primary goals and principles of RAI therapy. The developments in theoretical physics and nuclear instrumentation and the scientists who made these developments in the early years contributed greatly to the development of the concept. In the field of nuclear medicine, William H. Beierwaltes has gone down in our history as a clinical researcher with his most important contributions. The classical paradigm that started with him has carried us to today's molecular theranoistic viewpoint. This paper examines controversial topics in the advent of thyroid theranostics, and applies historical significance to current discussions on the role of RAI in thyroid cancer management. Another paradigm shift is on the horizon as thyroidology enters the age of genomics. The molecular theranostic profiles will soon be incorporated into a dynamic clinical decision-making and management algorithm for thyroid surgery and RAI therapy. From now on, nuclear oncology will gain a new ontological identity with molecular pathology and new theranostic expansions.

Keywords: Radioactive iodine, theranostics, nuclear oncology, Saul Hertz, Irving Ariel, Samuel Seidlin, Henry Beierwaltes, thyroid cancer, genomics

Öz

Tiroit hastalıklarında radyoaktif iyot (RAI) kullanımının ilk yıllarına ait çalışmalar hipertiroidi konusunda yoğunlaşmıştır. Saul Hertz'in tirotoksikozda RAI ile elde ettiği başarı, Samuel Seidlin'in tiroid kanseri tedavisi üzerinde RAI araştırmalarını kolaylıkla tetiklemiştir. Bu dönüm noktası niteliğindeki olaylar, günümüz klinik uygulamalarını etkileyen radyoterapötik ilkelerin oluşturulması için felsefi bir temel olan nükleer ontolojiyi somutlaştırmıştır. Bu ontolojik temeli atan Dr. Saul Hertz, Harvard Üniversitesi ile bağlantılı çalışan Massachusetts General Hospital Tiroit Kliniği'nin kurucu direktörüdür. Hertz preklinik deneyler ve klinik olgular ile, bugünkü bilgilerimize esas teşkil eden tiroid teranostik çalışmalarını 1937-1942 yılları arasında gerçekleştirmiştir. RAI ile tiroit kanseri tedavisi ilk kez 1942 yılında Samuel Seidlin tarafından uygulanmıştır. İlk uygulamanın sansasyonel etkisi, ilginç olarak, bilimsel verileri gölgeleyecek denli güçlü olmuştur. Seidlin ve meslektaşları, benzersiz bir durumu sergileyen on altı hasta serisini bir araya getirmiştir: RAI'ye yanıt veren fonksiyonel tiroit metastazları. O zamanki diğer araştırmalar, RAI'nın terapötik bir ajan olarak etkinliğinin az olduğunu göstermiştir, çünkü çoğu tiroit tümörleri kolloid oluşturmaz ve bu nedenle RAI'yı konsantre edemezler. Bu bulgular kısa süre sonra Life dergisinin Ekim 1949 sayısında

Address for Correspondence: Seza Güleç MD, Miami Cancer Research Center, Miami, USA
Phone: +90 786-693-0821 **E-mail:** sezagulec@gmail.com ORCID ID: orcid.org/0000-0002-4321-5453
Received: 24.04.2020 **Accepted:** 27.04.2020

RAI'yi tiroid kanseri için hayat kurtaran bir tedavi olarak tasvir eden ana akım bir makale tarafından gölgede bırakılmıştır. Ardından paradigma belirlenmiş ve daha sonra William H. Beierwaltes ve diğer önde gelen nükleer tıp doktorlarının yazıları ile RAI tedavisinin birincil hedef ve ilkeleri belirlenmiştir. Kavramın gelişmesinde, erken yıllarda teorik fizik ve nükleer instrumentasyonlardaki gelişmelerin ve bu gelişmelere imza atan bilim adamlarının büyük katkıları olmuştur. Nükleer tıp alanında ise en önemli katkılarıyla William H. Beierwaltes bir klinik araştırmacı olarak tıp tarihine geçmiştir. Onunla başlayan klasik paradigma, bizleri bugünün moleküler teranostik bakış açısına kadar taşımıştır. Bu makale, tiroid teranostiklerinin ortaya çıkışındaki tartışmalı konuları incelemekte ve RAI'nın tiroid kanseri yönetimindeki rolü konusundaki güncel tartışmalarda tarihsel önemi vurgulamaktadır. Tiroidoloji genomik çağına girerken bir başka paradigma dönüşümü ufuktadır. Moleküler teranostik profiller yakında tiroid cerrahisi ve RAI tedavisi için dinamik bir klinik karar verme ve yönetim algoritmasına dahil edilecektir. Bundan böyle moleküler patoloji ve yeni teranostik açılımlar ile, nükleer onkoloji artık yeni bir ontolojik kimliğe kavuşacaktır.

Anahtar kelimeler: Radyoaktif iyot, teranostik, nükleer onkoloji, Saul Hertz, Irving Ariel, Samuel Seidlin, Henry Beierwaltes, tiroid kanseri, genomik

"Today is only one day in all the days that will ever be. But what will happen in all the other days that ever come can depend on what you do today".
*- **Ernest Hemingway***

Radio-iodine Halts One Type of Cancer

On October 31, 1949, the *Life* Magazine ran an article titled "Radio-iodine Halts One Type of Cancer" with the subheading "Radioactive chemical brings about history-making recovery of patient dying from thyroid tumors" (1). This article (Figure 1) featured the "before and after" photographs of Bernard Brunstein, the Brooklyn shoe salesman who was "cured" of thyroid cancer with the use of radioactive iodine (RAI). The "before" photograph from the year 1942 shows him as cachectic and frail, which is in stark contrast with the "after" photograph, which showcases him as a healthy-appearing man with a full face. This convincing portrayal of RAI as a miraculous therapy for thyroid cancer left a strong impression on the public and practicing clinicians. The article's profound rhetoric permeated medical teaching and influenced

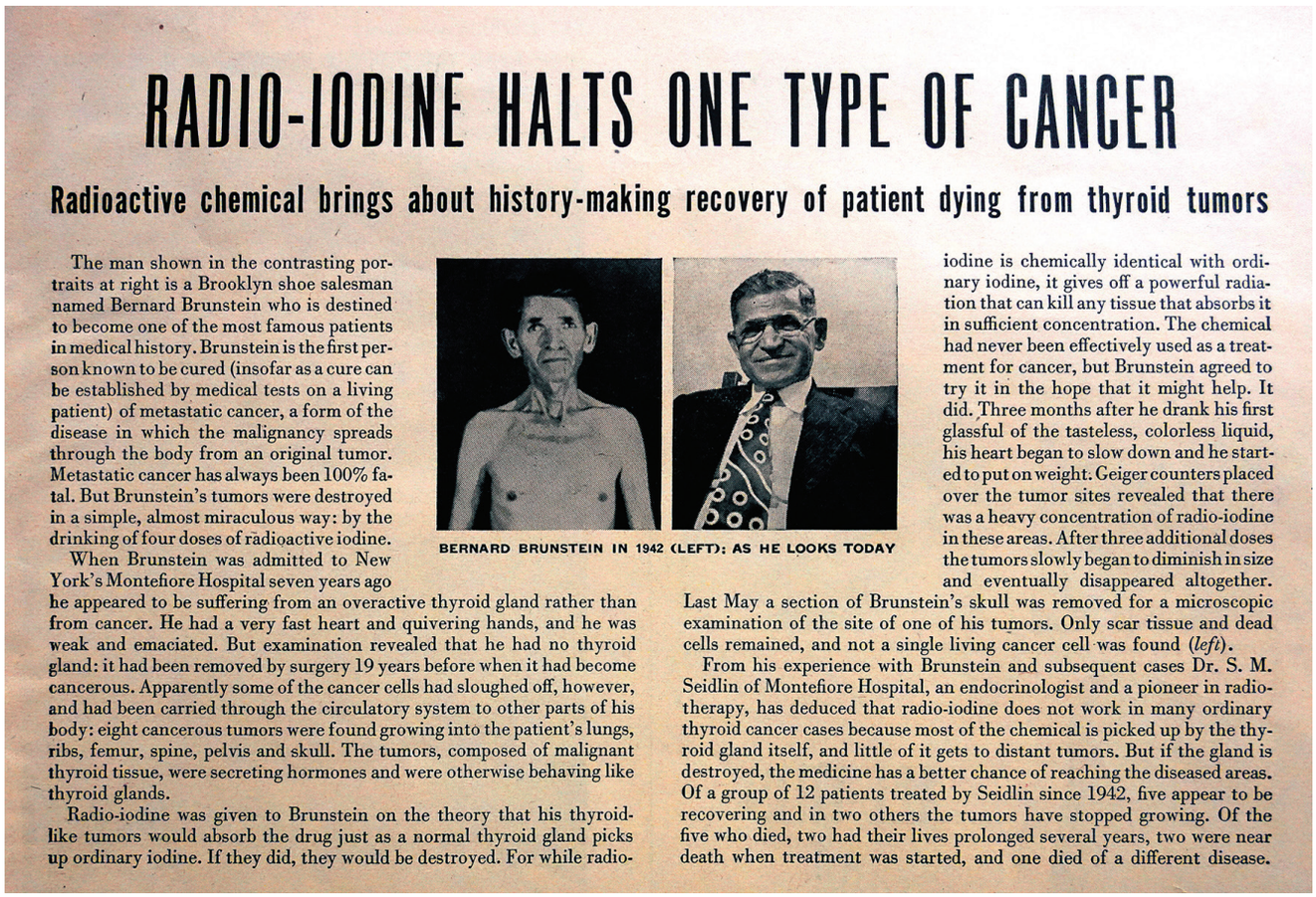

RADIO-IODINE HALTS ONE TYPE OF CANCER

Radioactive chemical brings about history-making recovery of patient dying from thyroid tumors

The man shown in the contrasting portraits at right is a Brooklyn shoe salesman named Bernard Brunstein who is destined to become one of the most famous patients in medical history. Brunstein is the first person known to be cured (insofar as a cure can be established by medical tests on a living patient) of metastatic cancer, a form of the disease in which the malignancy spreads through the body from an original tumor. Metastatic cancer has always been 100% fatal. But Brunstein's tumors were destroyed in a simple, almost miraculous way: by the drinking of four doses of radioactive iodine.

When Brunstein was admitted to New York's Montefiore Hospital seven years ago he appeared to be suffering from an overactive thyroid gland rather than from cancer. He had a very fast heart and quivering hands, and he was weak and emaciated. But examination revealed that he had no thyroid gland: it had been removed by surgery 19 years before when it had become cancerous. Apparently some of the cancer cells had sloughed off, however, and had been carried through the circulatory system to other parts of his body: eight cancerous tumors were found growing into the patient's lungs, ribs, femur, spine, pelvis and skull. The tumors, composed of malignant thyroid tissue, were secreting hormones and were otherwise behaving like thyroid glands.

Radio-iodine was given to Brunstein on the theory that his thyroid-like tumors would absorb the drug just as a normal thyroid gland picks up ordinary iodine. If they did, they would be destroyed. For while radio-iodine is chemically identical with ordinary iodine, it gives off a powerful radiation that can kill any tissue that absorbs it in sufficient concentration. The chemical had never been effectively used as a treatment for cancer, but Brunstein agreed to try it in the hope that it might help. It did. Three months after he drank his first glassful of the tasteless, colorless liquid, his heart began to slow down and he started to put on weight. Geiger counters placed over the tumor sites revealed that there was a heavy concentration of radio-iodine in these areas. After three additional doses the tumors slowly began to diminish in size and eventually disappeared altogether. Last May a section of Brunstein's skull was removed for a microscopic examination of the site of one of his tumors. Only scar tissue and dead cells remained, and not a single living cancer cell was found (*left*).

BERNARD BRUNSTEIN IN 1942 (LEFT); AS HE LOOKS TODAY

From his experience with Brunstein and subsequent cases Dr. S. M. Seidlin of Montefiore Hospital, an endocrinologist and a pioneer in radiotherapy, has deduced that radio-iodine does not work in many ordinary thyroid cancer cases because most of the chemical is picked up by the thyroid gland itself, and little of it gets to distant tumors. But if the gland is destroyed, the medicine has a better chance of reaching the diseased areas. Of a group of 12 patients treated by Seidlin since 1942, five appear to be recovering and in two others the tumors have stopped growing. Of the five who died, two had their lives prolonged several years, two were near death when treatment was started, and one died of a different disease.

Figure 1. A popular article featuring Samuel Seidlin's famous patient who was "cured" of thyroid cancer by radioactive iodine therapy, dated October 31, 1949 (*Life* Magazine)

clinical reasoning, which soon placed RAI treatment as the core modality for the management of "differentiated" thyroid cancer. RAI, which is the first theranostic radiopharmaceutical approach, has ontological origins that date back to November 12, 1936, which forever changed the management paradigm for thyroid diseases.

Saul Hertz, Father of Theranostics

Saul Hertz (Figure 2), Chief of the Thyroid Clinic at the Massachusetts General Hospital (MGH), joined the Chief of Medicine, James H. Means, for a luncheon at the Harvard Medical School's Vanderbilt Hall on November 12, 1936. The keynote speaker was Massachusetts Institute of Technology (MIT)'s President Karl Compton, whose talk on "What Physics Could do for Biology and Medicine" sparked Hertz's creativity. From the audience, Hertz asked, "Can iodine be made artificially radioactive?" He was already several years deep into experiments on thyroid iodine physiology at the MGH in his quest for a non-operative solution to hyperthyroidism. Compton was unsure how to answer, maybe partially because his lecture's focus on artificial radioisotopes came recommended last-minute by the MIT physicist Robley Dunglison Evans. Nonetheless, Compton jotted a reminder to himself and wrote to Hertz a month later on December 15, 1936 (Figure 3): "To my chagrin I have just come across the memorandum which I made on your question about the radioactivity of iodine. Iodine can be made artificially radioactive. It has a half-period of decay of twenty-five minutes and emits gamma rays and beta rays (electrons) with a maximum energy of 2.1 million volts. It is probable that there are several other periods of decay, but if so they correspond to types of radioactivity like the one indicated, and they are not as yet very definitely established" (2).

To this, Hertz replied 8 days later on December 23, 1936, hinting at his hypothesis, he wrote "...hope that iodine, which is made radioactive as you indicated will be a useful method of therapy in cases of over-activity of the thyroid gland". From a historical perspective, the correspondence between Compton and Hertz is an indisputable proof that the idea of RAI theranostic arose from Hertz. The Hertz family later released these letters; however, several histories, even 21st century publications, have presented the 1936 Vanderbilt Hall interaction in a way that credited the Chief of Medicine J.H. Means for presenting the RAI idea (3,4,5). We can thus be sure, beyond any reasonable doubt, that it was Saul Hertz who posed the question first.

Hertz's RAI research work began in the early 1937. Then, Evans was appointed to manage the physics laboratory at MIT, where we designed for the small-scale production of non-cyclotron ^{128}I. The experimental protocol followed was the one proposed by the 1934 *Nature* paper article by Fermi (6), an Italian-American physicist who later became famous as the architect of the atomic bomb. Evans recruited a junior faculty, the MIT nuclear physicist Arthur Roberts to perform the grunt work of isolating ^{128}I. Nearby at the MGH, James H. Means, who had previously told Hertz that he intended to let his contract expire at the thyroid clinic, renewed Hertz's directorial position and charged him with the job of overseeing all biological and medical aspects of the radioiodine project. Under this Hertz-Roberts collaboration, an experimental study of 48 rabbits was first undertaken, which demonstrated that the goitrous thyroid glands retained more RAI than the normal control glands. They ran experiments at the MIT because the 25-minute half-life of ^{128}I prohibited transportation of the radionuclide across the Charles River to the MGH. The scholars later speculated that their original experiment produced only 0.05 miliCurie (mCi) of activity, which is extremely small in comparison with the 100-mCi therapeutic activity that is commonly applied presently for RAI treatments (7). Although successful in laboratory, Hertz realized that

Figure 2. Saul Hertz, Chief of the Thyroid Clinic at the Massachusetts General Hospital (MGH) who introduced the concept of RAI theranostics

the small experimental yield and the short half-life of ^{128}I made its clinical application impractical. To ramp up the production, the MIT outlined plans to build a cyclotron for the mass creation of radioiodine. The then President Compton and the Hertz-Roberts laboratory manager Evans took a day trip to Manhattan in May 1938 and secured a $30.000 grant (equivalent of $530.000 today) from the John and Mary Markle Foundation to fund the proposed MIT cyclotron. Construction was arduous and MIT soon consulted the University of California at Berkeley, where Ernest O. Lawrence's original cyclotron possessed novel capabilities to create different radioisotopes, each with longer half-lives than ^{128}I. Building the MIT cyclotron was believed to solve the problem of experimental yield, albeit solutions for short half-lives remained unresolved.

Lawrence's cyclotron had established the University of California at Berkeley as the west coast hub for radionuclide research. The work progress continued when Glenn Seaborg and Jack Livingood discovered the popular ^{131}I there in 1938 by irradiating tellurium targets (8). This breakthrough came after a conversation between Seaborg with fellow laboratory associate Joseph A. Hamilton, a physician-scientist who explained that the short half-life of ^{128}I placed great constraints on its clinical application. In collaboration with Livingood, Seaborg then produced ^{131}I roughly 1 week after that his dialogue with Hamilton. Several of the radioisotopes discovered at the Berkeley cyclotron, including ^{131}I, were pursued out of passion for pure physics. Seaborg later reflected that they "usually gave little thought to the possibility that one of the objects of our search would have practical value. But we were in for some surprises" (9). However, the l arge-scale synthesis of ^{131}I remained a problem until 1941. Seaborg could live to see the impact of his contribution to thyroid diseases when his mother later required RAI treatment for hyperthyroidism (10). The fission-derived radioiodine was made freely available in the year 1946 as a consequence of the Manhattan project in the "secret town of Oak Ridge" in Tennessee.

Despite all the technical hitches, the RAI research continued to expand. Irving Ariel, a surgeon by occupation, performed animal studies using 12.5-hour half-life I-130 at the University of Rochester. Ariel (Figure 4) later continued his clinical and research studies in New York's Memorial Hospital. Ariel's career as a "Nuclear Surgeon" flourished in the later years, and he became best known as an

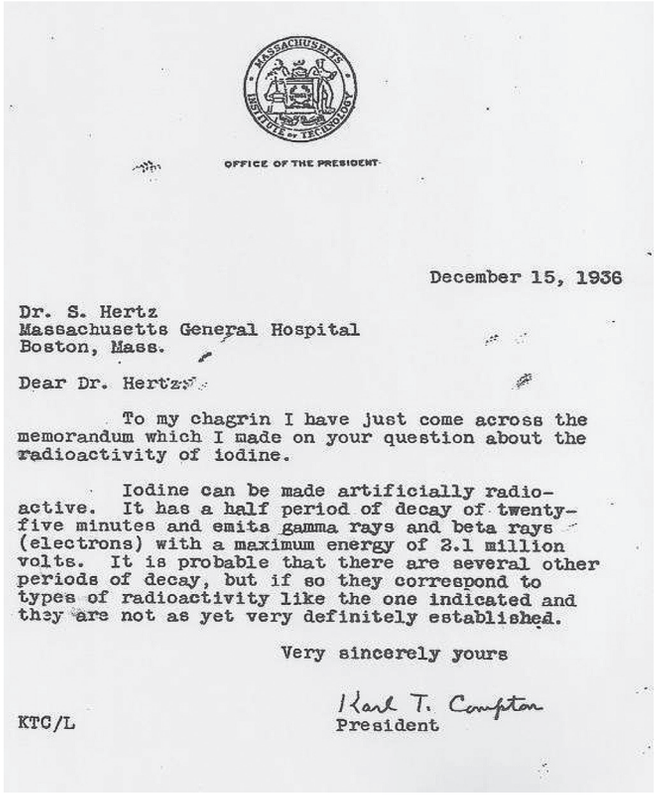

OFFICE OF THE PRESIDENT

December 15, 1936

Dr. S. Hertz
Massachusetts General Hospital
Boston, Mass.

Dear Dr. Hertz:

To my chagrin I have just come across the memorandum which I made on your question about the radioactivity of iodine.

Iodine can be made artificially radioactive. It has a half period of decay of twenty-five minutes and emits gamma rays and beta rays (electrons) with a maximum energy of 2.1 million volts. It is probable that there are several other periods of decay, but if so they correspond to types of radioactivity like the one indicated and they are not as yet very definitely established.

Very sincerely yours

Karl T. Compton
President

KTC/L

Figure 3. Massachusetts Institute of Technology (MIT) president Karl Compton's letter to Saul Hertz, the undisputable proof that Hertz is the father of Nuclear Theranostics

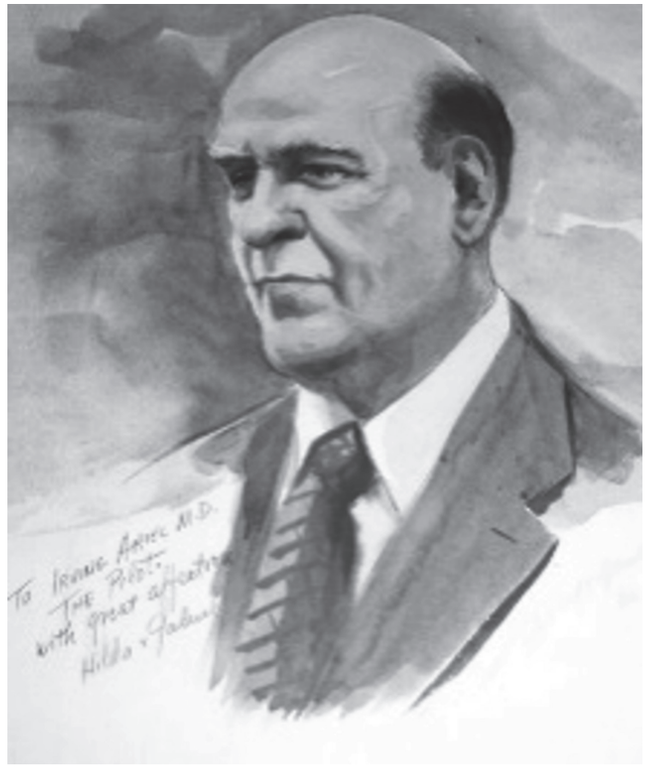

Figure 4. Irving Ariel, a New York Surgeon, who is well recognized for his clinical and translational Nuclear Medicine research introduced I-131 to the surgical world

innovator in the radiomicrosphere therapy (11). In fact, he was among the first to shift to ^{131}I when it became more available. The Ariel group later demonstrated the clinical importance of dose rate, which suggested that ^{131}I had a higher therapeutic potential than other radioisotopes with longer half-lives, namely the 60-day ^{125}I (12). In addition, Ariel spent most of his career as a clinician and a professor of surgical oncology in New York, affiliated with the Memorial Hospital and the Albert Einstein College of Medicine. The surgeon was one of the founding members of the Society of Nuclear Medicine. He also served as the trustee of the National Society of Nuclear Medicine and the president of the Greater New York Chapter.

At this juncture, radioiodine from the original cyclotron, for which Lawrence later won the 1939 Nobel Prize in Physics, became available as ^{126}I ($t_{1/2}$=13 days) and ^{131}I ($t_{1/2}$=8 days), which were ready-to-ship first-class from Berkeley to Cambridge (13). This Berkeley-MIT-MGH collaboration continued for nearly 2 years until the MIT cyclotron opened in 1940. Distinct from other cyclotrons, MIT devoted theirs to biological and medical research, albeit for a profit. Evans initially charged researchers $25 for radiotracers from the newly minted MIT radioactivity center. He later admitted that this became their primary revenue source, generating over $88.000 by 1945, largely paid through federal military research contracts at the indirect expense of taxpayers. In contrast, Lawrence's Nobel Prize-winning cyclotron at Berkeley continued shipping radioisotopes for free throughout the Second World War, supporting biomedical research as well as the Manhattan Project toward developing the atomic bomb (14).

Longer half-life ^{131}I shipped to MIT throughout the years 1938-1939 allowed Hertz and Roberts to confirm radiotracer avidity in normal rabbit thyroid and goiter. However, one mishap occurred during these early experiments when the amount of stable-carrier iodide was administered with the radioiodide. The scholars never foresaw that stable iodide would compete for thyroid uptake and thereby reduce the radionuclide tissue penetrance. As a result, their dosage predictions for future clinical trials were exorbitantly high, estimated at 750 mCi for the effective treatment of hyperthyroidism (7).

The Hertz-Roberts team was academically productive, which was a blessing and a curse that strained relationships with the supervisors. For instance, their 1938 manuscript was intercepted after acceptance because they had neglected to add the lab supervisor of Evans as a co-author, despite the fact that he reportedly contributed nothing to the experiments, analysis, or scientific writing process. Evans forced Hertz to draft a letter to the editors requesting an amended author list (15). Their subsequent 1940 manuscript included both Evans and Means as co-authors, with Hertz and Roberts at the helm, independently operating their own laboratory. This glimpse of academic hierarchy foreshadowed what was yet to come. Scholarly disputes festered against the backdrop of rising political concerns-the rise of the Third Reich, palpable antisemitism, and radio broadcasts bringing battlefield scenes into American homes-all while two of the greatest thyroid investigators, Hertz and Roberts, were Jewish.

The War and Subsequent *JAMA* Controversy

Hertz and Roberts began translating knowledge from their rabbit experiments to patients at the thyroid clinic. Hertz treated their first patient on March 31, 1941 and documented the process in his handwriting as "Elizabeth D.", with 2.1-mCi RAI. Hertz's case logs of RAI treatments grew steadily, with the addition of roughly 1 new patient every month. By 1943, his series had grown to include 27 patients with hyperthyroidism who were treated solely with RAI. His term as the director of the thyroid clinic ended during the summer of 1942. Means, however, agreed to pay Hertz a partial salary to continue his hyperthyroidism research. Thus, Hertz transitioned to private practice by opening his own Boston clinic from which he occasionally funneled patients into his ongoing RAI case series. At this time point, his MIT research partner Roberts was no longer involved, as he had turned his focus to other projects in particle physics and never returned to the thyroid subject again.

Hertz joined the US Navy and left for active duty in April 1943. Means was floored by Hertz's abrupt departure, but he agreed to allocate any new hyperthyroid patients to the study and follow-up their progress. Their conceptual understanding at that point was to attempt two rounds of oral RAI, for which Hertz deemed 12-15 mCi an appropriate activity. After which, patients with persistent symptoms were referred to a surgeon for possible thyroidectomy. Means was taken aback by Hertz's unexpected departure and hired Earle Chapman to coordinate Hertz's enrolled research patients at the MGH. Chapman, although he joined the group from his private clinical practice, actually attended the fateful lecture at the Vanderbilt Hall in December 1936 and followed the MGH-MIT progress with RAI through regular attendance at the weekly Thyroid Clinic meetings.

Hertz returned home to Brookline in the early 1945 and worked at the Chelsea Naval Hospital while attempting to re-enter the research circles at the MGH. Collegial relations had changed, and Hertz sensed it in the work atmosphere.

Academic hierarchy, stained by personal ambitions and political sentiments, were blatant now. Hertz received a phone call in November 1945 from Morris Fishbein, the then editor-in-chief of *JAMA*, who confirmed Hertz's ongoing suspicions. Fishbein in fact explained that the thyroid clinic had submitted a manuscript for a series of patients treated with RAI without consulting Hertz or including him as an author (16). *JAMA* initially rejected the paper for being excessively lengthy, and Hertz requested a copy in the interim while Chapman distilled the MGH manuscript down to an appropriate length. Understandably frustrated, Hertz wrote and submitted his own manuscript to *JAMA* with Arthur Roberts as a co-author. *JAMA* ultimately published both the articles, one by Hertz-Roberts and another by Chapman-Evans, side-by-side in the May 11, 1946 issue (17,18). Both the studies reached positive findings with RAI in the treatment of hyperthyroidism. Moreover, there was no patient overlap between the papers. In fact, the patients mentioned were in correspondence with Hertz during his active duty in the Navy, when Chapman was "really going to town", were never included in Hertz's series as promised. Chapman omitted to tell Hertz that he had slightly altered the experimental protocol, against the desire of Chief Means, to not administer a stable chaser dose of iodine after giving RAI, which added novelty to his series.

Despite the inner turmoil at the thyroid clinic, Hertz gained national recognition in other venues. He was inducted as a Young Turk to the American Society of Clinical Investigators (ASCI) in 1946 for his revolutionary work in developing the first theranostic modality in medicine: RAI treatment for thyroid disorders. ASCI inductees were called "young Turks" as an homage to the moniker for the members of the Committee of Union and Progress, a Turkish liberal reform movement in the Ottoman Empire that fought against Abdulhamid Han, the last Ottoman sultan to rule with absolute power. The sultan was deposed by the young Turks in the year 1909, when the ASCI held its inaugural meeting. The founding members based their new society on a revolutionary approach to research that emphasized newer physiological methods, with the hope of bringing sweeping reforms to research, which was analogous to the original young Turks in the Ottoman Empire (19).

Early Days of RAI in Thyroid Cancer

Success with hyperthyroidism fueled a seamless, almost intuitive transition to the use of RAI in thyroid carcinoma. In the recent years, the Hertz family communicated that Saul Hertz planned to study RAI as a therapy for thyroid cancer treatment while at the MGH thyroid clinic (20,21). Indeed, Samuel Seidlin consulted Hertz in the year 1943 for his RAI expertise when managing a patient with metastatic thyroid cancer; this case later gained fame and was widely publicized on the national and international stages. Hertz articulated in 1946 that his research would focus on "cancer of the thyroid which I believe holds the key to the larger problem of cancer in general", and that, after the War, "(new) demand expected in the fields of cancer and leukaemia for other radioactive medicines" (19).

The first research that focused on RAI in thyroid carcinoma were clinical reports led by a Berkeley physician-scientist Joseph G. Hamilton. A 1942 study by Hamilton's team administered tracer radioiodine in 2 preoperative patients undergoing thyroidectomy (22). Pathological examination demonstrated diffused radioiodine avidity in the surgical specimen, although they found "no significant deposition" in malignant foci of the gland by autoradiography.

Metastatic thyroid carcinoma with avidity for radioiodine was first reported on April 3, 1942 by a group from the Columbia University (23). Although he was most interested in unrelated research on spirochetes, dermatologist Albert S. Keston was the lead author because he owned the Geiger-Müller counter they borrowed to study the RAI uptake. Their patient had known bone metastases and had the status of 35-years post-thyroidectomy. Keston et al. hand-scanned the patient together with the then radiotherapy resident Robert P. Ball on the morning of December 7, 1941; he later recalled that they learned of the attacks at Pearl Harbor mid-examination via radio broadcast (24). After locating a single functional metastasis in the right distal femur, they administered a therapeutic dose of 10-mCi RAI obtained from both the cyclotrons at Berkeley and at MIT. A 3-week follow-up tracer study demonstrated little uptake in the femoral lesion, hinting at a therapeutic role of RAI in functional metastases. However, when they later published an autopsy report for the same patient in 1944, they noted that the bulk of metastatic tumor burden proved to be undifferentiated tissue that "did not concentrate radioiodine" (25).

The aforementioned experiences seemed to dispel the possibility that RAI could "cure" thyroid cancer. However, the discussion was far from finished as the literature continued to evolve. On December 7, 1946, at the 5-year anniversary of the Pearl Harbor attack, *JAMA* published Samuel Seidlin's extensive report of the first successful "treatment" of metastatic thyroid carcinoma with RAI (26). Seidlin (Figure 5) was an endocrinologist at Montefiore Hospital in New York when he consulted Hertz for an RAI advice in 1943. He subsequently followed his patient's progress for 3 years before releasing the groundbreaking

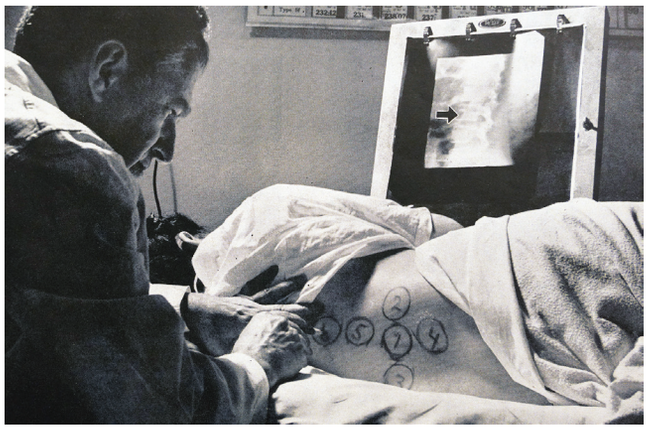

Figure 5. Samuel Seidlin examining a patient with a Geiger counter probe to detect RAI tracer uptake in metastatic thyroid lesions of the vertebrae in correlation with a radiograph of the spine (Life Magazine)
RAI: Radioactive iodine

case. Seidlin's coauthors in this case were Leonidas Marinelli, a physicist at Memorial Hospital (now Memorial Sloan-Kettering) who worked on dosimetry, and Eleanor Oshry, an applied physicist who was also the first woman to graduate from the Carnegie-Mellon's engineering school.

Their landmark paper presented the extensive history of B.B., a then 51-year-old man with metastatic thyroid cancer. The patient underwent total thyroidectomy at the age of 30 years for a large substernal goiter that compressed his trachea. Microscopic examination of his surgical specimen revealed no normal structures, and the pathological diagnosis was "malignant adenoma". Postoperatively, despite complete excision of the gland, B.B. did not become hypothyroid as was expected. In fact, he lived on for 15 years as a strong, healthy man before developing any classic symptoms of hyperthyroidism. His conditions of weight loss, palpitations, and anxiety progressively worsened until he was brought to surgical attention in November 1939 with a basal metabolic rate of +40 and a pulsatile tumor at the level of the twelfth thoracic vertebra. Accordingly, he underwent laminectomy at T12 and L1 for excisional biopsy, which revealed metastatic thyroid carcinoma. His postoperative course was complicated by thyroid storm, which in turn prompted his return for surgical neck exploration a few weeks later that turned out unremarkable.

B.B.'s condition worsened until his admission at the Montefiore Hospital on April 20, 1942, when he presented as a "small, emaciated, poorly developed man" standing at 4-feet, 10-inches tall and weighing 84 pounds. Seidlin's clinical team treated B.B. with daily doses of 1-6-mL Lugol's aqueous iodine for nearly 10 months to inhibit iodine organification through the Wolff-Chaikoff effect, thereby downregulating thyroid hormone production from his metastases. B.B. showed symptomatic relief at first, but, by January 1943, his condition worsened.

Seidlin consulted Saul Hertz soon after this incidence to discuss the possibility of using RAI to manage B.B.'s functional metastases. Hertz agreed with the management, and Seidlin only needed a contact for the supply of RAI. His decision to call Robey Evans at MIT was based solely on the fact that it was cheaper to call Massachusetts from New York than to connect with Berkeley, California. If that were not a factor, based on Hertz's past professional disagreements with Evans, he would have probably recommended that Seidlin send his RAI inquiry elsewhere. Marshall Brucer, the past-president of the Society of Nuclear Medicine and cogent medical historian, later recalled an anecdote about Seidlin's initial phone call with Evans, as follows:

Seidlin: "How much does it (RAI) cost?"

Evans: "Eighteen-hundred dollars an hour".

Seidlin: (not expecting such a high price): "Send me some".

Evans: "How many miliCuries do you want?"

Seidlin: "Send me a whole hour's worth".

When Brucer (27) wrote his 1966 *Vignettes in Nuclear Medicine*, he called this historic phone transaction "the beginning of radioisotope dosimetry". The decision-making underlying their negotiation was driven by financial considerations more than scientific evidence. Seidlin later admitted that neither he nor his patient had $1.800 and that he did not understand what Evans meant by "miliCuries". Eighteen-hundred dollars was possibly the operating price for the MIT cyclotron, and not the price for a therapeutic dose of RAI. Nevertheless, at this moment, Seidlin was a determined physician hoping to acquire a promising experimental therapy for his patient.

RAI shipments began arriving at the Montefiore Hospital from MIT, and Seidlin administered the first tracer dose to B.B. on March 11, 1943. Geiger-Müller counter hand-scanning confirmed all known metastases and revealed 2 new lesions: one focus was in the skull and another in the ischium. The first therapeutic RAI dose administered on May 11, 1943 contained 17 mCi of 12.6-h ^{130}I with <0.5 mg of carrier iodine. Over the following 22 months, B.B. received a total of 16 therapeutic doses, of both ^{130}I and ^{131}I, the largest dose being 55.4 mCi, and the final dose was administered on March 6, 1945. The cumulative quantity of RAI administered throughout his clinical course totaled 268.8 mCi.

Urinary RAI excretion was tracked, and the specimens were often held for reclamation. Owing to the exorbitant cost of cyclotron-generated radionuclide, the Montefiore team extracted and recycled RAI from B.B.'s urine to re-

administer by the oral route. On one such occasion, after administering the largest 55.4-mCi dose, they recovered 20.1-mCi from the urine and reused the rapidly decaying RAI. Although the laboratory assistants at Montefiore conducted the frugal practice of recycling RAI from urine for economic reasons, this practice later formed the basis for groundbreaking original research. One notable Montefiore laboratory assistant named Rosalyn Yalow translated the practice to albumin and insulin as well, and later won the 1977 Nobel Prize in Physiology or Medicine for her discovery of radioimmunoassay (28).

Seidlin's (26) team noted marked clinical improvement in the early stages that steadily improved with successive treatments. B.B. gained weight and reached an equilibrium at 106 pounds by April 1944, occasionally commenting that he was "getting fat". His bone pain drastically improved, he no longer had palpitations, and his basal metabolic rate dropped to -27. Seidlin's clinic at the Montefiore Hospital followed B.B.'s case and were amazed by his subjectively well constitution, which seemed to represent that he was "cured" from metastatic thyroid carcinoma.

B.B. dropped his anonymity in 1949, coming out as Bernard Brunstein in the popular weekly *Life* Magazine. Seidlin organized this opportunity for the humble Brooklyn shoe salesman to share his story. The inspiring account portrayed Brunstein as having experienced near-death from metastatic cancer before he was recovered with the "atomic cocktail" regimen. The cover photo for the October 31, 1949 issue featured Princess Margaret, the younger sister of Queen Elizabeth II. The thyroid cancer article spanned 3 pages and included several photographs to accompany the 5 paragraphs of text. No authors were listed for the piece. The second-to-last sentence of this article mentioned that Seidlin had performed RAI treatment on 12 patients since 1942, 5 of whom "appear to be recovering", presumably from their hyperthyroid state. Only 2 patients from that case series had tumors that appeared to stop growing.

RAI was brought to national attention and was presented as a cure for metastatic thyroid cancer based on the clinical improvement in just 1 patient. *Life* Magazine was arguably one of the most influential and widely-read weekly publication at the time. They covered all-important social topics ranging from World War II to U.S. presidential elections and served as a platform for famous authors, debuting important literature like Ernest Hemingway's *Old Man and the Sea*. While Seidlin's famous patient did improve clinically with respect to hyperthyroidism, *Life* somewhat misrepresented the claim that Seidlin "cured" metastatic thyroid carcinoma. In fact, only a little more than 2 years after this popular article, Brunstein reportedly died in 1952 from autopsy-proven anaplastic carcinoma (29).

Edward Siegel (30), the Physicist-in-Charge for Seidlin's laboratory during 1949-1952, later wrote his recollection of the famous case. He described an interaction in which Seidlin became "frustrated and disappointed" when Brunstein initially failed to meet with the photographers from *Life*, saying to his patient, "Is this how you show your gratitude? After all, I cured you of cancer". Brunstein replied, "Dr. Seidlin, you are supposed to be a smart man; if I had cancer five years ago, you know I'd be dead now!" (31). Essentially, even the patient himself believed that he was cured of something other than cancer, namely his hyperthyroidism.

Despite his interactions with the popular media, Seidlin himself was somewhat skeptical of having truly cured cancer. When examining the original December 7, 1946 *JAMA* case report, he wrote, "In spite of remarkable clinical improvement, it cannot be concluded that the functioning tumors have been completely destroyed, because recent tracer studies, although showing a marked increase in excretion, still show localization of RAI in these lesions" (26).

The *Harvard Crimson* ran a headline in May 1949 titled "Hertz to Use Nuclear Fission in Cure for Cancer". On closer examination, the article discussed how "it has been demonstrated that the majority of cancerous thyroids do not take up the RAI" (32). Saul Hertz published a comprehensive chapter in January 1950, 2 months after the popular *Life* article. His commentary on RAI in thyroid carcinoma was captured best by the following statement: "On the whole the results of RAI treatment in cancer of the thyroid, while promising, have not indicated any great percentage of cures in the short time in which the procedure has been used" (33). He was well-aware of Seidlin's patient and followed Brunstein's treatment progress. Hertz recounted the case and added, "of course, it will take a number of years to demonstrate many such cases as this original one" (33).

Building the Classic Age

Seidlin's "radioablation" of thyroid cancer raised an important question about what is the appetite of thyroid tumors for RAI? A relevant autoradiography study appeared in the January 1950 issue of *Cancer* by a Sloan-Kettering group led by Fitzgerald et al. (34) Their paper discussed original research on the concentration of ^{131}I in 100 consecutive cases of thyroid carcinoma, demonstrating that only 47 of the 100 patients had carcinoma with concentrated ^{131}I (34). From the 100 patients, they studied 258 total lesions, and found that 47% had concentrated ^{131}I. With respect to papillary thyroid carcinoma, the most

common type, only 26% of the tumors demonstrated ^{131}I uptake. The possibility that a tumor would concentrate radioiodine correlated with those follicular lesions that make functional colloid. This interesting research did not go unnoticed.

Beierwaltes et al. (35), one of the most pre-eminent nuclear medicine pioneer, cited the Fitzgerald paper in his authoritative 1957 book *Clinical Use of Radioisotopes*, stating that "less than 50 per cent of carcinomas of the thyroid have been demonstrated to pick up measurable amounts of RAI". In several ways, Seidlin et al. (26) and Beierwaltes et al. (35) carried forward the foundation laid by Hertz with RAI in hyperthyroidism and built a conceptual basis for RAI in thyroid cancer. The rationale for applying RAI in thyroid cancer was clearly stated in 1957, in that "it is advisable to administer RAI to finish the job the surgeon started". The purpose of RAI in thyroid cancer was to completely ablate the normal thyroid tissues to make surveillance easier. If any tumor remains *in situ* after surgical thyroidectomy that is amenable to RAI, it is an added benefit, but not the primary purpose. In fact, small clusters of thyroid remnant are a normal post-operative product of ligating vascular pedicles at the thyroid poles (36). Beierwaltes (35) (Figure 6) reflected on the role of RAI in thyroid cancer in his autobiography *Love of Life*: "We were the first to insist on a total surgical thyroidectomy as the first step in treating all patients with thyroid cancer. The second step was to keep the patient off thyroid hormone for six weeks. The third step was to do a radio-iodine scan of the neck and whole body to look for thyroid remnant or metastasis. Then we gradually found that the usual effective dose of radio-iodine treatment was (1) 150 mCi to ablate the thyroid remnant; (2) 175 mCi for regional node metastasis; (3) 200 mCi for spreads outside the neck" (37). Beierwaltes provided the original framework, but the methodology for RAI ablation in cancer became morphed in subsequent decades and continues to remain debatable until date.

Leaning into the Age of Genomics

Molecular theranostics is the new paradigm in thyroid cancer risk stratification. More refined classification schemes based on genomics and their downstream phenotypic expressions are currently being formulated. Genomics with molecular pathology and molecular imaging reflect the true biological nature of different cancer types that are currently defined by the conventional morphologic features. The tumor differentiation/de-differentiation and clinical behavior for each individual cancer are now definable by molecular markers in addition to the standard

Figure 6. William Henry Beierwaltes, the pioneer nuclear medicine physician, 1955 (U.S. National Library of Medicine)

morpho-pathology. In 2014, the first comprehensive study on genomic characterization of thyroid cancer was published, which involved compiling of large data on the morphological and molecular features of papillary thyroid cancer (38). This work marked the beginning of a new paradigm for thyroid cancer diagnosis and management. First and foremost, this study identified pathways of thyroid cancer oncophysiology and their impact on iodine metabolism. Correlations between morphology and driver genetic mutations as well as thyroid differentiation score were first clearly described in a systematic fashion with this study. It is clearly evident that the conventional postoperative risk stratification criteria were to vacate their roles in molecular diagnostics and in the state-of-the-art RAI theranostics. This new paradigm promises to resolve the long-winded equipoise and facilitate research in optimal care of thyroid cancer patients.

Epilogue

Nuclear Oncology has an inspiring and thought-provoking history. This article is a tale of its "Ontology", the core philosophy behind the concept of theranostics. Thyroidology has evolved into a new paradigm with advances in genomics and molecular medicine. The molecular theranostic profiles are expected to be incorporated into dynamic clinical

decision-making and management algorithms for thyroid surgery and RAI therapy remaining faithful to the ontology of nuclear oncology.

Ethics

Peer-review: Internally peer-reviewed.

Authorship Contributions

Surgical and Medical Practices: S.G., J.E., Concept: S.G., J.E., Design: S.G., J.E., Data Collection or Processing: S.G., J.E., Analysis or Interpretation: S.G., J.E., Literature Search: S.G., J.E., Writing: S.G., J.E.

Conflict of interest: We hereby declare that we have no conflict of interest with any institution or person regarding this guide.

Financial Disclosure: The authors declared that this study received no financial support.

References

1. Radio-iodine halts one type of cancer: radioactive chemical brings about history-making recovery of patient dying from thyroid tumors. Life Magazine 1949;27:54-56.
2. Compton K. Letter to Saul Hertz: Hertz Family Archive December 15;1936.
3. Ell PJ. The contribution of medical physics to nuclear medicine: a physician's perspective. EJNMMI Phys 2014;1:3.
4. Adelstein SJ. Robley Evans and what physics can do for medicine. Cancer Biother Radiopharm 2001;16:179-185.
5. Brucer M. Robley Evans makes radioiodine. In: A Chronology of Nuclear Medicine (ed. Marshall Brucer). St. Louis: Robert R. Butaine Publishing; 1990:223.
6. Fermi E. Radioactivity induced by neutron bombardment. Nature 1934;133:757.
7. Sawin CT, Becker DV. Radioiodine and the treatment of hyperthyroidism: the early history. Thyroid 1997;7:163-176.
8. Livingood JJ, Seaborg GT. Radioactive Iodine Isotopes. Phys Rev 1938;53:1015.
9. Unknown Author. Distinguished Nuclear Pioneer––1971 Glenn Theodore Seaborg, Ph.D. J Nucl Med 1971;12:328-331.
10. Seaborg D. The life and contributions to the periodic table of Glenn T. Seaborg, the first person to have an element named after him while he was still alive. Pure Appl Chem 2019;91:1929-1939.
11. Gulec SA, O'Leary JP. A tribute to a nuclear surgeon. Arch Surg 2007;142:683-684.
12. Ariel IM. Treatment of tumors of the thyroid gland. GP 1952;6:32-42.
13. Ganz JC. Medical physics—particle accelerators—the beginning. Prog Brain Res 2014;215:25-35.
14. Creager ANH. Life atomic: a history of radioisotopes in science and medicine. Chicago, University of Chicago Press 2013;54-55.
15. Hertz S, Roberts A, Evans RD. Radioactive iodine as an indicator in thyroid physiology. Am J Physiology 1940;38:510.
16. Kigner E. Daughter gets dad his due: Dr. Saul Hertz honored for pioneering thyroid work. The Jewish Advocate 2012;203:1-4.
17. Hertz S, Roberts A. Radioactive iodine in the study of thyroid physiology VII. The use of radioactive iodine therapy in hyperthyroidism. JAMA 1946;131:181.
18. Chapman EM, Evans RD. The treatment of hyperthyroidism with radioactive iodine. JAMA 1946;11:186.
19. Howell JD. A history of the American Society for Clinical Investigation. J Clin Invest 2009;119:682-697.
20. Hertz B. Hertz S. (1905-1950) discovers the medical uses of radioactive iodine: the first targeted cancer therapy. In: Thyroid Cancer—Advances in Diagnosis and Therapy (ed. Hojjat Ahmedzadehfar). London: Intech Open Publishing 2016;1-14.
21. Hertz B. A tribute to Dr. Saul Hertz: The discovery of the medical uses of radioiodine. World J Nucl Med 2019;18:8-12.
22. Hamilton JG. The use of radioactive tracers in biology and medicine. Radiology 1942;39:541-572.
23. Keston AS, Ball RP, Frantz VK, Palmer WW. Storage of radioactive iodine in a metastasis from thyroid carcinoma. Science 1942;95:362-363.
24. Brucer M. The first 10 years of thyroid uptake (No. 38). (ed. Marshall Brucer). In: Vignettes in Nuclear Medicine St. Louis: Mallinckrodt Inc, 1967.
25. Frantz VK, Ball RP, Keston AS, Palmer WW. Thyroid carcinoma with metastasis: studied with radioactive iodine. Ann Surg 1944;119:668-669.
26. Seidlin SM, Marinelli LD, Oshry E. Radioactive iodine therapy: effect on functioning metastases of adenocarcinoma of the thyroid. JAMA 1946;14:838-847.
27. Brucer M. From surgery without a knife to the atomic cocktail (No. 2). (ed. Marshall Brucer). In: Vignettes in Nuclear Medicine. St. Louis: Mallickrodt Inc, 1966.
28. Becker DV. The early history of the use of radioiodine in thyroid disease. American Thyroid Association: Presidential Address. October 7, 1983.
29. Surks MJ. Milestones in thyroid research at Einstein and Montefiore: 1920-2011. https://www.einstein.yu.edu/departments/medicine/divisions/endocrinology-diabetes/division.aspx?id=35245. Accessed on February 3, 2020.
30. Seigel E. Some recollections of my tenure at Montefiore Hospital: a half-life with radioiodine and the thyroid gland. https://www.einstein.yu.edu/departments/medicine/divisions/endocrinology-diabetes/division.aspx?id=35245. Unpublished manuscript. Accessed on February 3, 2020.
31. Siegel E. The beginnings of radioiodine therapy of metastatic thyroid carcinoma: a memoir of Samuel M. Seidlin, M. D. (1895-1955) and his celebrated patient. Cancer Biother Radiopharm 1999;14:71-79.
32. Vincent DG. Hertz to use nuclear fission in cure for cancer. Harvard Crimson 1949;24 https://www.thecrimson.com/article/1949/5/24/hertz-to-use-nuclear-fission-in/. Accessed on February 3, 2020.
33. Hertz S. Use of radioactive iodine in the diagnosis, study and treatment of diseases of the thyroid. (ed. Samuel Soskin) In: Progress in Clinical Endocrinology 1950;65-78.
34. Fitzgerald PJ, Foote Jr FW, Hill RF. Concentration of I131 in thyroid cancer, shown by autoradiography: a study of 100 consecutive cases showing the relation of histological structure and the function of thyroid carcinoma. Cancer 1950;3:86-105.
35. Beierwaltes WH, Johnson PC, Solari AJ. Clinical use of radioisotopes. Philadelphia: W.B. Saunders Co.; 1957:150.
36. Gulec SA, Kuker R. Radioactive iodine remnant ablation: the beta-knife completion thyroidectomy. Mol Imaging Radionucl Ther 2017;26:16-23.
37. Beierwaltes WH. Love of life: autobiographical sketches. New York: Vantage Press; 1996;76-77.
38. Cancer Genome Atlas Research Network. Integrated genomic characterization of papillary thyroid carcinoma. Cell 2014;159:676-690.

Original Article
Mol Imaging Radionucl Ther 2020;29:98-104 DOI:10.4274/mirt.galenos.2020.89421

The Role of Ga-68 PSMA PET/CT Scan on Differentiating of Oligometastatic and High Risk Prostate Cancer

Oligometastatik ve Yüksek Riskli Prostat Kanserinin Ayrımında Ga-68 PSMA PET/BT Taramasının Rolü

Mehmet Erdoğan[1], Emine Elif Özkan[2], Sefa Alperen Öztürk[3], Mustafa Yıldız[1], Sevim Süreyya Şengül[1]

[1]*Süleyman Demirel University Faculty of Medicine, Department of Nuclear Medicine, Isparta, Turkey*
[2]*Süleyman Demirel University Faculty of Medicine, Department of Radiation Oncology, Isparta, Turkey*
[3]*Süleyman Demirel University Faculty of Medicine, Department of Urology, Isparta, Turkey*

Abstract

Objectives: In this study, we aimed to investigate whether Ga-68 prostate-specific membrane antigen positron emission tomography/computed tomography (PSMA PET/CT) scanning is adequate to predict intermediate risk, high risk, or oligometastatic prostate cancer (PCa) as an initial staging modality.

Methods: The Ga-68 PSMA PET/CT scan images of 50 PCa patients pathologically proven by transrectal ultrasound guided biopsy were evaluated retrospectively. The association of standard uptake value maximum (SUV_{max}) value of the area with the highest PSMA expression within the primary tumor with the risk groups and metastatic burden is investigated.

Results: The SUV_{max} value was 6.18 in oligometastatic patients where it was measured as 10.93 in patients with higher metastatic burden (p=0.037). The cut-off SUV_{max} value for multiple metastases was 7.96 (p=0.047). According to the regression model, SUV_{max} value has a positive influence [odds ratio (OR)=1.42], which was statistically significant (p=0.038). SUV_{max} values for intermediate and high risk patients were 6.91 and 11.44, respectively (p=0.014). The cut-off SUV_{max} value for the high risk group was 10.55 (p=0.006). In the regression model, SUV_{max} value has a positive influence (OR=1.198), which was statistically significant (p=0.021).

Conclusion: In this paper, we demonstrated the association between SUV_{max} value of primary tumor and Gleason score. Our results also allowed us to suggest that primary tumor SUV_{max} is a sufficiently accurate predictor of D'Amico risk groups in newly diagnosed PCa cases. Additionally, Ga-68 PSMA PET/CT turns out to be a useful tool in determining oligometastatic PCa, which requires a different treatment approach.

Keywords: Ga-68 PSMA PET/CT, prostate cancer, oligometastasis, SUV_{max}

Öz

Amaç: Çalışmamızda, Ga-68 prostat spesifik membran antijen pozitron emisyon-bilgisayarlı tomografi (PSMA PET/BT) taramanın maksimum standardize uptake değerini (SUV_{maks}), başlangıç evrelemede orta ve yüksek riskli prostat kanserini (PCa) tahmin edebilir mi? Oligometastatik PCa'yi tahmin edebilir mi? sorularına cevap aradık.

Yöntem: TRUS-Bx temelinde PCa tanısı almış ve Ga-68 PSMA PET/BT tarama yapılmış 50 hastanın görüntüleri retrospektif olarak incelendi. Primer tümörde PSMA ekspresyonunun en yüksek olduğu alanın SUV_{maks} değeri ile risk gruplarının ve metastaz durumunun korelasyonu yapıldı.

Bulgular: Oligometastatik hastalarda SUV_{maks} değeri 6,18 iken, multipl metastazı olan olgularda 10,93 olarak bulundu (p=0,037). Multipl metastaz için cut-off SUV_{maks} değeri 7,96 olarak bulundu (p=0,047). Regresyon modelinde, SUV_{maks}'nın katkısı pozitif yönlü [göreceli olasılıklar oranı (OR)=1,42] ve anlamlı bulundu (p=0,038). Orta risk grubunda SUV_{maks} değeri 6,91 iken, yüksek risk grubunda 11,44 olarak bulundu (p=0,014). Yüksek risk grubu için cut-off SUV_{maks} değeri 10,55 olarak bulundu (p=0,006). Regresyon modelinde, SUV_{maks}'nın katkısı pozitif yönlü (OR=1,198) ve anlamlı bulundu (p=0,021).

Address for Correspondence: Mehmet Erdoğan MD, Süleyman Demirel University Faculty of Medicine, Department of Nuclear Medicine, Isparta, Turkey
Phone: +90 211 246 28 10 **E-mail:** mdr_erdogan@yahoo.com ORCID ID: orcid.org/0000-0001-7724-778X
Received: 13.01.2020 **Accepted:** 31.05.2020

Sonuç: Bu çalışma ile yeni tanı almış PCa'da primer tm'nin SUV_{maks} değerinin, Gleason skoru ile korele olduğunu gösterdik. SUV_{maks}'nin, D'Amico risk sınıflamasına göre orta ve yüksek riskli PCa'sı yüksek doğrulukla tahmin edebileceğini düşünüyoruz. SUV_{maks}'nin tedavi yaklaşımı açısından önem arz eden oligometastatik PCa'sı yüksek doğrulukla tahmin edebileceğini düşünüyoruz.

Anahtar kelimeler: Ga-68 PSMA PET/BT, prostat kanseri, oligometastaz, SUV_{maks}

Introduction

Prostate cancer (PCa) is the second most frequent cancer in men and the cause of 5.2% of all cancer-related deaths (1). Prostate-specific antigen (PSA), digital rectal examination, Gleason score (GS), and specific imaging modalities are the most widely used parameters for initial clinical staging. These specific imaging tools are transrectal ultrasound (TRUS), multiparametric magnetic resonance imaging, thoracoabdominal computed tomography (CT), and bone scan (2). The goal of clinical staging in PCa is to determine the burden of disease and predict the prognosis via pretreatment clinical parameters to direct the patient for the most appropriate treatment plan. Procedures to be chosen for staging are specified according to risk stratification. The most widely used risk grouping for PCa is the one defined by D'Amico (3).

Ga-68 prostate-specific membrane antigen positron emission/CT (PSMA PET) scanning in PCa is found to have a higher sensitivity and specificity in distant lymph node metastasis and bone metastasis according to conventional imaging modalities (4). PSMA is a type II transmembrane glycoprotein consisting of 750 amino acids (5). It shows little or no expression in normal prostate cells, whereas it is significantly expressed in prostate carcinoma or metastasis (6). Besides, although it does not enter the circulation, PSMA is an ideal molecular target for nuclear medicine procedures with Ga-68 PSMA PET/CT (7).

As determining oligometastatic patients became crucial in terms of individualizing treatment strategy, PSMA PET/CT became increasingly used as initial staging modality. Hellman and Weichselbaum (8) first suggested the definition of the term "oligometastasis-oligometastatic" in 1995 that means "low burden metastatic patients whose prognostic features are between localized and metastatic disease". However, a consensus was not constituted on the final definition of oligometastatic disease. Some authors use only the number of metastases, whereas others consider both the number and localization (9).

The Chemo-Hormonal Therapy Versus Androgen Ablation Randomized Trial for Extensive Disease (CHAARTED) study suggested the widely accepted definition in the literature. Patients were stratified as high-volume disease in the presence of visceral metastases or four bone lesions with at least one beyond the vertebral bodies and pelvis and low-volume disease if out of high-volume definition (10). Radical treatment strategies such as surgery or stereotactic radiotherapy may be appropriate alternatives for a limited number of metastatic lesions that are so-called oligometastatic (11). Several studies reported increased overall survival with radical treatment approaches in oligometastatic PCa patients. Therefore, differentiating oligometastatic from multimetastatic disease during initial staging is important.

In this study, we aimed to investigate whether Ga-68 PSMA PET/CT scanning is adequate to predict the risk group or metastatic burden in PCa as an initial staging modality.

Materials and Methods

Patients

Images of 50 PCa patients who were diagnosed with 12-24 core TRUS-biopsy were retrospectively investigated. The patients had suspicious metastatic lesions in the bone scan or other conventional imaging techniques and underwent Ga-68 PSMA PET/CT for initial staging. Patients who underwent transurethral resection or radical prostatectomy were excluded.

The Scientific Research Ethics Committee of Medical Faculty of the Süleyman Demirel University (desicion no: 177, 21.05.2019) approved the study. All procedures were performed in terms of the ethical standards of the institutional research committee in alliance with the 1964 Helsinki Declaration and its later amendments. Informed consent was waived owing to the retrospective nature of the study. Pretreatment PSA values of patients were obtained from their electronical charts, and time between PSA test and Ga-68 PSMA PET/CT was maximum of 45 days. Biopsy specimens were reported according to the GS system and Gleason grade system suggested by The International Society of Urological Pathology in 2014 (12): Grade group 1 (GS ≤6), Grade group 2 (GS 3+4=7), grade group 3 (GS4+3=7), Grade group 4 (GS 4+4=8.3+5=8.5+3=8), and grade group 5 (GS 9-10). Consequently, patients were stratified according to D'Amico risk grouping, which classified Gleason grade groups 2 and 3 as intermediate risk group and Gleason grade groups 4 and 5 as high risk group (3). Gleason grade group 1, which is the low risk group,

was excluded in these two groups. Patients were then divided into three groups: non-metastatic, oligometastatic, and multimetastatic. Three or less metastatic lesions none or only one of them out of pelvis or vertebra was accepted as oligometastasis as in CHAARTED trial (10). Four or more bone metastasis and lymph node metastasis were included in the multiple metastatic group. None of the patients had visceral metastasis.

Image Acquisition and Analysis

Images were gathered via Philips Time of Flight PET/CT camera. PET/CT images were obtained 60 min after intravenous injection of 111-185 MBq (3-5 mCi) Ga-68 PSMA ligand. A low-dose CT scan was performed before PSMA PET/CT for attenuation correction and anatomic localization purposes and, consequently, a 3-min caudocranial PET emission scanning in the supine position. CT data were used for attenuation correction, and image reconstruction was done via the standard recursive algorithm. Transaxial, coronal, and sagittal plans were reformed. Maximum intensity projection images were also obtained. Two experienced nuclear medicine specialists evaluated the PET/CT fusion images. (The interrater agreement was high, and ICC=0.926). The highest standard uptake value maximum (SUV_{max}) value calculated from the whole prostate tissue is accepted as the highest region of PSMA expression, and it was recorded. Whole body scan was reviewed, especially for bony structure and abdominopelvic lymph nodes. The number and localization of PSMA-expressing bony structures and lymph nodes were also recorded.

Statistical Analysis

The statistical analysis was performed using SPSS 20.0 (IBM Inc., Chicago, IL, USA) software. Descriptive statistics were presented as frequency (percent ratio) for categorical variables and median; interquartile range for numeric variables. Normal distribution evaluation of PSA and SUV_{max} values were analyzed by Kolmogorov-Smirnov test, and both variables revealed non-parametric results. Therefore, the comparisons were performed by Mann-Whitney U and Kruskal-Wallis tests. Post-hoc analysis of significant results is shown in the tables by superscript letters. Receiver operating characteristic (ROC) analysis was performed for SUV_{max} values to calculate the diagnostic ratios. All tests are presented as two sided with 95% confidence intervals and relevant p values ($p<0.05$). The association between SUV_{max} values of primary tumor and these two risk groups is statistically analyzed, and logistic regression analysis was also performed. Subgroups of intermediate risk (Gleason grades 2 and 3) were additionally analyzed with each SUV_{max} values of the primary tumor in terms of association. The power analysis was not performed because of the small study sample size. In the SUV_{max} comparisons according to grade categories, power and partial eta square values were 0.853 and 0.200, respectively. Therefore, it appeared that the sample size was sufficient, and 20% of the variance according to categories was clarified.

Results

Fifty patients were enrolled to our study. The median age was 67.50 (12.25) years. When categorized, the distribution of age ranges was <55 (4%), 55-65 (40%), 65-75 (34%), and >75 (22%) years. More than half (58%) of patients were metastatic. Lymph node metastasis was found in 34% of patients, bone metastasis 40%, and both 16%. Of patients, 1 (2%), 9 (18%), 11 (22%), 15 (30%), and 14 (28%) were reported as grade groups 1, 2, 3, 4, and 5 respectively. No statistically significant difference was found between the Gleason grade groups. According to D'Amico risk classification, 20 (40%) patients were intermediate risk, whereas 29 (58%) were in the high risk group. Seven (14%) patients were found to be oligometastatic, and multiple bone and lymph node metastases were seen in 13 (26%) and 9 (18%) patients, respectively. Patients were also divided into nonmetastatic (42%), oligometastatic (14%), and multimetastatic (44%) groups.

Demographic features of patients are shown in Table 1.

SUV_{max} values in patients with positive biopsy ratio of >50% were higher, but the difference was nonsignificant. When three PSA groups (<10, 10-20, and >20 ng/mL) were analyzed, SUV_{max} values increased with higher PSA values, and this difference was statistically significant (p=0.011). No statistically significant difference was found between the SUV_{max} values of metastatic and non-metastatic patients. The median SUV_{max} value was 10.93 (14.94) and 6.18 (2.49) in multiple metastatic and oligometastatic groups, respectively, which is statistically significant (p=0.037). In intermediate and high risk patients, the SUV_{max} values were 6.91 (3.54) and 11.44 (14.83), respectively, which was also statistically significant (p=0.014). The difference in the SUV_{max} values between grade groups 2 and 3 was not statistically significant (p=0.056). SUV_{max} values in patients with vesicula seminalis invasion were significantly higher (p=0.001; Table 1).

Although SUV_{max} values in oligometastatic and multiple metastatic cases were significantly different, ROC analysis was performed. Area under the curve was significant 0.753 (p=0.047), and the cut-off value for SUV_{max} was 7.96 (Figure 1). The sensitivity and specificity of this cut-off value for predicting multiple metastases were 68.18% and 85.71%, respectively. The positive predictive value (PPV)

was high as 93.75%, whereas the negative predictive value (NPV) was only 46.15% (Table 2).

ROC analysis was also performed for the risk groups. Area under the curve was statistically significant at 0.727 (p=0.006). The cut-off value for SUV_{max} was 10.55 (Figure 2). The specificity and PPV of this cut-off value for predicting high risk group was 90.00%. The sensitivity and NPV were similar and found to be 62.07% (Table 3).

PSA values were not significantly different between age groups. In contrast, it was significantly higher in patients with positive biopsy ratio of >50% (p=0.002). In patients with lymph node metastasis, the PSA value was significantly higher than patients in the non-metastatic group (p<0.001). The difference was also statistically significant between the oligometastatic and multiple metastatic group (p=0.015), which is higher in multiple metastatic patients. No significant difference was found between the PSA values of D'Amico risk groups. However, it was significantly higher in patients with vesicula seminalis invasion (p=0.006; Table 1)

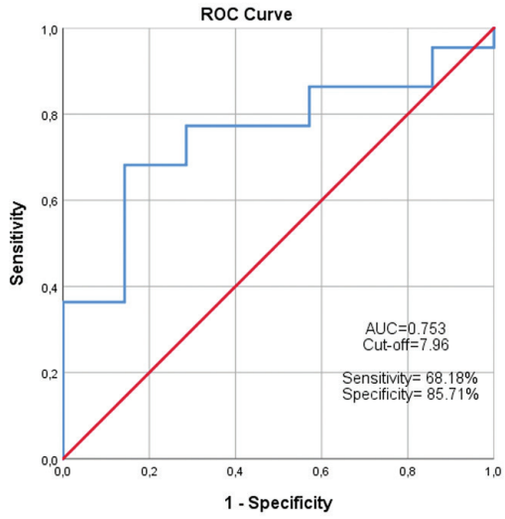

Figure 1. Receiver operating characteristic curve of standard uptake value on oligometastasis and multimetastasis
ROC: Receiver operating characteristic, AUC: Area under the curve

Table 1. SUV_{max} and PSA according to some characteristics of patients

Characteristics		PSA		SUV_{max}	
		Median (IQR)	p	Median (IQR)	p
BX ratio (%)	<50	7.01 (7.44)	0.002*	7.61 (7.38)	0.136
	>50	21.36 (34.38)		10.55 (14.73)	
PSA groups (ng/mL)	<10	5.18 (4.66)[a.b]	<0.001*	5.97 (5.85)[a.b]	0.011*
	10-20	11.87 (4.24)[a.c]		10.72 (13.02)[a]	
	>20	41.72 (63.16)[b.c]		10.93 (14.08)[b]	
Grades	1	14.79	0.091	11.91	0.056
	2	5.75 (10.86)		7.45 (4.15)	
	3	12.05 (27.35)		6.38 (2.66)	
	4	9.50 (44.76)		12.14 (12.97)	
	5	16.45 (37.07)		11.37 (14.89)	
Metastasis	None	10.14 (8.59)	0.089	8.19 (9.72)	0.426
	Exist	20.05 (41.56)		8.46 (8.12)	
Bone metastasis	None	11.44 (16.34)	0.593	10.58 (10.67)	0.406
	Exist	11.23 (49.01)		7.43 (7.22)	
Oligometastasis	None	10.14 (8.59)	0.015*	8.19 (9.72)	0.037*
	Oligo metastatic	9.50 (9.09)[a]		6.18 (2.49)[a]	
	Multiple metastatic	26.07 (52.61)[a]		10.93 (14.94)[a]	
Grade	Intermediate risk	9.49 (17.67)	0.120	6.91 (3.54)	0.014*
	High risk	12.98 (40.22)		11.44 (14.83)	
Vesicula seminalis	None	10.21 (9.56)	0.006*	7.49 (5.97)	0.001*
	Exist	29.44 (80.65)		14.28 (15.00)	

*Significant at 0.05 level, [a, b, c]The same superscript letter denotes the significant pairwise comparisons, SUV_{max}: Standard uptake value maximum, PSA: Prostate-specific antigen, IQR: Interquartile range, BX: Biopsy

Univariate logistic regression model was performed between oligometastatic and multiple metastatic patients. PSA and SUV_{max} were the variables to be specified as factors. Oligometastasis is investigated as a reference category. Goodness of fit results for this model were found to be significant and acceptable (-2LL=21.406; Hosmer & Lemeshow X^2=7.207 (p=0.514). The explanatory ratio of these factors to the multiple metastasis category was sufficiently high (Nagelkerke R^2=0.459). The contribution of SUVmax to the model was positive [odds ratio (OR=1.42) and significant (p=0.038; Table 4).

Univariate logistic regression model was also used between D'Amico risk groups. PSA, SUV_{max}, and age were the variables to be specified as factors. The intermediate risk group was the reference category. Goodness of fit results for this model were found significant (-2LL=51.698; Hosmer & Lemeshow X^2=4.491 (p=0.810), and the explanatory ratio was R^2=0.347. Contribution of SUV_{max} to the model was positive (OR=1.198) and significant (p=0.021; Table 4).

Discussion

Low burden metastatic PCa is considered to have a different behavioral pattern compared with high burden multiple metastatic counterparts. Although some reports have shown an outcome improvement with radical strategies, optimal treatment approach is still a matter of debate. Moreover, it is a controversy whether it is appropriate to perform aggressive modalities such as surgery or high-dose radiotherapy for both metastasis and primary lesions (13). Considering these discussions to constitute the most appropriate individual approach for low metastatic burden disease, we searched for an answer whether Ga-68 PSMA PET/CT scanning is adequate to predict intermediate risk, high risk, or oligometastatic PCa as an initial staging modality in this study (Figure 3).

According to our results, median SUV_{max} values in oligometastatic and multiple metastatic patients were 6.18 and 10.93, respectively, and this was statistically significant (p=0.037). Further ROC analysis revealed a cut-off value of 7.96 for SUV_{max}, and values higher than this predicted high burden disease with a sensitivity, specificity, PPV, and NPV of 68.18%, 85.71%, 93.75%, and 46.15%, respectively. To our knowledge, this is the first study to investigate the SUV_{max} value in Ga-68 PSMA PET/CT in staging and determining the disease burden (oligometastatic or multimetastatic) for PCa patients.

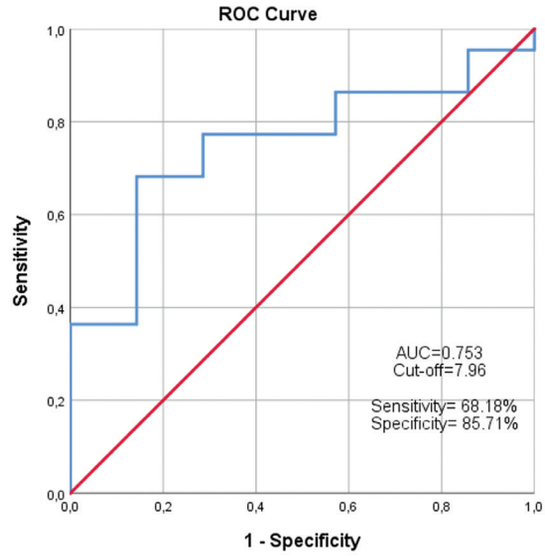

Figure 2. Receiver operating characteristic curve of standard uptake value on intermediate and high risk groups
ROC: Receiver operating characteristic, AUC: Area under the curve

Table 2. ROC analysis results and diagnostic ratios between oligometastatic and multiple metastatic groups

				% (95% CI)			
	AUC	**p**	**Cut-off**	**Sensitivity**	**Specificity**	**PPV**	**NPV**
SUV_{max}	0.753 (0.565-0.942)	0.047*	7.96	68.18 (45.13-86.14)	85.71 (42.13-99.94)	93.75 (70.50-98.95)	46.15 (30.23-62.91)

*Significant at 0.05 level, ROC: Receiver operating characteristics, CI: Confidence interval, SUV_{max}: Standard uptake value maximum, AUC: Area under the curve, PPV: Positive predictive value, NPV: Negative predictive value

Table 3. ROC analysis results and diagnostic ratios between intermediate and high risk groups

				% (95% CI)			
	AUC	**p**	**Cut-off**	**Sensitivity**	**Specificity**	**PPV**	**NPV**
SUV_{max}	0.727 (0.587-0.867)	0.006*	10.55	62.07 (42.26-79.31)	90.00 (68.30-98.77)	90.00 (70.10-97.19)	62.07 (50.11-72.72)

*Significant at 0.05 level, ROC: Receiver operating characteristics, CI: Confidence interval, SUV_{max}: Standard uptake value maximum, AUC: Area under the curve, PPV: Positive predictive value, NPV: Negative predictive value

Table 4. Predictive model of factors affecting metastasis and risk groups				
Model 1. Oligometastatic[R] and multiple metastatic groups				
			-2LL= 21.406	Nagelkerke R^2 = 0.459
	Hosmer & Lemeshow X^2=7.207 (p=0.514)			
Factors	Beta	p	OR	95% CI
PSA	0.075	0.120	1.078	0.981-1.186
SUV_{max}	0.412	0.038*	1.420	1.240-1.676
Model 2. Intermediate risk[R] and high risk				
			-2LL=51.698	Nagelkerke R^2=0.347
			Hosmer & Lemeshow X^2=4.491 (p=0.810)	
PSA	0.013	0.420	1.013	0.982-1.044
SUV_{max}	0.181	0.021*	1.198	1.028-1.397

[R]Reference category, *Significant at 0.05 level, log likelihood, -2LL=-2, SUV_{max}: Standard uptake value maximum, PSA: Prostate-specific antigen

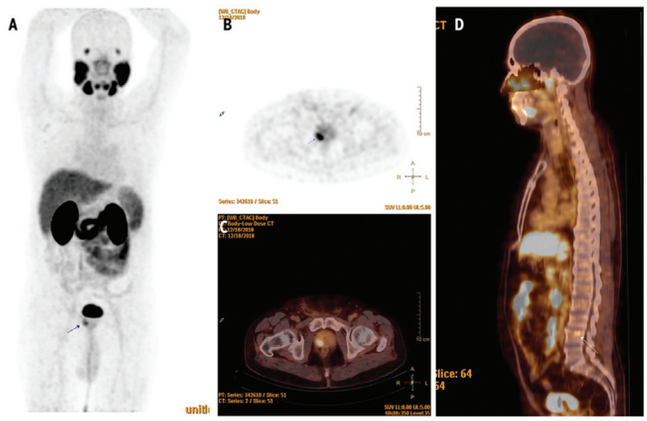

Figure 3. The prostate-specific membrane antigen positron emission (Ga-68 PSMA PET) image of 67 years old prostate carcinoma patient (A), transraxial PET/computed tomography (CT) image of Ga-68 PSMA expressing primary tumor in right lobe apex (B), transraxial PET/CT fusion image (C), sagittal plan PET/CT image of metastatic lesion in the lumbar 4th spine expressing Ga-68 PSMA (D)

PSMA: Prostate-specific membrane antigen, PET: Positron emission tomography, CT: Computed tomography

Currently, D'Amico risk group is still the main clinical feature directing treatment decision. Therefore, some studies investigated the association of SUV_{max} with these risk groups. An example of these studies is published by Uprimny et al. (14). The authors found mean SUV_{max} values in intermediate and high risk groups as 8.25 and 20.5, respectively, in their 82-patient sample, which was statistically significant (p<0.001). In another study by Sachpekidis et al. (15) in 24 patients, SUV_{max} values of low and intermediate risk groups were significantly lower compared with that of high risk group in concordance with our study. Likewise, Demirci et al. (16) also found that high risk group had significantly higher SUV_{max} value (p<0.001).

In our study, median SUV_{max} values of intermediate and high risk groups were 6.91 and 11.44, respectively, which were statistically significant (p=0.014), in accordance with previous reports. Related SUV_{max} cut-off value calculated via ROC analysis was 10.55. The specificity and PPV were 90%, and sensitivity and NPV were both 62.07% for the predicting risk group. Demirci et al. (16) found SUV_{max} cut-off value as 9.1 for high risk group, which is close to ours. The difference between SUV_{max} values of Gleason grade groups 2 and 3 was not statistically significant (medians 7.45 and 6.38, respectively) in the same line with the results of several previous studies (14,15). However, Demirci et al. (16) reported significant difference between SUV_{max} values of grades 2 and 3 subgroups. This discordance may be attributed involvement of post radical prostatectomy specimens rather than biopsy when the contradiction between GS reported with biopsy and prostatectomy is considered (17).

As a secondary aim, SUV_{max} values were investigated according to three PSA subgroups. SUV_{max} values increased with increasing PSA, and the difference was found to be statistically significant (p<0.001). Reports addressing the same issue (14,15) also found that primary tumor SUV_{max} value was significantly higher in patients with PSA ≥10 ng/mL.

Study Limitations

Our study has limitations specific to the retrospective design. Although this study was conducted in a small environment in a restricted time, a small sample size fulfilling the inclusion criteria was enrolled. As a last limitation, the GSs were not verified with radical prostatectomy specimens, although it was not available for all patients.

Conclusion

Eventually, this study is rewardable in particularly two main aspects. First, we have shown that primary tumor SUV_{max} value in initial Ga-68 PSMA PET/CT would predict the D'Amico risk group with high accuracy, which is to date the main directory of treatment algorithm. Second, to our concern, our study is the first to prove the high accuracy of SUV_{max} and determine a cut-off value for predicting oligometastatic and multimetastatic PCa. In the era of radical approaches for oligometastatic disease, this is crucial for individualizing treatment approach. Further studies with large samples addressing the prognostic value of SUV_{max}

on differentiating oligometastatic and multimetastatic PCa, and its prognostic roles are warranted.

Ethics

Ethics Committee Approval: The Scientific Research Ethics Committee of Medical Faculty of the Süleyman Demirel University (desicion no: 177, 21.05.2019) approved the study.

Informed Consent: Informed consent was waived owing to the retrospective nature of the study.

Peer-review: Externally peer-reviewed.

Authorship Contributions

Surgical and Medical Practices: M.E., S.S.Ş., M.Y., Concept: S.A.Ö., Design: E.E.Ö., Data Collection or Processing: M.E., Analysis or Interpretation: S.A.Ö., E.E.Ö., Literature Search: M.E., S.A.Ö., E.E.Ö., Writing: M.E., E.E.Ö.

Conflict of Interest: No conflict of interest was declared by the authors.

Financial Disclosure: The authors declared that this study has received no financial support.

References

1. SEER Cancer Statistics Review (CSR) 1975-2016 Updated April 15, 2019, https://seer.cancer.gov/statfacts/html/corp.html
2. Mottet N, Bellmunt J, Bolla M, Briers E, Cumberbatch MG, de Santis M, Fossati N, Gross T, Ann M Henry AM, Joniau S, Lam TB, Mason MD, Matveev VB, Moldovan PC, van den Bergh RCN, den Broeck TV, van der Poel HG, van der Kwast TH, Rouvière O, Schoots IG, Wiegel T, Cornford P. EAU-ESTRO-SIOG guidelines on prostate cancer. Part1: screening, diagnosis and local treatment with curative intent. Eur Urol 2017;71:618-629.
3. D'Amico AV, Whittington R, Malkowicz SB, Schultz D, Blank K, Broderick GA, Renshaw AA, Kaplan I, Beard CJ, Wein A. Biochemical outcome after radical prostatectomy, external beam radiation therapy, or interstitial radiation therapy for clinically localized prostate cancer. JAMA 1998;280:969-74.
4. Maurer T, Gschwend JE, Rauscher I, Souvatzoglou M, Haller B, Weirich G, Wester H-J, Heck M, Kübler H, Beer AJ, Schwaiger M, Eiber M. Diagnostic efficacy of (68) gallium-PSMA positron emission tomography compared to conventional imaging for lymph node staging of 130 consecutive patients with intermedi- ate to high risk prostate cancer. J Urol 2016;195:1436-1443.
5. Mease RC, Foss CA, Pomper MG. PET imaging in prostate cancer: focus on prostate specific membrane antigen. Current Topics in Medicinal Chemistry 2013;13:951-962.
6. Vargas HA, Grimm J, O FD, Sala E, Hricak H. Molecular imaging of prostate cancer: translating molecular biology approaches into the clinical realm. Eur Radiol 2015;25:1294-1302.
7. Schafer M, Bauder-Wust U, Leotta K, Zoller F, Mier W, Haberkorn U, Eisenhut M, Eder M. A dimerized ureabased inhibitor of the prostate-specific membrane antigen for Ga-68 PET imaging of prostate cancer. EJNMMI Res 2012;2:23.
8. Hellman S, Weichselbaum RR. Oligometastases. J Clin Oncol 1995;13:8-10.
9. Reyes DK, Pienta KJ. The biology and treatment of oligometastatic cancer. Oncotarget 2015;6:8491-8524.
10. Sweeney CJ, Chen YH, Carducci M, Liu G, Jarrard DF, Eisenberger M, Wong Y-N, Hahn N, Kohli M, Cooney MM, Dreicer R, Vogelzang NJ, Picus J, Shevrin D, Hussain M, Garcia JA, DiPaola RS. Chemohormonal Therapy in Metastatic Hormone-Sensitive Prostate Cancer. N Engl J Med 2015;373:737-746.
11. Ost P, Bossi A, Decaestecker K, De Meerleer G, Giannarini G, Karnes RJ, Roach M, Briganti A. Metastasis directed therapy of regional and distant recurrences after curative treatment of prostate cancer: a systematic review of the literature. Eur Urol 2015;67:852-863.
12. Epstein JI, Egevad L, Amin MB, Delahunt B, Srigley JR, Humphrey PA, Committee G. the Grading Committee. The 2014 International Society of Urological Pathology (ISUP) Consensus Conference on Gleason Grading of Prostatic Carcinoma: Definition of Grading Patterns and Proposal for a New Grading System. Am J Surg Pathol 2016;40:244-252.
13. Slaoui A, Albisinni S, Aoun F, Assenmacher G, Al Hajj Obeid W, Diamand R, Regragui S, Touzani A, Bakar A, Mesfioui A, Karmouni T, Ameur A, Elkhader K, Koutani A, Ibnattya A, Roumeguere T, Peltier A. A systematic review of contemporary management of oligometastatic prostate cancer: fighting a challenge or tilting at windmills? World J Urol 2019;37:2343-2353.
14. Uprimny C, Kroiss AS, Decristoforo C, Fritz J, von Guggenberg E, Kendler D, Kendler D, Scarpa L, di Santo G, Roig LG, Maffey-Steffan J, Horninger W, Virgolini IJ. ^{68}Ga-PSMA-11 PET/CT in primary staging of prostate cancer: PSA and Gleason score predict the intensity of tracer accumulation in the primary tumour. Eur J Nucl Med Mol Imaging 2017;44:941-949.
15. Sachpekidis C, Kopka K, Eder M, Hadaschik BA, Freitag MT, Pan L, Haberkorn U, Dimitrakopoulou-Strauss A. ^{68}Ga-PSMA-11 dynamic PET/CT imaging in primary prostate cancer. Clin Nucl Med 2016;41:e473-e479.
16. Demirci E, Kabasakal L, Şahin OE, Akgün E, Gültekin MH, Doğanca T, Tuna MB, Öbek C, Kiliç MK, Esen T, Kural AR. Can SUVmax values of Ga-68-PSMA PET/CT scan predict the clinically significant prostate cancer? Nucl Med Commun 2019;40:86-91.
17. Barzell WE, Melamed MR, Cathcart P, Moore CM, Ahmed HU, Emberton M. Identifying candidates for active surveillance: an evaluation of the repeat biopsy strategy for men with favorable risk prostate cancer. J Urol 2012;188:762-767.

Original Article
Mol Imaging Radionucl Ther 2020;29:105-111 DOI:10.4274/mirt.galenos.2020.05657

Metabolic Characterization of Anterior Mediastinal Masses by ^{18}F-FDG PET/CT

^{18}F-FDG PET/BT ile Anterior Mediastinal Kitlelerin Metabolik Karakterizasyonu

Zehra Pınar Koç[1], Pınar Pelin Özcan[1], Erhan Ayan[2], Rabia Bozdoğan Arpacı[3]
[1]*Mersin University Faculty of Medicine, Department of Nuclear Medicine, Mersin, Turkey*
[2]*Mersin University Faculty of Medicine, Department of Thoracic Surgery, Mersin, Turkey*
[3]*Mersin University Faculty of Medicine, Department of Pathology, Mersin, Turkey*

Abstract

Objectives: To evaluate the role of ^{18}F-fluorodeoxyglucose (FDG) positron emission tomography/computed tomography (PET/CT) for the diagnosis of anterior mediastinal masses.

Methods: The oncological ^{18}F-FDG PET/CT images of 41 patients (17 women, 24 men; age: 16-83 years, mean age: 50.5±19.5 years) who attended the nuclear medicine department between November 2016 and September 2017 were retrospectively evaluated for the metabolic characterization of their anterior mediastinal masses.

Results: Based on our results, the lesions of 4 patients were benign [maximum standard uptake value (SUV_{max}) <3] and that of 2 patients were non-tumoral (i.e., tuberculosis and sarcoidosis). The mean dimensions and the SUV_{max} levels of the malignant lesions were 6.4±3.7 cm and 11.9±9.6, respectively. The pathological results for the malign tumors were thymus tumors (n=8), lymphoma (n=8), lung cancer (n=11), carcinoid metastasis (n=2), thyroid carcinoma (n=2), germ cell carcinoma (n=1), schwannoma (n=1), and sarcoma (n=1). The degree of ^{18}F-FDG accumulation could precisely identify the malign and benign tumors.

Conclusion: Thus, contrary to the known causes, it is possible that anterior mediastinal masses originate from structures other than the anterior mediastinal structures. In this study, the lymphoma and lung carcinoma pathology were more frequent than thymic lesions.

Keywords: Anterior mediastinum, mass, ^{18}F-FDG, PET/CT

Öz

Amaç: Bu çalışmada anterior mediastinal kitlelerin karakterizasyonunda ^{18}F-florodeoksiglukoz (FDG) pozitron emisyon tomografi/bilgisayarlı tomografinin (PET/BT) rolü değerlendirilecektir.

Yöntem: Anterior mediastinal kitle tanısıyla nükleer tıp bölümüne Kasım 2016-Eylül 2017 tarihleri arasında metabolik karakterizasyon amacıyla başvuran hastaların onkolojik ^{18}F-FDG PET/BT görüntüleri geriye dönük olarak değerlendirildi. Kırk bir hasta (17 kadın, 24 erkek; 16-83, ortalama yaş: 50,5±19,5) çalışmaya dahil edildi.

Bulgular: Çalışmaya dahil edilen hastalardan iki hastanın lezyonu benign olarak tanımlandı [maksimum standart alım değeri (SUV_{maks}) <3] ve ikisinin patolojisi tümör dışı lezyonlardı (tüberküloz ve sarkoidoz). Malignite tanısı konulan hastaların kitlelerinin ortalama boyutu ve SUV_{maks} değerleri sırasıyla; 6,4±3,7 cm ve 11,9±9,6 idi. Malign tümörlerin patolojik tanıları; timik tumörler (n=8), lenfoma (n=8), akciğer kanseri (n=11), karsinoid metastazı (n=2), tiroid karsinomu (n=2), germ hücreli tümör (n=1), schwannoma (n=1) ve sarkom (n=1) idi.

Sonuç: Bilinen nedenlerin aksine anterior mediastinal kitlelerin patoloji sonuçları anterior mediastinal yapıların tümörlerinin veya karsinomlarının dışındaki patolojilerden kaynaklanabilir. Bu seride timik tümörlere göre lenfoma ve akciğer karsinomu daha sık rastlanan patolojilerdi.

Anahtar kelimeler: Anterior mediasten, kitle, ^{18}F-FDG, PET/BT

Address for Correspondence: Zehra Pınar Koç MD, Mersin University Faculty of Medicine, Department of Nuclear Medicine, Mersin, Turkey
Phone: +90 324 241 00 00 **E-mail:** zehrapinarkoc@gmail.com ORCID ID: orcid.org/0000-0002-3274-5790
Received: 03.01.2020 **Accepted:** 19.07.2020

Introduction

Several causes of anterior mediastinal masses, either benign or malignant, have been reported. In fact, it has been reported that anatomic structures in the anterior mediastinum either enlarge or become malignant or metastasize from another tumor. Several studies have also evaluated thymus enlargement as a differential diagnosis of anterior mediastinal masses (1). In addition, numerous cases have been reported related to the origin of anterior mediastinal masses in the literature (1). The other reasons of development of anterior mediastinal mass are benign enlargement of anatomic structures involving or invading the mediastinum (2,3).

It has been previously documented that the ^{18}F-fluorodeoxyglucose (FDG) positron emission tomography/computed tomography (PET/CT) is an accurate modality in the staging and restaging of anterior mediastinal tumors. In fact, a recent study suggested that the diagnostic power of ^{18}F-FDG PET/CT for anterior mediastinal mass is high, but its negative predictive value is higher (4). Another small series of study determined the cut-off level for the determination of malignancy in anterior mediastinal mass (5). The present study aimed to evaluate the pathological outcomes of adult patients presenting with anterior mediastinal mass in conjunction with the ^{18}F-FDG PET/CT findings.

Materials and Methods

Patients

The following were the patient inclusion criteria: age of 16-85 years and presenting with anterior mediastinal mass without histopathological diagnosis.

Informed consents were obtained from the patients for conducting PET/CT examinations.

The following were the patient exclusion criteria: pregnancy and lactation, age <16 or >85 years, presenting with another malign tumor elsewhere, and those with contraindication for PET/CT examinations.

The study was approved by the Local Ethics Committee and conducted according to the revised Helsinki Declaration, 2010. Mersin University Rectorate Clinical Research Ethics Committee (date: 05/10/2017, no: 2017/285).

The PET/CT images of 41 patients (17 women, 24 men, age: 16-83 years, mean age: 50.5±19.5 years) who were referred to the nuclear medicine department with the diagnosis of anterior mediastinal mass by a previous CT examination conducted between November 2016 and September 2017 were obtained. The data were retrospectively evaluated by 2 experienced nuclear medicine physicians without any knowledge of the final diagnosis of the patients. The PET/CT study was not performed for patients with anamnesis of pregnancy and lactation and for those with contraindication for the examination. In addition, we did not prefer pediatric patients with interfering problems that involved the anterior mediastinum frequently (such as physiological thymus activity) and elder patients (age: >85 years) because they probably could not be operated.

PET/CT Examinations

The patients were prepared for the examination by ensuring at least 6 h of fasting and decreased physical activities since at least 24 h prior to the examination. The patients were first injected with the radiopharmaceutical agent [mean 370 MBq (10 mCi), according to the body weight] via the venous line 60 min before the imaging. Imaging was performed by using a PET/CT scanner (discovery PET/CT 610; GE, US) with a low-dose CT scan (130 kV, 50 mAs, 1.5 pitch, 5-mm thickness, 70-cm field of view) for attenuation correction without intravenous contrast administration via oral contrast administration from the skull base to the upper thigh region with the acquisition time of 3 min/bed position and the matrix size of 256x256. Attenuation-corrected PET images were then reconstructed by using an iterative reconstruction algorithm, VUE point HD with 3 iterations and 32 subsets.

Diagnostic Criteria

The images were evaluated with respect to the metabolic characteristics of the anterior mediastinal lesions [maximum standard uptake value (SUV_{max})] levels obtained from the workstation (Mac iOs, Osirix MD programme). The SUV_{max} levels were retrieved by the circular region of interest covering the most active portions of the lesions in addition to the CT characteristics of the lesions and the dissemination to other structures (metastatic dissemination, lymphadenopathies elsewhere in the body, and other possible malignant primary sites). The anterior mediastinal mass lesions were determined to be benign in case of a single site with low uptake of ^{18}F-FDG (SUV_{max} <3).

Interventions and Histopathological Analysis

Surgical procedures were decided with reference to the PET/CT imaging and suspected malignancy. The types of surgical procedures conducted (such as thoracotomy, minithoracotomy sternotomy procedures, or biopsy) for each patient are summarized in Table 1. The final pathological outcomes obtained from the specimens of surgery including hematoxylene and eosine or immunohistochemistry (in case it was necessary) staining procedures were analyzed by an experienced pathology

physician, and the results of the PET/CT and pathology were compared.

Statistical Analysis

The statistical analysis was performed by using a package program (MedCalc®v10.3.0). The receiver operating curve (ROC) analysis was performed in order to determine the power of the SUV_{max} parameter to differentiate between the benign and malignant lesions.

Results

Of the 41 study participants, 37 underwent different surgeries based on their imaging findings (Table 1). The pathological results including those of 2 patients with the diagnosis of granulomatous diseases (Figure 1) are listed in Table 1. A total of 4 patients were considered to be benign based on their PET/CT imaging, these patients did not undergo any surgical procedure and were also out of the follow-up program (Figure 2). In this series, 10 patients were diagnosed with lymphoma, while 2 were diagnosed with neuroendocrine tumor metastases with a relatively low ^{18}F-FDG uptake. One of the patients had immature teratoma with a significantly high metabolic activity (Figure 3). The patient diagnosed with differentiated thyroid carcinoma also showed high ^{18}F-FDG affinity; however, those with medullary thyroid carcinoma showed a relatively low uptake. Unexpected results, such as lung carcinoma, were recorded in the study group as well (Figure 4).

The distribution of the pathological results and the SUV_{max} levels of the lesions are summarized in Table 1. The ^{18}F-FDG avid lesions outside of the anterior mediastinum of the patients are listed under Table 1. Thirteen patients underwent follow-up ^{18}F-FDG PET/CT imaging (mean 7.4±5.2 month), while 3 patients died within 1 month of PET/CT examination during the disease course. The progression of the disease was noted in 4 patients, with partial response in 2 and complete metabolic response in 5. One patient was diagnosed with interfering infection and 2 with recurrent mediastinal lesion.

The cut-off SUV_{max} level during the determination of malignant and benign tumors was 6.04 as per the ROC curves, and, with this cut-off value, the sensitivity and specificity of the diagnostic modality was 74% and 80%, respectively (Figure 5). The SUV_{max} level was found to be significantly (p=0.05) successful in the determination of malignant lesions, while this level in patients with thymoma was 3-5.95. The SUV_{max} levels of thymic carcinoma was significantly higher than those of thymoma lesions (3-19,39).

Discussion

The benign anterior mediastinal masses may be benign metastasizing leiomyoma, inflammatory endobronchial pseudotumor, physiological thymus activity, or rebound thymus activity (1). The benign metastasizing leiomyoma is a rare tumor of the middle-age women occurring years after hysterectomy (6). Inflammatory pseudotumor is a benign lesion of children or young adults that may be associated with trauma, paraneoplastic syndrome, or inflammatory reactions (7). It is therefore important to discriminate the thymus uptake or thymic rebound from the pathological uptake in PET/CT among young people and children (1). Unfortunately, patients with benign lesions in this case series were also out of the follow-up and did not want to undergo an operation.

Although some pitfalls and false-positive results are associated with the ^{18}F-FDG uptake of the surrounding tissues (8), the ^{18}F-FDG PET/CT remains the most important modality in the preoperative evaluation of anterior mediastinal lesions. In this case series, only a limited number of patients showed false-positive results, including sarcoidosis (Figure 1) and tuberculosis. Granulomatous infections frequently interfere with malignant tumor metastasis or primary tumors, especially for PET/CT examinations in endemic countries and provides false-positive results. However, the ratio of false-positive results of patients with granulomatous diseases was found to be in an acceptable range in this study.

The most common tumors of the anterior mediastinum are thymic tumors "thymoma" in adults, and previous studies have demonstrated a close correlation between the World Health Organization and Mosaka stage of the thymic tumors and SUV_{max} levels (9). This study group included only 3 patients with thymoma, which is rarer than expected, while the SUV_{max} levels of these patients were in an acceptable range. The thymic carcinoma group showed higher SUV_{max} levels, as expected, than the thymoma group. CT or magnetic resonance showed extension and invasion into the adjacent mediastinal structures of the thymic tumors (9). The ^{18}F-FDG PET/CT may differentiate the subgroup of thymic epithelial tumors such as thymoma, thymic carcinoma, and carcinoid tumors and accurately stage these tumors (10). Complete surgical removal of the thymic tumors with the involved adjacent structures is hence the popular treatment modality (11). A special subgroup of thymic tumors is the cystic thymus tumor that is characterized by multiple cysts (12). The ^{18}F-FDG PET/CT imaging may demonstrate an increased uptake in the cystic thymomas related to the septum or margins of the tumor (12). The SUV_{max} cut-off level for malignant and

Table 1. The ^{18}F-FDG PET/CT imaging, pathology results, and biopsy/surgery sites of the patients

No	SUV	Other hypermetabolic lesions in PET/CT	Surgery	Pathology	Follow-up
1	5.73	Pleura	Biopsy mediastinum	Metastasis of thymic carcinoma	Progression in 1 year
2	7.56	Disseminated lymphadenopathy	Biopsy nasopharynx	Hodgkin lymphoma	
3	4.42	-	Excision of mass	Schwannoma	
4	4.6	Lung tumor, pleura, lymph nodes	Broncoscopic biopsy	NSCLC	
5	10.35	Cervical lymph nodes	Cervical node biopsy	Hodgkin lymphoma	Partial response in 4 months
6	17.19	Disseminated lymph nodes	Inguinal node biopsy	Nonhodgkin lymphoma	
7	3.17	Lung	Lung wedge	Neuroendocrine tumor met	
8	5.52	Mediastinal, axillary, cervical nodes	Axillary node biopsy	Neuroendocrine tumor met	Thymic rebound in 10 months
9	21.69	Liver, femur met	FNAB of liver	Lung adenocancer met	
10	19.89	Cervical lymph nodes	Cervical node biopsy	Thymus carcinoma met	Residual thymus
11	14.15	Lung, spleen uptake, cervical	Cervical node biopsy	NSCLC	Died in 10 days
12	12.68	Lung, bone, liver met	FNAB of liver	Lung adenocarcinoma met	Died in 1 month
13	8.18	Cervical lymph nodes	Cervical node biopsy	Thymus carcinoma met	
14****	12.29	Lung, liver, bone met	Cervical node biopsy	Small cell lung cancer met	
15	10.24	Mediastinal cervical lymph nodes	Cervical node biopsy	Hodgkin lymphoma	
16	10.64	-	Bone marrow biopsy	Hodgkin lymphoma	Complete response in 1 year
17***	13.68	-	Thymus biopsy	Immature teratoma	Abdominal progress in 7 months
18	13.8	-	Mediastinal tru-cut biopsy	Nonhodgkin lymphoma	
19*	15.6	Cervical lymph nodes	Cervical node biopsy	Sarcoidosis	
20	3.69	Lung	Lung wedge	Medullary thyroid carcinoma	Metabolic and Ga-68 progression
21	17.2	Cervical, axillary, liver, bone	Axillary biopsy	Burkitt lymphoma	
22	12.5	Cervical, spleen, bone marrow, bone	Cervical node biopsy	Hodgkin lymphoma	
23	6.04	Abdominal, mesentary, colon	Mediastinal biopsy	Tuberculosis	
24	11.8	Bone	Mediastinal biopsy	Neuroendocrine carcinoma met	Partial response in 3 months
25	3.3	Cervical lymph node	Mediastinal tumor excision	Thymoma type AB	
26	11.16	Cervical lymph node	Mediastinal biopsy	Hodgkin lymphoma	Nearly complete response in 3 months
27	27.43	Lung, surrenal	Mediastinal biopsy	Lung adenocarcinoma met	Nearly complete response in 3 months
28	4.5	-	Mediastinal tumor excision	Thymoma type AB	Suspicious anterior mediastinal lesion in 5 months
29	56.5	-	Thyroidectomy	Folliculary, Papillary carcinoma	
30	3	-	Mediastinal biopsy	Thymic carcinoma	Died in 10 days
31	10.9	Lung, bone	Broncoscopic biopsy	NSCLC	

32	3.3	Cervical, abdominal lymph nodes, lung	Cervical lymph node	Lung adenocarcinoma met.	
33	11.72	Cervical lymph node	Cervical node biopsy	Small cell lung cancer	Progression in 2 months
34	14.3	-	Pericardial biopsy	Undifferentiated carcinoma	Complete remission in 20 months
35	5.95	-	Mediastinal tumor excision	Thymoma type B1	
36	10.94	-	Mediastinal tumor excision	Undifferentiated carcinoma	
37	12.93	-	Paraphayngeal biopsy	Squamous cell carcinoma met	

*Patient indicated in Figure 1, ***Figure 3, ****Figure 4, ^{18}F-FDG: ^{18}F-fluorodeoxyglucose, PET/CT: Positron emission tomography/computed tomography, NSCLC: Non-small cell lung cancer, FNAB: Fine needle aspiration biopsy, met: Metastasis, SUV: Standardized uptake value

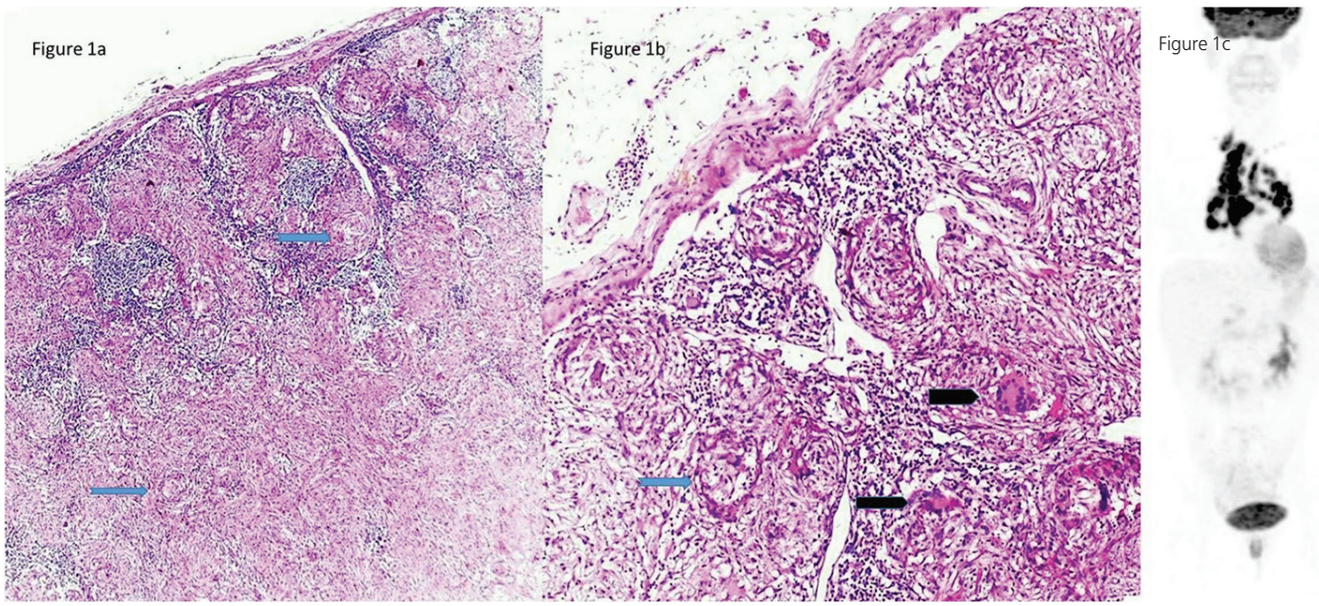

Figure 1. A 39-year-old woman with pathological diagnosis of sarcoidosis was evaluated. Her histological sections revealed well-defined, small, non-necrotizing granulomas composed of epithelioid cells with scattered (a) Langhans giant cells in the lymph node. Necrosis was absent. Granuloma was noted at higher power. Non-necrotizing granulomas composed of epithelioid cells with scattered Langhans giant cells (H&E, x40). (b) Langhans giant cells can be observed in the middle area. These cells are presenting with mediastinal multiple lymph nodes with significantly increased ^{18}F-FDG affinity (H&E, x200), as demonstrated by the (c) multiple intensity projection image of ^{18}F-FDG PET/CT
H&E: Haemotoxylin and eosin, ^{18}F-FDG: ^{18}F-fluorodeoxyglucose

benign thymomas have not been determined, although the previous reports accepted the 4.5-6.3 levels (13). The SUV_{max} cut-off value for the determination of the benign and malignant lesions by ^{18}F-FDG PET/CT was 6.04 in this study by the ROC analysis. We noted that the diagnostic sensitivity and specificity of the test was acceptably high with this determined cut-off level.

Another problem with the anterior mediastinum is the physiological uptake related to thymus and a phenomenon called the "thymic rebound" that occurs especially in the pediatric age. Thymic rebound refers to the thymus regression during and enlargement after the completion of chemotherapy (1). A previous related study concluded that the SUV_{max} cut-off level of 3.1 may accurately differentiate thymic rebound from lymphoma recurrence (1). Another study about benign and malignant anterior mediastinal mass indicated the cut-off level of 3 (5). Other malignant tumors of anterior mediastinum include lymphoproliferative diseases such as lymphoma, neuroendocrine tumors, and mesenchymal tumors. The most important change in the patients' management was observed in the lymphoma group since the biopsy sites were altered due to the PET results. In a case series on patients with lymphoma, it was suggested that mild ^{18}F-FDG accumulating lesions in the

Figure 2. The ^{18}F-FDG PET/CT images of a 56-year-old man with anterior mediastinal mass in the transaxial projection of fusion, PET, and CT with low ^{18}F-FDG uptake who was out of the follow-up program without any pathological outcome
^{18}F-FDG: ^{18}F-fluorodeoxyglucose, PET/CT: Positron emission tomography/computed tomography

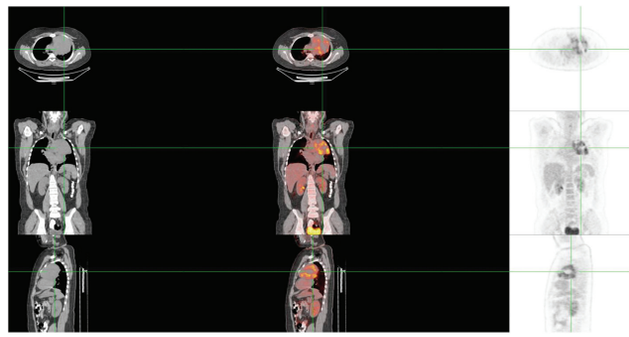

Figure 3. Heterogeneous uptake with increased ^{18}F-FDG accumulation in large anterior mediastinal mass, which was immature teratoma, as shown by the transaxial, coronal, and sagittal plane CT, fusion, and PET images
^{18}F-FDG: ^{18}F-fluorodeoxyglucose, PET: Positron emission tomography, CT: Computed tomography

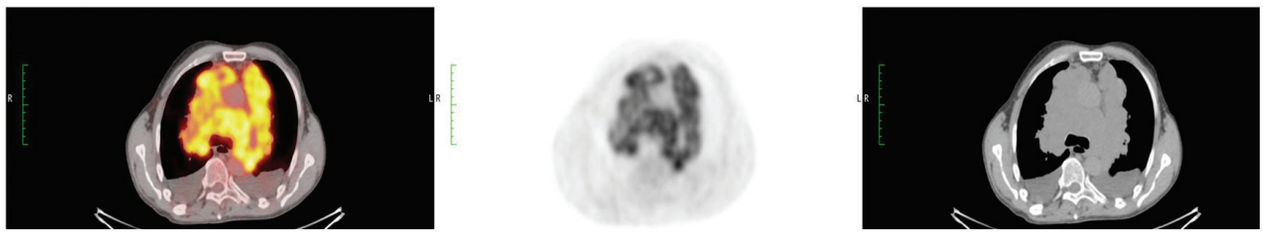

Figure 4. Transaxial fusion, PET, and CT images of anterior mediastinal conglomerated hypermetabolic mass lesion diagnosed as small cell lung carcinoma
PET: Positron emission tomography, CT: Computed tomography

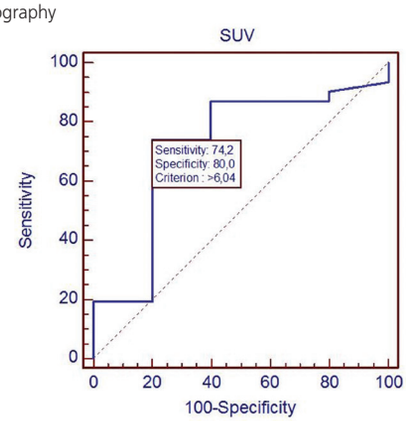

Figure 5. ROC analysis of sensitivity and specificity of the ^{18}F-FDG PET/CT according to the SUV_{max} cut-off value (6.04). Graphical demonstration of ROC curves
ROC: Receiver operating curve, ^{18}F-FDG: ^{18}F-fluorodeoxyglucose, PET/CT: Positron emission tomography/computed tomography, SUV_{max}: Maximum standard uptake value

anterior mediastinal region may indicate benign lesions like thymic hyperplasia even in lymphoma patients (14). However, in the case of the presence of diagnostic criteria indicating malignancy in lymphoma patients, secondary malignant tumors of the anterior mediastinum have been indicated in previous case reports (15).

Study Limitations

The study limitations include the retrospective design that limits the patient selection. In addition, relatively small number of patients could be included since the main subject of the study considered specific patient population.

Conclusion

This study thus demonstrated that adult patients, especially, may have several unexpected other primary malignancies, especially lung cancer (30%). No study has so far reported the pathological outcomes of anterior mediastinal mass in comparison with the ^{18}F-FDG PET/CT imaging results. We demonstrated that ^{18}F-FDG PET/CT is an essential imaging modality for the characterization of anterior mediastinal mass. This modality may change the patients' management by determines other possible biopsy sites.

Acknowledgment

We want to thank Associate Professor Dr. Gülhan Örekici from the Biostatistics Department of Mersin University Faculty of Medicine for performing the statistical analysis of this study.

Ethics

Ethics Committee Approval: The study was approved by the Local Ethics Committee and conducted according to the revised Helsinki Declaration, 2010. Mersin University Rectorate Clinical Research Ethics Committee (date: 05/10/2017, no: 2017/285).

Informed Consent: Informed consents were obtained from the patients for conducting PET/CT examinations.

Peer-review: Externally and internally peer-reviewed.

Authorship Contributions

Surgical and Medical Practices: Z.P.K., P.P.Ö., E.A., R.B.A., Concept: Z.P.K., P.P.Ö., Design: Z.P.K., P.P.Ö., Data Collection or Processing: Z.P.K., P.P.Ö., E.A., R.B.A., Analysis or Interpretation: Z.P.K., P.P.Ö., E.A., R.B.A., Literature Search: Z.P.K., P.P.Ö., Writing: Z.P.K., P.P.Ö.

Conflict of Interest: No conflict of interest was declared by the authors.

Financial Disclosure: The authors declared that this study has received no financial support.

References

1. Gawande, RS, Khurana A, Messing, S, Zhang D, Castañeda RT, Goldsby RE, Hawkins RA Daldrup-Link HE. Differentiation of normal thymus from anterior mediastinal lymphoma and lymphoma recurrence at pediatric PET/CT. Radiology 2012;262:613-622.
2. Dua, SG, Purandare, NC, Shah S, Maitra R, Rangarajan V. Cervical extension of the thymus mimicking metastatic recurrence of Ewing sarcoma on PET/CT. Indian J Nucl Med 2010;25:176-177.
3. Sulu E, Damadoğlu E, Takır HB, Okur HK, Köroğlu E, Yılmaz A. A case of endobronchial inflammatory pseudotumor invading the mediastinum. Tuberk Toraks 2011;59:77-80.
4. Proli C, De Sousa P, Jordan S, Anikin V, Devaraj A, Love SM, Shackcloth M, Kostoulas N, Papagiannopoulos K, Haqzad Y, Loubani M, Sellitri F, Granato F, Bush A, Marchbank A, Iyer S, Scarci M, Lim E, UK Thoracic Surgery Research Collaborative. A diagnostic cohort study on the accuracy of 18-fluorodeoxyglucose ((18)FDG) positron emission tomography (PET)-CT for evaluation of malignancy in anterior mediastinal lesions: the DECiMaL study. BMJ Open 2018;6;8:e019471.
5. Kumar A, Regmi SK, Dutta R, Kumar R, Gupta SD, Das P, Halanaik D, Jindal T. Characterization of thymic masses using (18)F-FDG PET-CT. Ann Nucl Med 2009;23:569-577.
6. Ogawa, M, Hara, M, Ozawa, Y, Moriyama S, Yano M, Shimizu S, Shibamoto Y. Benign metastasizing leiomyoma of the lung with malignant transformation mimicking mediastinal tumor. Clin Imaging 2011;35:401-404.
7. Melloni, G, Carretta, A, Ciriaco, P, Arrigoni G, Fieschi S, Rizzo N, Bonacina E, Augello G, Belloni PA, Zannini P. Inflammatory pseudotumor of the lung in adults. Ann Thorac Surg 2005;79:426-432.
8. Wang, Y, Kalra M, Scott, J. Compensatory asymmetric hemidiaphragmatic uptake secondary to contralateral hemidiaphragmatic paresis. Clin Nucl Med 2013;38:53-55.
9. Srirajaskanthan R, Toubanakis, C, Dusmet M, Caplin ME. A review of thymic tumours. Lung Cancer 2008;60:4-13.
10. Sung YM, Lee KS, Kim BT, Choi JY, Shim YM, Yi CA. 18F-FDG PET/CT of thymic epithelial tumors: usefulness for distinguishing and staging tumor subgroups. J Nucl Med 2006;47:1628-1634.
11. De Palma, A, Pagliarulo, V, Lorusso, M, Verardo L, Gennaro FD, Genualdo M, Quercia R, Montrone T, Gentile A, Loizzi M. A rare case of necrotic thymoma. G Chir 2014;35:43-46.
12. Romeo V, Esposito A, Maurea S, Camera L, Mainenti PP, Palmieri G, Buonerba C, Salvatore M. Correlative Imaging in a Patient with Cystic Thymoma: CT, MR and PET/CT Comparison. Pol J Radiol 2015;80:22-26.
13. Kaira K, Sunaga N, Ishizuka T, Shimizu K, Nobuyuki Yamamotoa N. The role of [^{18}F]fluorodeoxyglucose positron emission tomography in thymic epithelial tumors. Cancer Imaging 2011;11:195-201.
14. Ustaalioglu BB, Seker M, Bilici A, Canpolat N, Yıldirim E, Kefeli U, Ustaalioglu R, Yilmaz BE, Salepci T, Ozdemir N, Gumus M. The role of PET-CT in the differential diagnosis of thymic mass after treatment of patients with lymphoma. Med Oncol 2011;28:258-264.
15. Yi WL, Chen TP, Chiu NT, Liu CS, Lin YH. Parapharyngeal Ganglioneuroma Detected by 18F-FDG PET/CT in a Patient With Hodgkin Lymphoma. Clin Nucl Med 2019;44:240-243.

Original Article
Mol Imaging Radionucl Ther 2020;29:112-117 DOI:10.4274/mirt.galenos.2020.88261

Value of C-reactive Protein/Albumin Ratio for Predicting Ischemia in Myocardial Perfusion Scintigraphy

C-reaktif Protein/Albümin Oranının Miyokardiyal Perfüzyon Sintigrafisinde İskemi Öngörmedeki Rolü

Süleyman Çağan Efe[1], Özlem Özdemir Candan[2], Cihan Gündoğan[3] , Ahmet Öz[4], Yasin Yüksel[4], Burak Ayca[4], Tevfik Fikret Çermik[3],

[1]*Kartal Koşuyolu Cardiovascular Diseases Training and Research Hospital, Clinic of Cardiology, İstanbul, Turkey*
[2]*İstanbul Training and Research Hospital, Clinic of Internal Medicine, İstanbul, Turkey*
[3]*İstanbul Training and Research Hospital, Clinic of Nuclear Medicine, İstanbul, Turkey*
[4]*İstanbul Training and Research Hospital, Clinic of Cardiology, İstanbul, Turkey*

Abstract

Objectives: Several studies demonstrate the relationship between coronary artery disease and inflammatory parameters. Nevertheless, there is paucity of data regarding the role of high sensitivity (hs)-C-reactive protein (CRP) to albumin ratio (CAR) in patients with ischemia on gated single photon emission tomography (SPECT) myocardial perfusion imaging (MPI). This study was aimed at demonstrating the relationship between CAR and the occurrence of ischemia on gated SPECT MPI.

Methods: We retrospectively evaluated 2.048 referred patients for gated SPECT MPI from a cardiology outpatient clinic between October 2017 and June 2019. After applying exclusion criteria and measuring serum CRP and albumin levels, we included 126 patients in the study. We then classified subjects into different groups according to the absence or presence of ischemia on gated SPECT MPI.

Results: According to laboratory findings, hs-CRP and CAR were significantly higher in the ischemia group, while the serum albumin was significantly lower in ischemia group ($p<0.05$ for each). The independent predictors of presence of ischemia in multivariate analysis were hypertension and CAR (CAR; odds ratio: 5.720, 95% confidence interval: 2.697-12.133, $p<0.001$). The optimal value of CAR for presence of ischemia was 0.96 with 76% sensitivity and 71% specificity.

Conclusion: We found CAR values as a predictor for ischemia before MPI.

Keywords: Myocardial perfusion scintigraphy, stable coronary artery disease, C-reactive protein/albumin ratio

Öz

Amaç: Birçok çalışmada, koroner arter hastalığı ile enflamatuvar parametreler arasında ilişki bulunduğu gösterilmiştir. Bununla birlikte, tek foton emisyon tomografisi (SPECT) miyokard perfüzyon görüntülemesinde (MPI) iskemi bulunan hastalardaki C-reaktif proteinin (CRP)/albümin oranının (CAR) rolü ile ilgili yeterli veri bulunmamaktadır. Bu çalışmada, SPECT MPI'da CAR ve iskemi varlığı arasındaki ilişkiyi araştırmayı amaçladık.

Yöntem: Ekim 2017 ve Haziran 2019 tarihleri arasında kardiyoloji polikliniğinden yönlendirilerek SPECT MPI yapılan 2,048 hasta retrospektif olarak değerlendirildi. Tarama popülasyonu değerlendirildiğinde serum CRP ve albümin düzeyleri ölçülen ve dışlama ölçütlerini karşılamayan 126 hasta çalışma grubunu oluşturdu. SPECT MPI'da iskemi varlığı ve yokluğuna göre hastalar iki gruba ayrılarak veriler değerlendirildi.

Bulgular: Laboratuvar bulguları açısından değerlendirildiğinde iskemi bulunan grupta CRP ve CAR anlamlı olarak daha yüksek iken, bu grupta serum albümini anlamlı olarak daha düşük bulundu (her biri için $p<0,05$). Çok değişkenli analizde, iskemi varlığının bağımsız prediktörleri hipertansiyon ve CAR idi (CAR; göreceli olasılıklar oranı: 5,720,%95 CI: 2,697-12,133, $p<0,001$). İskemi varlığı için en uygun CAR değeri %76 hassasiyet ve %71 özgüllük ile 0,96 olarak bulunmuştur.

Address for Correspondence: Süleyman Çağan Efe MD, Kartal Koşuyolu Cardiovascular Diseases Training and Research Hospital, Clinic of Cardiology, İstanbul, Turkey
Phone: +90 535 695 24 88 **E-mail:** scaganefe@gmail.com ORCID ID: orcid.org/0000-0002-6067-6841
Received: 14.05.2020 **Accepted:** 12.08.2020

Sonuç: Çalışmamız miyokard iskemisi ve CAR değerleri arasındaki ilişkiyi araştıran ilk çalışma olarak değerlidir. Miyokard perfüzyon sintigrafisi öncesi bakılan CAR değerleri iskemi için prediktör olarak bulundu.

Anahtar kelimeler: Miyokard perfüzyon sintigrafisi, kararlı koroner arter hastalığı, C-reaktif protein/albümin oranı

Introduction

In daily practice, many patients with chest pain and similar cardiac complaints are evaluated in outpatient clinics. Appropriate patients are oriented to perform stress electrocardiography, stress echocardiography, or gated single photon emission computed tomography (SPECT) myocardial perfusion imaging (MPI) to investigate myocardial ischemia. In addition, MPI is known to evaluate the prevalence and severity of myocardial ischemia (1,2).

Inflammatory process has an important role in atherosclerosis, plaque development, and plaque progression. High-sensitivity C-reactive protein (hs-CRP), neutrophile count, lymphocyte count, monocyte count, and albumin are the most studied and clinically evaluated inflammatory markers (3,4). Inflammatory markers can be used to determine patients' risk and improving their clinical outcomes. Published studies on the prevention of cardiovascular diseases (CVD) highlight the availability of hs-CRP levels for determining risk stratification in selected patients (5). Adverse cardiovascular outcomes and prevalence of atherosclerosis have a significant association with elevated CRP levels (6). There is also an association with coronary artery disease (CAD) and other acute phase reactants like albumin. The fact that CRP and albumin are easily accessible markers in daily practice increases the frequency of using these markers. The CRP to albumin ratio (CAR) is a new marker, which is calculated by the ratio of these acute phase reactants. CAR is thought to be better at predicting inflammatory events (7,8,9). This study was aimed to investigate the predictability of ischemia from inflammatory markers, before performing MPI in stable CAD patients.

Materials and Methods

We retrospectively evaluated 2048 patients referred for gated SPECT MPI from a cardiology outpatient clinic between October 2017 and June 2019. Out of these, we enrolled patients with serum CRP and albumin levels measured one day before MPI. After applying exclusion criteria, we included 146 patients in the study. We contacted patients through telephone to obtain cardiovascular risk factors and diseases that might affect acute phase reactants. We further excluded participants having a history of CAD (with revascularization), chronic kidney disease (estimated glomerular filtration rate <60 mL/dk), hepatic disease (aspartate aminotransferase, alanine aminotransferase two-fold above normal limits), history of cancer or systemic inflammatory disease, patients taking statins, anti-inflammatory drugs, or antibiotic medications within one week from the study. Finally, we had 126 eligible patients for the analysis (Figure 1). The nuclear medicine department and myocardial perfusion studies (MPS) reports confirmed that all patients had taken dipyridamole or adenosine as a pharmacological stressor. We obtained a written patient informed consent. The Local Ethics Committee approval from İstanbul Training and Research Hospital with decision number 1.935 was taken for the present study.

Myocardial Perfusion Imaging

We performed a two-day stress/rest imaging protocol using Technetium 99-m methoxy-isobutylisonitrile (Tc-99m MIBI) in order to evaluate myocardial perfusion. During peak exercise, we injected radiopharmaceutical agents on modified Bruce protocol or at peak hyperemia. For stress imaging, we used dipyridamole (0.142 mg/kg/min) or adenosine (0.28 mg/min) infusion as a radiopharmaceutical agent. Imaging began 30-45 min after injecting 15-20 mCi Tc-99m MIBI. We injected a similar dose for rest imaging if there was any suspected perfusion defect on stress images.

SPECT Imaging Protocol

We obtained all images over a 180° angle orbit from right anterior oblique, 45° angle to left posterior oblique, 45° angle using a dual-head γ-camera (General Electric Optima NM/CT 640, GE Healthcare, Wauwatosa, WI, USA) equipped with ultra-high resolution collimator, 64x64 matrix, an elliptic orbit with step and shoot acquisition at 3° intervals over 180° angle, 60 projections and 9-13 s per projection using a 20% energy window centered on the 140 keV photopeak of Tc-99m. The patients lay in supine position on the surface with their arms raised straight above the head. Image sets obtained by SPECT analysis were reconstructed on a dedicated workstation (Xeleris, GE Healthcare, Haifa, Israel) using WBR and Evolution for Cardiac recommended manufacturer relative risk and noise reduction parameters, with and without CT based AC (12 iterations and 10 subsets). At the end of each acquisition, a single low-dose CT scan (100 keV; 1.0 mA; 0.2-0.3 mS) of the chest was performed to obtain attenuation maps

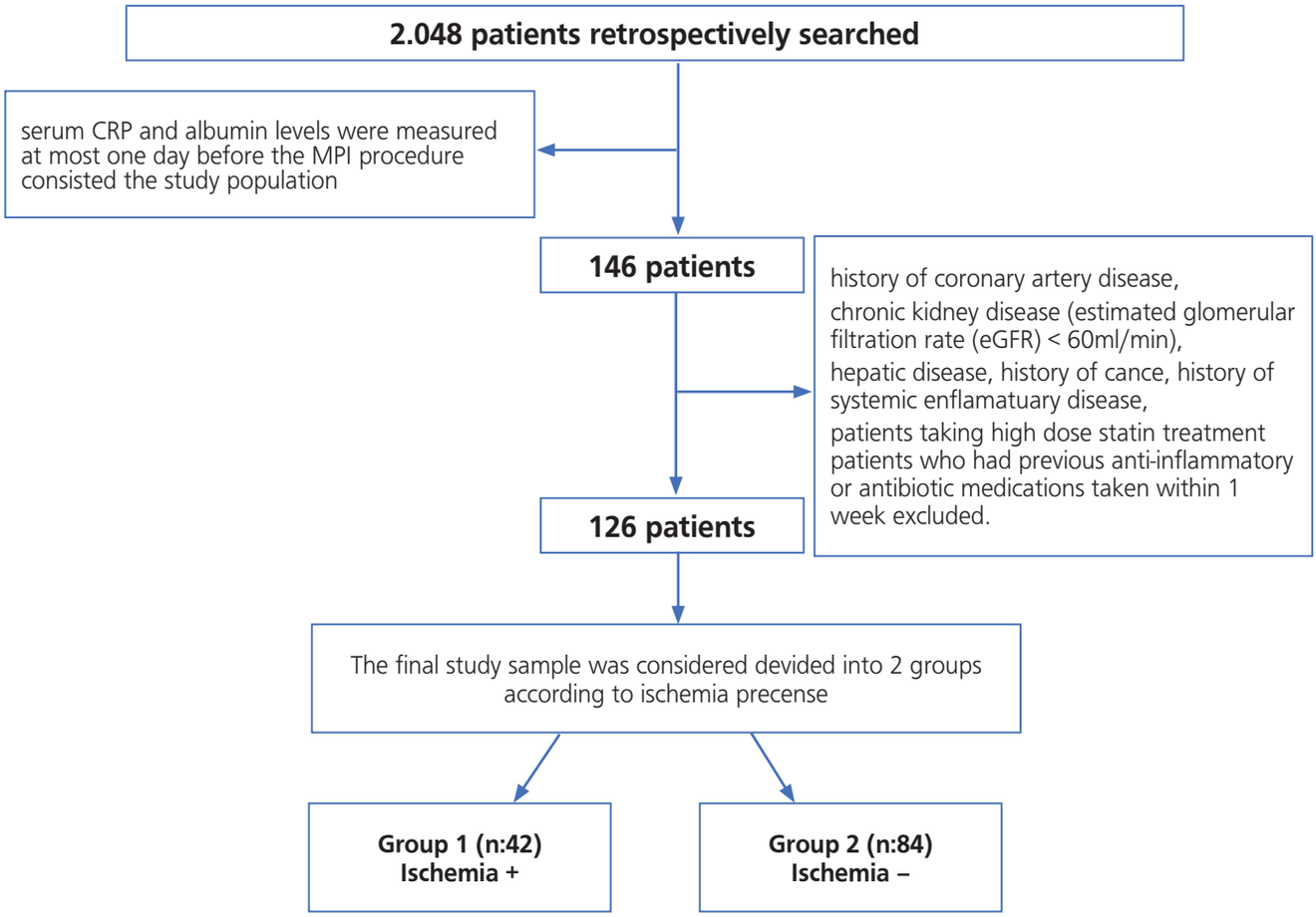

Figure 1. Study population flow chart
CRP: C-reactive protein, MPI: Myocardial perfusion imaging, eGFR: Glomerular filtration rate

automatically applied by the processing software in order to correct the emission data. The MPI dataset was carefully re-matched with the CT attenuation map to produce the attenuation corrected images.

Laboratory Measurements

We performed routine blood chemistry measurements including hs-CRP (mg/L) in the morning. In addition, we measured albumin and hs-CRP levels using Roche Diagnostics Cobas 8000 analyzer. We deduced the CAR (mg/g) value by dividing hs-CRP level to albumin level, and results were obtained from the same blood samples.

Statistical Analysis

We performed overall analysis using Statistical Package for Social Sciences (SPSS statistical version 17.0 Inc, Chicago, IL). We described continuous variables as mean ± standard deviation or median values, while categorical variables as frequencies and percentages (%). We verified the normality of continuous variables using Kolmogorov-Smirnov statistics. Meanwhile, we performed Mann-Whitney U test and independent t-test to evaluate parametric variables. We used χ2-test or Fisher's Exact test to evaluate categorical variables. Statistical significance was set at $p<0.05$. The variables that showed marginal association in univariate analysis were moved to multivariate logistic regression analyzes. We performed multivariate logistic regression analyzes to obtain independent predictors of ischemia in MPI. The receiver operating characteristics curve analysis was used for calculating the CAR value that predicts presence of ischemia with the best possible specificity and sensitivity.

Results

All participants in the study underwent gated SPECT MPI. The mean age of participants was 59.8±11.3 years and 56 patients (44%) were male. The subjects were classified into

groups according to the absence or presence of ischemia on gated SPECT MPI. Table 1 shows the demographic characteristics of all the study population. The frequencies of diabetes mellitus and history of hypertension were significantly more frequent in patients with ischemia (p<0.05 for each). Based on laboratory findings (Table 2), hs-CRP and CAR were significantly higher in the ischemia group, but serum albumin was significantly lower in this group (p<0.05 for each). Other laboratory findings were not different between the groups. Hypertension, diabetes mellitus, and CAR were the predictors of presence of ischemia in univariate analysis (Table 3). From multivariate regression analysis using a model adjusted for the aforementioned parameters, hypertension [odds ratio (OR): 4.012, 95% confidence interval (CI): 1.580-10.118, and p=0.003] and CAR (OR: 5.720, 95% CI: 2.697-12.133, and p<0.001) were independently correlated with the presence of ischemia. The area under curve of CAR for gated SPECT MPI in the ischemia group was 0.77 (0.67-0.87 95% CI, p<0.001) (Figure 2). Moreover, the optimal value of CAR in the group with the presence of ischemia was 0.96 (sensitivity=76%; specificity=71%).

Table 1. Baseline demographic characteristics findings of all patients

	Presence of ischemia (n=42)	Absence of ischemia (n=84)	p value
Gender, male (%)	22 (52.4)	34 (40.5)	0.206
Age	60.5±11.1	59.4±11.9	0.812
Use of smoking (%)	19 (45.2)	35 (41.7)	0.703
Hypertension (%)	24 (57.1)	23 (27.4)	0.001
Diabetes mellitus (%)	22 (52.4)	28 (33.3)	0.040
Dyslipidemia	8 (19.0)	14 (16.7)	0.741

Nominal variables presented as frequency (%)

Table 2. Laboratory findings of all patients

	Presence of ischemia (n=42)	Absence of ischemia (n=84)	p value
White blood cell count (cells/µl)	8.20±2.02	7.90±2.00	0.501
Neutrophil (cells/µL)	4.59±1.62	4.37±1.63	0.478
Lymphocyte (cells/µL)	2.55±0.87	2.46±0.80	0.566
Monocyte (cells/µL)	0.64±0.26	1.26±5.71	0.318
Neutrophil-to-lymphocyte ratio	1.98±0.91	1.95±1.01	0.864
Platelet count (cells/µL)	274.0±91.9	269.2±84.6	0.774
Hemoglobin (g/dL)	12.86±1.90	13.3±1.68	0.134
Creatinine (mg/dL)	0.87±0.27	0.80±0.29	0.265
Blood urea nitrogen (mg/dL)	40.3±16.4	35.8±14.5	0.174
CRP, mg/L	5.83±3.06	3.10±2.13	<0.001
Serum albumin, g/L	4.02±0.57	4.22±0.49	0.038
CAR, mg/g	1.48±0.81	0.73±0.47	<0.001

Continuous variable are presented as mean ± SD
CAR: C-reactive protein/albumin ratio, CRP: C-reactive protein, SD: Standard deviation

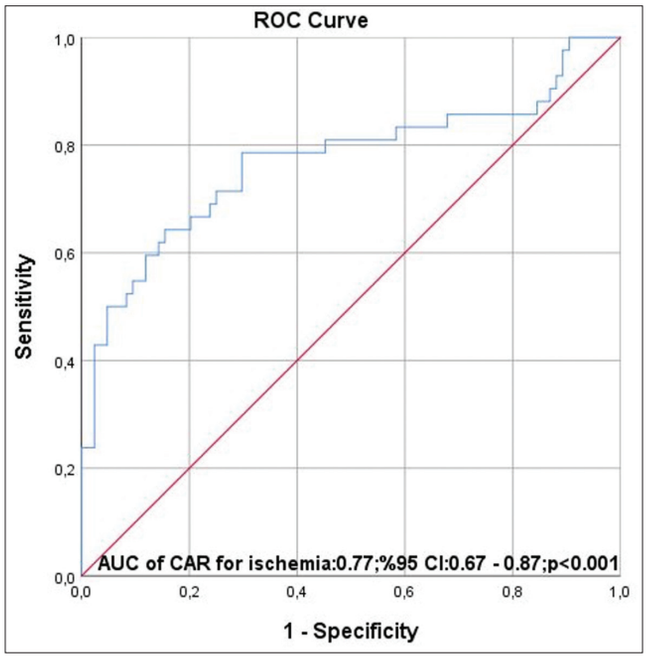

Figure 2. ROC curve analysis
ROC: Receiver operating characteristics, AUC: Area under curve, CAR: CAR: C-reactive protein/albumin ratio, CI: Confidence interval

Table 3. Uni-multivariable logistic regression analysis for presence of ischemia

	Univariate			Multivariate		
	OR	95% CI	p value	OR	95% CI	p value
Hypertension	3.836	1.626-7.690	0.001	4.012	1.580-10.118	0.003
Diabetes mellitus	2.200	1.032-4.688	0.041			
CAR	6.235	2.989-13.006	<0.001	5.720	2.697-12.133	<0.001

CAR: C-reactive protein/albumin ratio, OR: Odds ratio, CI: Confidence interval

Discussion

In this study, we evaluated the association between CAR and MPI detected ischemia in patients with stable CAD. Among various inflammatory parameters, CAR showed the best capability to discriminate myocardial ischemia detected by MPI. This association was independent of other predictors.

Hs-CRP is considered to be an independent cardiovascular event marker used in cardiovascular risk classification, and in some scores like Reynolds score, hs-CRP is present (3,10). Redberg et al. (6) hypothesized that hs-CRP is both an inflammatory marker and a predictor of an increased risk of CVD. As a result, there is a clear relationship between increased hs-CRP levels and higher CV risk (11,12).

There is an ongoing debate on whether hs-CRP is an indicator of inflammation or whether it contributes to the development of atherosclerosis (6). In atherosclerotic plaques, elevated hs-CRP levels were associated with increased number of monocytes, increased vascular endothelial plasminogen actıvator inhibitor-1 expression, and reduced low density lipoprotein uptake by tissue macrophages. The hs-CRP is a known cause of oxidative stress, resulting in remodeling of the vascular wall through angiotensin activity increase. It also activates the prothrombotic states in blood. There is evidence that demonstrates the presence of abundant CRP in atherosclerotic lesions and also defines CRP as the trigger for various pathogenic pathways causing atherogenic events (13). Plasma level of hs-CRP is known to increase with the complexity of CAD (5). Hs-CRP can be used as a predictor of CVD, ischemic stroke, and myocardial infarction (14). Increased CRP at admission in patients with unstable angina or non-ST-segment myocardial infarction is associated with increased 14-day mortality, even in patients with a negative rapid cardiac troponin test (15). In other studies with stable CAD patients treated with PCI, CRP independently associated with an increased risk of 1-year mortality (16). In STEMI patients, CAR was found to be effective as prognostic marker for in-hospital and long-term all-cause mortality (17). As already known, our study determined the relationship between CRP and myocardial ischemia.

Albumin is known as an acute phase marker with reduced levels in cases of infection and chronic inflammation. Low albumin levels are known to have prognostic significance in cases such as acute coronary syndrome, heart failure, and stable coronary heart disease (18). Hypoalbuminemia is also known as an independent prognostic indicator in many CVDs (19). In our study, low albumin levels were associated with ischemia.

It is well-known that inflammatory reactions take place in all stages of myocardial ischemia. In ischemic myocardial tissue, pro-inflammatory chemokines are strongly secreted thereby activating leukocytes leading to leukocyte migration to the inflammation area. A growing set of clinical evidence suggests that neutrophil-to-lymphocyte ratio (NLR), CRP, albumin, and lymphocyte are easily accessible and cheap markers to assess inflammation, especially in acute coronary syndromes (20). NLR was found as an independent predictor for acute and stable CAD in some studies (21,22). In a study where CAR values were compared with other inflammatory parameters, CAR was found to be a better predictor than other parameters for significant CAD in patients with stable CAD (23). Despite previous studies, NLR was not associated with myocardial ischemia in our study.

Several reports show that the severity and extent of myocardial ischemia can be determined accurately using SPECT MPI; they have also highlighted the prognostic value of this method. Spectral perfusion screening has been reported to have lower CRP levels in patients with normal myocardial functions than with myocardial ischemia (24).

The CAR is a marker that is calculated by the ratio of these acute phase markers; and is believed to be more sensitive in predicting inflammatory events. In some CVD (such as stable angına pectoris and acute coronary syndromes), CAR values were higher than in control groups and disease severity was associated with CAR values (7,8,9). In our study, ischemia group in MPS had significantly higher CAR values than those without ischemia.

Although CRP and albumin are both acute phase markers, there is experimental evidence that demonstrates the presence of CRP in atherosclerotic lesions. The exertion and measurable values of these markers vary slightly in patients with ischemia due to myocardial ischemia in daily life efforts. Our study is a novel one which investigates the relationship between myocardial ischemia and CAR values. Therefore, CAR values at any time in patients with stable CAD may be predictive for ischemia detection in outpatient clinics.

Study Limitations

Owing to the retrospective nature of this study, we could not assess myocardial viability by MPI, and hence could determine the ischemia percentage from MPI reports.

Conclusion

CAR is an independent variable in detecting myocardial ischemia in stable CAD patients. CAR values can be used to predict the presence of ischemia prior to invasive procedures in daily in daily practice.

Ethics

Ethics Committee Approval: The Local Ethics Committee approval from İstanbul Training and Research Hospital with decision number: 1935 was taken for the present study.

Informed Consent: Obtained a written patient informed consent.

Peer-review: Externally and internally peer-reviewed.

Authorship Contributions

Surgical and Medical Practices: S.Ç.E., Concept: S.Ç.E., C.G., Design: S.Ç.E., T.F.Ç., B.A., Data Collection or Processing: Ö.Ö.C., C.G., Analysis or Interpretation: S.Ç.E., A.Ö., Literature Search: Y.Y., S.Ç.E., Writing: S.Ç.E., Ö.Ö.C., C.G., A.Ö., Y.Y., T.F.Ç., B.A.

Conflict of Interest: No conflict of interest was declared by the authors.

Financial Disclosure: The authors declared that this study has received no financial support.

References

1. Doukky R, Frogge N, Balakrishnan G, Hayes K, Collado FM, Rangel MO, Golzar Y, Garcia-Sayan E, Hendel RC. The prognostic value of cardiac SPECT performed at the primary care physician's office. J Nucl Cardiol 2013;20:519-528.
2. Hachamovitch R, Berman DS, Kiat H, Cohen I, Cabico JA, Friedman J, Diamond GA. Exercise myocardial perfusion SPECT in patients without known coronary artery disease: Incremental prognostic value and use in risk stratification. Circulation 1996;93:905-914.
3. Hosseinsabet A, Mohebbi A, Almasi A. C-reactive protein and Coronary Calcium Score association in coronary artery disease. Cardiol J 2008;15:431-436.
4. Duffy BK, Gurm HS, Rajagopal V, Gupta R, Ellis SG, Bhatt DL. Usefulness of an elevated neutrophil to lymphocyte ratio in predicting long-term mortality after percutaneous coronary intervention. Am J Cardiol 2006;97;993-996.
5. Blaha MJ, Budoff MJ, DeFilippis AP, Blankstein R, Rivera JJ, Agatston A, O'Leary DH, Lima J, Blumenthal RS, Nasir K. Associations between C-reactive protein, coronary artery calcium, and cardiovascular events: Implications for the JUPITER population from MESA, a population-based cohort study. Lancet 2011;378:684-692.
6. Redberg RF, Rifai N, Gee L, Ridker PM. Lack of association of C-reactive protein and coronary calcium by electron beam computed tomography in postmenopausal women: Implications for coronary artery disease screening. J Am Coll Cardiol 2000;36:39-43.
7. Wang W, Ren D, Wang CS, Li T, Yao HC, Ma SJ. Prognostic efficacy of high-sensitivity C-reactive protein to albumin ratio in patients with acute coronary syndrome. Biomark Med 2019;13:811-820.
8. Duman H, Çinier G, Bakırcı EM, Duman H, Şimşek Z, Hamur H, Değirmenci H, Emlek N. Relationship Between C-Reactive Protein to Albumin Ratio and Thrombus Burden in Patients With Acute Coronary Syndrome. Clin Appl Thromb Hemost 2019;25:1076029618824418.
9. Karabağ Y, Çağdaş M, Rencuzogullari I, Karakoyun S, Artaç İ, İliş D, Atalay E, Yesin M, Gürsoy MO, Halil Tanboğa I. Relationship between C-reactive protein/albumin ratio and coronary artery disease severity in patients with stable angina pectoris. J Clin Lab Anal 2018;32:e22457.
10. Mahabadi AA, Möhlenkamp S, Moebus S, Dragano N, Kälsch H, Bauer M, Jöckel K-H, Erbel R, Heinz Nixdorf Investigator Group. The heinz nixdorf recall study and its potential impact on the adoption of atherosclerosis imaging in European primary prevention guidelines. Curr Atheroscler Rep 2011;13:367-372.
11. Malik S, Zhao Y, Budoff M, Nasir K, Blumenthal RS, Bertoni AG, Wong ND. Coronary artery calcium score for long-term risk classification in individuals with type 2 diabetes and metabolic syndrome from the multi-ethnic study of atherosclerosis. JAMA Cardiol 2017;2:1332-1340.
12. Dong Y, Wang X, Zhang L, Chen Z, Zheng C, Wang J, Kang Y, Shao L,Tian Y, Wang Z, China CVD study investigators. High-sensitivity C reactive protein and risk of cardiovascular disease in China-CVD study. J Epidemiol Community Health 2019;73:188-192.
13. Bisoendial RJ, Boekholdt SM, Vergeer M, Stroes ES, Kastelein JJ. C-reactive protein is a mediator of cardiovascular disease. Eur Heart J 2010;31:2087-2091.
14. Paoletti R, Bolego C, Poli A, Cignarella A. Metabolic Syndrome, Inflammation and Atherosclerosis. Vasc Health Risk Manag 2006;2:145-152.
15. Morrow DA, Rifai N, Antman EM, Weiner DL, McCabe CH, Cannon CP, Braunwald E. C-reactive protein is a potent predictor of mortality independently of and in combination with troponin T in acute coronary syndromes: a TIMI 11A substudy. Thrombolysis in Myocardial Infarction. J Am Coll Cardiol 1998;31:1460-1465.
16. Sabatine MS, Morrow DA, Jablonski KA, Rice MM, Warnica JW, Domanski MJ, Hsia J, Gersh BJ, Rifai N, Ridker PM, Pfeffer MA, Braunwald E, PEACE Investigators. Prognostic significance of the Centers for Disease Control/American Heart Association high-sensitivity C-reactive protein cut points for cardiovascular and other outcomes in patients with stable coronary artery disease. Circulation 2007;115:1528-1536.
17. Askin L, Tanriverdi O, Tibili H, Turkmen S. Prognostic value of C-reactive protein / albumin ratio in ST-segment elevation myocardial infarction. Interventional Medicine and Applied Science 2019:1-4.
18. McMillan DC, Watson WS, O'Gorman P, Preston T, Scott HR, McArdle CS. Albumin concentrations are primarily determined by the body cell mass and the systemic inflammatory response in cancer patients with weight loss. Nutrition and cancer 2001;39:210-213.
19. Arques S. Human serum albumin in cardiovascular diseases. Eur J Intern Med 2018;52:8-12.
20. Tamhane UU, Aneja S, Montgomery D, Rogers E-K, Eagle KA, Gurm HS. Association between admission neutrophil to lymphocyte ratio and outcomes in patients with acute coronary syndrome. Am J Cardiol 2008;102;653-657.
21. Azab B. Medhat Zaher, Weiserbs KF, Torbey E, Lacossiere K, Gaddam S, Gobunsuy R, Jadonath S, Baldari D, McCord D, Lafferty J. Usefulness of neutrophil to lymphocyte ratio in predicting short- and long-term mortality after non-ST-elevation myocardial infarction. Am J Cardiol 2010;106;470-476.
22. Park JJ, Jang HJ, Oh IY, Yoon CH, Suh JW, Cho YS, Youn TJ, Cho GY, Chae IH,Choi DJ. Prognostic value of neutrophil to lymphocyte ratio in patients presenting with ST-elevation myocardial infarction undergoing primary percutaneous coronary intervention. Am J Cardiol 2013;111;636-642.
23. Tanriverdi Z, Gungoren F, Tascanov MB, Besli F, Altiparmak IH. Comparing the Diagnostic Value of the C-Reactive Protein to Albumin Ratio With Other Inflammatory Markers in Patients With Stable Angina Pectoris. Angiology 2020;71:360-365
24. Rashidinejad H, Moazanzadeh M, Mirshekarpoor H, Ebrahim F. The relationship between HS-CRP serum levels with the results of cardiac perfusion SPECT imaging in patients with suspected coronary artery disease. Asian Journal of Biomedical and Pharmaceutical Sciences 2015;5:30-33.

Original Article
Mol Imaging Radionucl Ther 2020;29:118-123 DOI:10.4274/mirt.galenos.2020.21549

Collimator and Energy Window Evaluation in Ga-67 Imaging by Monte Carlo Simulation

Ga-67 Görüntülemede Monte Carlo Simulasyonu Kullanılarak Kolimatör ve Enerji Penceresi Değerlendirmesi

Mina Ouahman[1], Rachid Errifai[1], Hicham Asmi[1], Youssef Bouzekraoui[1], Sanae Douama[1], Farida Bentayeb[1], Faustino Bonutti[2]

[1]*Mohammed V-Rabat University Faculty of Science, Laboratory of High Energy Physics Modelisation Simulation, Rabat, Morocco*
[2]*Academic Hospital of Udine, Clinic of Medical Physics, Udine, Italy*

Abstract

Objectives: Gallium-67 (Ga-67) imaging is affected by collimator penetration and scatter components owing to the high-energy (HE) gamma-ray emissions. The characterization of penetration and scatter distribution is essential for the optimization of low-energy high-resolution (LEHR), medium energy (ME), and HE collimators and for the development of an effective correction technique. We compared the image quality that can be achieved by 3 collimators for different energy windows using the SIMIND Monte Carlo code.

Methods: Simulation experiments were conducted for LEHR, ME, and HE collimators for Ga-67 point source placed at 12-cm distance from the detector surface using the Monte Carlo SIMIND simulation code. Their spectra point spread functions as well as the original, penetration, scattering, and X-rays curves were drawn and analyzed. The parameters full-width at half maximum and full-width at tenth maximum were also investigated.

Results: The original, penetration, and scatter curves within 10% for LEHR were 34.46%, 33.52%, 17.29%, and 14.72%, respectively. Similarly, the original, penetration, scatter, and X-rays within 10% for ME and HE were 83.06%, 10.25%, 6.69%, and 0% and 81.44%, 11.51%, 7.05%, and 0%, respectively. The trade-off between spatial resolution and sensitivity was achieved by using the ME collimator at 185 photopeak of Ga-67.

Conclusion: The Monte Carlo simulation outcomes can be applied for optimal collimator designing and for the development of new correction method in Ga-67 imaging.

Keywords: Ga-67 imaging, primary photons (original), penetration, scatter, SIMIND, sensitivity

Öz

Amaç: Galyum-67 (Ga-67) görüntüleme, yüksek enerjili gama ışını emisyonları nedeniyle kolimatör penetrasyonundan ve saçılma bileşenlerinden etkilenir. Penetrasyon ve saçılma dağılımının karakterizasyonu düşük enerjili yüksek çözünürlüklü (LEHR), orta enerjili (ME) ve yüksek enerjili (HE) kolimatörlerin optimizasyonu ve düzeltme yönteminin geliştirilmesi için önemlidir. Bu çalışma, SIMIND Monte Carlo kodunu kullanarak farklı enerji pencereleri için üç kolimatör ile elde edilebilen görüntü kalitesinin karşılaştırılmasını amaçlamaktadır.

Yöntem: Dedektör yüzeyinden 12 cm uzağa yerleştirilen Ga-67 nokta kaynağı ile LEHR, ME ve HE kolimatörleri için Monte Carlo SIMIND simülasyon kodu kullanılarak simülasyon yapıldı. Spektrumları yayılma fonksiyonlarına işaret ediyordu ve ayrıca orijinal, penetrasyon, saçılma ve X-ışınları eğrileri çizilerek analiz edildi. Yarı maksimumdaki tam genişlik ve 1/10 maksimumdaki tam genişlik araştırıldı.

Bulgular: LEHR için %10 içindeki orijinal, penetrasyon, saçılma ve X-ışınları sırasıyla %34,46, %33,52, %17,29 ve %14,72 idi. ME için %10 içindeki orijinal, penetrasyon, saçılma ve X-ışınları sırasıyla %83,06, %10,25, %6,69 ve %0 idi. HE için %10 içindeki orijinal, penetrasyon, saçılma ve X-ışınları sırasıyla %81,44, %11,51, %7,05 ve %0 idi. Uzamsal çözünürlük ve duyarlılık arasındaki denge, Ga-67'nin 185 fotopikli ME kolimatörü kullanılarak elde edildi.

Sonuç: Monte Carlo simülasyon sonuçları, Ga-67 görüntülemede optimum kolimatör tasarımı ve yeni düzeltme yönteminin geliştirilmesi için kullanılabilir.

Anahtar kelimeler: Ga-67 görüntüleme, primer fotonlar (orijinal), penetrasyon, saçılma, SIMIND, duyarlılık

Address for Correspondence: Youssef Bouzekraoui MD, Mohammed V-Rabat University Faculty of Science, Laboratory of High Energy Physics Modelisation Simulation, Rabat, Morocco **Phone:** 0623609312 **E-mail:** youssef0fsr@gmail.com ORCID ID: orcid.org/0000-0002-7877-1345
Received: 03.12.2019 **Accepted:** 20.04.2020

Introduction

Gallium-67 (Ga-67) disintegrates by electron capture to stable zinc 67 with a radioactive half-life of 3.26 days, and it has less costly imaging requirements. Despite that ^{18}F-fluorodeoxyglucose positron emission tomography is currently used for the diagnosis of non-Hodgkin's lymphoma, Ga-67 scintigraphy remains useful during the early period of treatment (1,2,3). The decay scheme of Ga-67 involves multiple emission energies with photopeak energies at 93, 185, and 300 keV. Therefore, the contributions of some photons are included in lower photopeak energy window. In addition, lead X-rays produced in the collimator can also be detected in the 93-keV photopeak energy windows. This contribution degrades the image quality and the quantitative accuracy, especially, when imaging with a low-energy collimator (4,5). All photons detected with the collimator were grouped into 3 categories as follows: original photons (i.e., photons detected on the detector without any scatter or penetration), penetration photons (those that passed through septa without attenuation), and scatter photons (those that scattered at least once in the septa) (6,7). Only the first photons provide correct information. Image quality is essentially affected by the penetration and scatter components of the collimator, particularly in high-energy imaging. The scattered photons depend on the photons energy, object study, and collimator design. Gamma-camera cannot classify the image-forming photons into original, penetrated, or scattered photons. The knowledge of penetration and scatter distribution is essential for the optimization of collimator design and for the development of a correction method (7,8). The typical energy resolution of NaI (Tl) has a full-width at half maximum (FWHM) of approximately 10% at 140 keV. Therefore, the contribution of scatter within the photopeak energy windows is huge (9). Accordingly, several compensation scatter methods have been proposed, for example, the triple-energy window method and the Compton window subtraction method (10,11). Therefore, the Monte Carlo simulation technique (12,13,14,15,16,17,18) separates the original, penetration, and scatter contribution inside the photopeak window. In this study, we compared the simulated energy spectra in Ga-67 imaging for different parallel-hole collimators for the Siemens Symbia gamma-camera (Table 1). The resolution and sensitivity (cps/MBq) were accordingly evaluated. We also estimated and compared the original, penetration, and scatter contribution inside the 20% and 10% energy windows around the 93, 185, and 300 keV photopeaks. Through this work, we aimed to determine the optimal energy window and collimators design [low-energy high-resolution (LEHR), medium energy (ME), and high energy (HE)] in Ga-67 imaging.

Materials and Methods

No statistical analysis was performed, and the study has no evident limitations.

Our study did not involve any patients.

All procedures performed in the experiments involving human participants were in accordance with the ethical standards of the institutional and/or national research committee and with the 1964 Helsinki Declaration and its later amendments or other comparable ethical standards.

We used the SIMIND Monte Carlo simulation code (version 6.1) to simulate a point source of Ga-67 isotope (Table 2) of dimension 0.1x0.1x0.1 cm^3 located at the center of a cylindrical water phantom of dimension 16x22x22 cm^3 and placed at 12 cm from the detector surface. In this simulation, we modeled the Siemens Medical System Symbia equipped by the following 3 collimators: LEHR, ME, and HE (Tables 1, 2) (19). A detector of 59.1x44.5-cm^2 area and 0.95-cm NaI (Tl) crystal thickness was used.

The detector was characterized by an intrinsic spatial resolution of 0.34 cm and an energy resolution of 8.80% at 140 keV. The photomultiplier tube (PM) back-scatter material with a thickness of 10 cm was used to simulate the backscattering of photons from the light guides and PM.

We included the contribution of lead X-rays scatter photons inside the collimator lead. The aluminum cover material thickness was 0.1 cm. The pixel size in the simulated planar images was 0.34 cm and 128x128 matrix size. We imported the binary image to the ImageJ software created by SIMIND. At the end of each simulation, SIMIND provided the value of original, penetration, and scatter photons as well as the efficiency, sensitivity, FWHM, and full-width at tenth maximum (FWTM) in separate files. Table 3 shows the abundance of Ga-67 as a function of energy, which is extremely useful in the selection of appropriate collimator.

Table 1. Specifications of the Siemens SYMBIA SPECT scanner

Characteristics	Value
Detector material	NaI (Tl)
Crystal dimensions (cm)	59.1x44.5x0.95
Number of photomultiplier tubes	59
Diagonal FOV (cm)	63.5

SPECT: Single photon emission tomography

Results

Figure 1 depicts the simulated energy spectra of a Ga-67 point source in water placed at 12-cm distance away from the detector surface. All energy spectra include both scattered and unscattered photons. The energies displayed in Figure 1 represent the energies of the main emission peaks of the isotope. The spectra characteristics help explain the choice of collimator type for imaging. The total number of photons detected with the collimators were degraded widely relative to that without the collimators. The peaks was detected in the energy region of 70-86-keV for each collimator, which matched the characteristic X-rays of lead produced by the photoelectric effect of HE photons. According to the contribution of penetration and scatter components in the projection data, the shape of Compton edge and Compton region were found to be different among the 3 collimators. In addition, as it can be seen, the contribution of septal penetration and scatter in the HE and ME were less than those in the LEHR.

Table 4 depicts the energy windows used for each collimator. The results of the simulation are detailed in Table 5. We evaluated the original, septal penetration, and scatter components in parallel-hole collimators LEHR, ME, and HE for Ga-67 point source using the Monte Carlo simulation program.

Figure 2 illustrates the comparison of the proportion of penetration (photons that penetrated the collimator), scatter (those that scattered in the collimator), and original (those that were detected on the detector without any scatter or penetration) inside the 20% and 10% energy windows around the 93-, 185-, and 300-keV photopeaks in the LEHR, ME, and HE collimators, respectively.

The point spread functions (PSF) were studied for Ga-67 imaging. A point source of 0.1-mm diameter was acquired with different collimators. The PSF obtained for all collimators are represented in Figure 3. The curves of Ga-67 with the ME and HE collimators demonstrate the effects of the septal that lowers the resolution. LEHR offers a poorer resolution than the HE and ME collimators within 20% and 10% windows (20,21,22) owing to the septal penetration and the scattering effects.

The indices of resolution used were FWHM to measure the collimator's spatial resolution, and the FWTM was used as an index of septal penetration and Compton scattering within the collimator. In order to quantify the resolution, FWHM and FWTM were computed on the PSF. The results for both FWHM and FWTM and the relevant sensitivities (Cps/MBq) are given in Table 6. These parameters were compared within the 20% and 10% energy windows. It can be seen from the table that, for each collimator, the FWTM increased with the width of the energy windows, especially for the LEHR and ME collimators, while, the FWHM remained approximately the same (21,22,23). On the other hand, the sensitivity decreased when the width of the energy window decreased, which was an extremely sharp transition for LEHR. Figure 4 depicts the images of Ga-

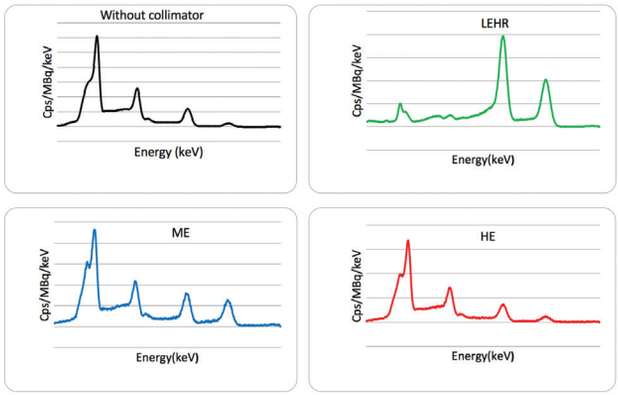

Figure 1. Comparison of the total simulated spectrum among the 3 different collimators for Ga-67 imaging
Ga-67: Gallium-67, LEHR: Low-energy high-resolution, ME: Medium energy, HE: High energy

Table 2. Collimators data of the Siemens SYMBIA systems during simulation

Imaging system	Collimators	Diameter (cm)	Septa (cm)	Length (cm)	Hole shape	Collimator type
Siemens SYMBIA	LEHR	0.111	0.016	2.405	Hexagonal	Parallel hole
	ME	0.294	0.114	4.064	Hexagonal	Parallel hole
	HE	0.400	0.200	5.970	Hexagonal	Parallel hole

LEHR: Low-energy high-resolution, ME: Medium energy, HE: High energy

Table 3. Energies and intensities of gamma rays emitted from the Ga-67 source

Energy (keV)	91.26	93.30	184.57	208.93	300.23	393.52	494.14	703.11	794.4	887.67
Abundance (%)	3.09	38.1	20.96	2.37	16.6	4.59	0.06	0.01	0.05	0.14

Ga-67: Gallium-67

Table 4. Acquisition energy windows used in the simulation		
Photopeak window (keV)	**Photopeak**	**Collimators**
10%	93 keV	LEHR
	185 keV	ME
	300 keV	HE
20%	93 keV	LEHR
	185 keV	ME
	300 keV	HE
LEHR: Low-energy high-resolution, ME: Medium energy, HE: High energy		

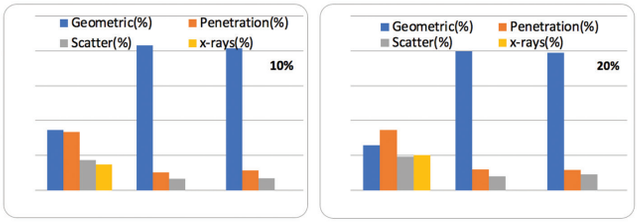

Figure 2. Comparison among the original, penetration, scatter, and X-rays for LEHR, ME, and HE collimators
LEHR: Low-energy high-resolution, ME: Medium energy, HE: High energy

Table 5. The result of the simulation performed in the study					
Energy windows	**Collimators**	**Original (%)**	**Penetration (%)**	**Scatter (%)**	**X-rays (%)**
10%	LEHR	34.46	33.52	17.29	14.72
	ME	83.06	10.25	6.69	0
	HE	81.44	11.51	7.05	0
20%	LEHR	25.94	34.7	19.31	20.05
	ME	79.98	12.03	8	0
	HE	79	11.8	9.2	0
LEHR: Low-energy high-resolution, ME: Medium energy, HE: High energy					

Table 6. Calculated FWHM and FWTM and sensitivities within the 20% and 10% energy windows for LEHR, ME, and HE collimators				
Energy windows	**Collimators**	**FWHM (mm)**	**FWTM (mm)**	**Sensitivity (Cps/MBq)**
10%	LEHR	3.47	33.12	21.11
	ME	5.04	10.09	12.8
	HE	5.53	10.26	5.82
20%	LEHR	3.88	52.05	42.37
	ME	5.20	15.67	19.40
	HE	5.64	11.87	7.41
FWHM: Full-width at half maximum, FWTM: Full-width at tenth maximum, LEHR: Low-energy high-resolution, ME: Medium energy, HE: High energy				

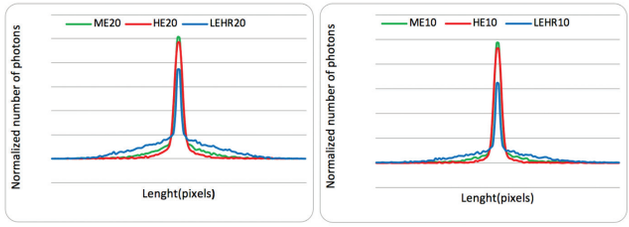

Figure 3. Comparison of PSF among the 3 different collimators for the Ga-67 point source inside the 20% and 10% energy windows with HE, ME, and LEHR collimators
PSF: Point spread functions, Ga-67: Gallium-67, LEHR: Low-energy high-resolution, ME: Medium energy, HE: High energy

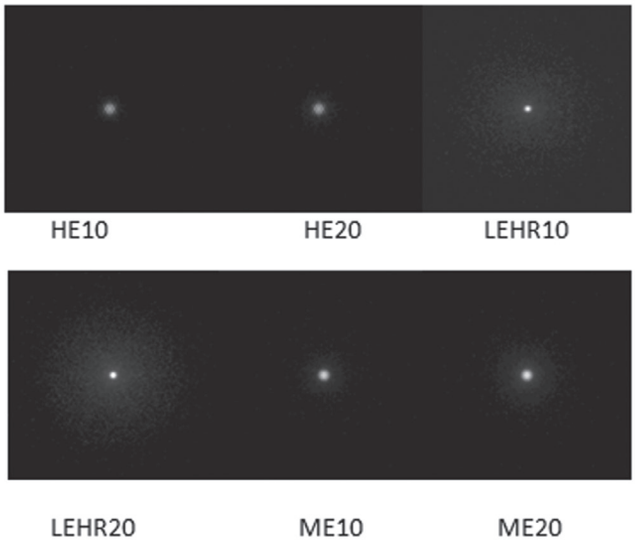

Figure 4. Images of the Ga-67 point sources created at the end of each simulation with LEHR, ME, and HE collimators within the 10% and 20% energy windows
Ga-67: Gallium-67, LEHR: Low-energy high-resolution, ME: Medium energy, HE: High energy

67 point sources obtained from the simulation performed with different collimators.

Discussion

The Monte Carlo simulation SIMIND code was used to store the history of the detected events, which was otherwise not possible with the experimental data. However, to compare i.e., equal acquisition time were employed. The collimator-detector response (CDR) of the single photon emission tomography imaging system depends on the following 4 components: the intrinsic response and the response of the detector and the original, penetration, and scatter distribution inside the collimator. Therefore, the characterization of this components helps compensate the CDR, which has a significant effect on accurate

quantification (20). As the Ga-67 radionuclide emits multiple-energy rays, a large scattered event is detected within the photopeak energy windows; this event degrades significant contrast and lesion detection (9).

The low original component in LEHR collimator may be attributed to the high level of penetration, scattering, and X-rays effects. This component is large for ME and HE collimators. The original component (primary photons) decreased with an increase in the photopeak window, especially for the LEHR collimator. Penetration and scatter component increased with an increase in the photopeak window, demonstrating smooth increase in all collimators. In addition, the X-rays component showed a slow increase with an increase in the photopeak window in the LEHR collimators. Although the number of detected photons from the main energy peak (93 keV) was high for LEHR, it is important to consider that a large amount from this peak was detected after septal penetration. The indices of resolution used were FWHM to measure the collimator's spatial resolution, while FWTM served as an index of septal penetration and Compton scattering within the collimator. In order to quantify the resolution, FWHM and FWTM were computed on the PSF.

The presence of a high level of penetrated and scattered photons from the LEHR collimator degrades spatial resolution, contrast, and quantification (20,21,22,23,24). Table 6 depicts that the use of LEHR collimator with Ga-67 imaging resulted in the most degraded spatial resolution, while the use of an HE collimator in Ga-67 imaging resulted in the loss of sensitivity and spatial resolutions (25). Data presented in Table 5 signify that the trade-off between the sensitivity and spatial resolution achieved with the ME collimator occurred when the photopeak was centered over the 185-keV photopeak with the use of 10% photopeak. We hence recommend Ga-67 imaging with a single peak around the 185-keV peak considering the high relative intensity of the 185-keV gamma peak (30%) and the high absorption efficiency of this photopeak within the NaI (Tl) crystal.

The fogginess in these images increased with an increase in the energy window, especially for LEHR. This observation can be attributed to the HE photons detected inside the energy window. Therefore, the LEHR collimators became virtually transparent, which was evident from the calculated value of high septa penetration and scattering obtained from the simulation experiments (Table 5).

Conclusion

We studied the LEHR, ME, and HE collimator in the Ga-67 imaging. Based on our results, we noted loss in sensitivity and spatial resolution by the HE collimator, as the LEHR collimator allows poorer spatial resolution. On the other hand, the trade-off between resolution and sensitivity was achieved with an ME collimator in the 10% energy window with a single peak at 185 keV. We believe that our results would facilitate the designing of optimal collimator and the development of a new correction method in Ga-67 imaging.

Ethics

Ethics Committee Approval: All procedures performed in studies involving human participants were in accordance with the ethical standards of the institutional and/or national research committee and with the 1964 Helsinki declaration and its later amendments or comparable ethical standards.

Informed Consent: The institutional review board of our institute approved this retrospective study, and the requirement to obtain informed consent was waived.

Peer-review: Externally and internally peer-reviewed.

Authorship Contributions

Surgical and Medical Practices: R.E., F.Bo., Concept: Y.B., F.B., H.A., Design: S.D., Data Collection or Processing: M.O., Analysis or Interpretation: Y.B., H.A., Literature Search: F.B., Y.B., Writing: Y.B., H.A.

Conflict of Interest: No conflict of interest was declared by the authors.

Financial Disclosure: The authors declared that this study received no financial support.

References

1. Mansberg R, Wadhwa SS, Mansberg V. Tl-201 and Ga-67 scintigraphy in non-Hodgkin's lymphoma. Clin Nucl Med 1999;24:239-242.
2. Tuli MM, Al-Shemmari SH, Ameen RM, Al-Muhanadi S, Al-Huda AF, Ballani N, Khoshi M, Al-Enezi F, Bajciova V, Mottl H. The use of gallium-67 scintigraphy to monitor tumor response rates and predict long-term clinical outcome in patients with lymphoma. Clin. Lymphoma 2004;5:56-61.
3. Shinohara H, Koga Y. Ga-67 imaging with scintillation camera – The selection of collimator. J Nucl Med 1981;22:169-176.
4. Farncombe TH, Gifford HC, Narayanan MV, Pretorius PH, Bruyant P, Gennert M, King M. An optimization of reconstruction parameters and investigation into the impact of photon scattering Ga-67 SPECT. IEEE Trans Nucl Sci 2002;49:2148-2154.
5. Moore SC, Kijewski MF, Fakhri GEE. Collimator Optimization for Detection and Quantitation Tasks: Application to Gallium-67 Imaging. IEEE Trans Med I 2005;24:1347-1356.
6. Vandenberghe ERS , Holen RV, Beenhouwer JD, Staelens S, Lemahieu I. Comparison of image quality of different iodine isotopes (I-123, I-124 and I-131). Cancer Biother Radiopharm 2007;22:423-430.
7. Dewaraja YK, Ljungberg M, Koral KF. Characterization of Scatter and Penetration Using Monte Carlo Simulation in 131I Imaging. J Nucl Med. 2000;41:123-130.

8. Lewis DP, Tsui BMW, Tocharoenchai C, Frey EC. Characterization of medium and high energy collimators using ray-tracing and Monte Carlo methods. 1998 IEEE Nucl Sc Symp and Med Imag Conf 1998. doi:10.1109/NSSMIC.1998.773931.
9. Farncombe TH, Gifford HC, Narayanan MV, Pretorius PH, Frey EC and King MA. Assessment of scatter compensation strategies for Ga-67 SPECT using numerical observers and human LROC studies. J Nucl Med 2004;45:802-812.
10. Jaszczak RJ, Greer KL, Floyd CE, Harris CC, Coleman RE. Improved SPECT quantitation using compensation for scattered photons. J Nucl Med 1984;25:893-900.
11. Ogawa K, Harata Y, Ichihara T, Kubo A, Hashimoto S. A practical method for position-dependent Compton-scatter correction in single photon emission CT. IEEE Trans Med Imaging 1991;10:408-412.
12. Ljungberg M. The SIMIND Monte Carlo program Home Page. Available from: http://www2.msf.lu.se/simind/index.asp.http://www.msf.lu.se/forskning/the-simind-monte-carlo-program
13. Yeh DM, Chang PC, Pan LK. The optimum Ga-67-citrate gamma camera imaging quality factors as first calculated and shown by the taguchi's analysis. Hell J Nucl Med 2013;16:25-32.
14. Ljungberg M. The SIMIND Monte Carlo program Home Page. http://www2.msf.lu.se/simind
15. Rong X, Du Y, Ljungberg M, Rault E, Vandenberghe S, Frey EC. Development and evaluation of an improved quantitative Y-90 bremsstrahlung SPECT method. Med Phys 2012;39:2346-2358.
16. Rong X, Frey EC. A collimator optimization method for quantitative imaging: application to Y-90 bremsstrahlung SPECT. Med Phys 2013;40:082504.
17. Toossi MB, Islamian JP, Momennezhad M, Ljungberg M, Naseri S. SIMIND Monte Carlo simulation of a single photon emission CT. J Med Phys 2010;35:42-47.
18. Roshan HR, Mahmoudian B, Gharepapagh E, Azarm A, Islamian JP. Collimator and energy window optimization for 90Y bremsstrahlung SPECT imaging: A SIMIND Monte Carlo stud. Appl Radia Isot 2016;108:124-128.
19. Lee YS, Kim JS, Kim KM, Lim SM, Kim HJ. Determination of energy windows for the triple energy window scatter correction method in I-131 on a Siemens SYMBIA gamma camera: a GATE simulation study. J Inst 2015;15;10:1-8.
20. Chun SY, Fessler JA, Dewaraja YK .Correction for Collimator-Detector Response in SPECT Using Point Spread Function Template. IEEE Trans Med Imaging 2013;32:295-305.
21. Bouzekraoui Y, Bentayeb F, Asmi H, Bonutti F. Comparison of image quality of different radionuclides technetium-99m, samarium-153, and iodine-123. Indian J Nucl Med 2019;34:201-204.
22. Bouzekraoui Y, Bentayeb F, Asmi H, Bonutti F. Energy window and contrast optimization for single-photon emission computed tomography bremsstrahlung imaging with yttrium-90. Indian J Nucl Med 2019;34:125-128.
23. Asmi H, Bentayeb F, Bouzekraoui Y, Bonutti F, Douama S. Energy window and collimator optimization in lutetium-177 single photon emission computed tomography imaging using Monte Carlo simulation. Indian J Nucl Med 2020;35:36-39.
24. Asmi H, Bentayeb F, Bouzekraoui Y, Bonutti F. Evaluation of acceptance angle in iodine-131 single photon emission computed tomography imaging with Monte Carlo simulation. Indian J Nucl Med 2019;34:24-26.
25. Bouzekraoui Y, Bentayeb F, Asmi H, Bonutti F. Determination of Energy Windows for Triple Energy Window Scatter Correction Method in Gadolinium-159 Single Photon Emission Computed Tomography Using Monte Carlo Simulation. Iran J Med Phys 2019;16:405-409.

Original Article
Mol Imaging Radionucl Ther 2020;29:124-131 DOI:10.4274/mirt.galenos.2020.71473

Red Marrow Absorbed Dose Calculation in Thyroid Cancer Patient Using a Simplified Excel Spreadsheet

Tiroid Kanseri Hastasında Basitleştirilmiş Bir Excel Elektronik Tablosu Kullanılarak Kırmızı İliğin Absorbe Ettiği Dozun Hesaplaması

Rangsee Songprakhon[1], Krisana Roysri[1], Putthiporn Charoenphun[2], Krisanat Chuamsaamarkkee[2]
[1]*Surin Hospital, Clinic of Radiology, Division of Nuclear Medicine, Surin, Thailand*
[2]*Mahidol University Faculty of Medicine Ramathibodi Hospital, Department of Diagnostic and Therapeutic Radiology, Bangkok, Thailand*

Abstract

Objectives: Absorbed dose to red marrow (D_{rm}) can be calculated using blood dosimetry. However, this method is laborious and invasive. Therefore, image-based dosimetry is the method of choice. Nonetheless, the commercial software is expensive. The goal of this work was to develop a simplified excel spreadsheet for image-based radioiodine red marrow dosimetry.

Methods: The serial whole-body images (acquired at 2nd, 6th, 24th, 48th, and 72th hours) of 29 patients from the routine pretherapeutic dosimetry protocol were retrospectively reanalyzed. The commercial OLINDA/EXM image-based dosimetry software was used to calculate the whole-body time-integrated activity coefficient ($TIAC_{WB}$) and D_{rm} [in terms of absorbed dose coefficient (d_{rm})]. For the simplified excel spreadsheet, the whole-body count was obtained from the vendor-supplied software. Then, the $TIAC_{WB}$ was computed by a fitting time-activity curve using an Excel function. S factor was taken from other publications and scaled according to the patient-specific mass. A comparison of the $TIAC_{WB}$ and d_{rm} from both methods was done using a non-inferiority test using a paired t-test or the Wilcoxon signed-rank test.

Results: The $TIAC_{WB}$ showed no significant difference between both methods (p=0.243). The calculated D_{rm} from a simplified Excel spreadsheet was assumed to be statistically non-inferior to the commercial OLINDA/EXM image-based dosimetry software with the non-inferiority margin of 0.02 ($p<0.05$).

Conclusion: The dose assessment from a simplified Excel spreadsheet is feasible and relatively low cost compared to the commercial OLINDA/EXM image-based dosimetry software.

Keywords: Red marrow absorbed dose, image-based dosimetry, radioiodine therapy, internal dosimetry

Öz

Amaç: Kırmızı iliğin absorbe ettiği doz (D_{rm}) kan dozimetresi kullanılarak hesaplanabilir. Ancak tam kan yöntemi zahmetli ve invaziftir. Bu nedenle, görüntü bazlı dozimetri tercih edilen yöntemdir. Bununla birlikte, ticari yazılım pahalıdır. Bu çalışmanın amacı, görüntü tabanlı radyoiyot kırmızı ilik dozimetrisi için basitleştirilmiş bir excel elektronik tablosu geliştirmektir.

Yöntem: Yirmi dokuz hastanın rutin tedavi öncesi dozimetri protokolündeki seri tüm vücut görüntüleri (2, 6, 24, 48 ve 72. saatlerde elde edilen) retrospektif olarak yeniden analiz edilmiştir. Rutin olarak, ticari OLINDA/EXM görüntü tabanlı dozimetri yazılımı, tüm vücut zamana entegre edilmiş aktivite katsayısı ($TIAC_{WB}$) ve D_{rm} [absorbe edilen doz katsayısı (d_{rm})] hesabı için kullanıldı. Basitleştirilmiş bir Excel elektronik tablosu için, tüm vücut sayısı satıcı tarafından sağlanan yazılımdan elde edilmiştir. Daha sonra $TIAC_{WB}$, Excel işlevi kullanılarak oluşturulan zaman-aktivite eğrisi ile hesaplandı. S faktörü diğer yayınlardan alınarak hastaya özel kitleye göre ölçeklendirildi. İki yöntem ile elde edilen $TIAC_{WB}$ ve d_{rm} değerlerinin karşılaştırması, bağımlı örneklem t-testi veya Wilcoxon işaretli sıralar testine dayalı bir non-inferiority test kullanılarak analiz edildi.

Bulgular: $TIAC_{WB}$ iki yöntem arasında anlamlı bir fark göstermedi (eşleştirilmiş örneklem t-testi ile p değeri 0,243). Basitleştirilmiş bir Excel elektronik tablosundan hesaplanan d_{rm} değerinin, 0,02'lik non-inferiority payı ile ticari OLINDA/EXM görüntü tabanlı dozimetri yazılımı ile hesaplanan değerden istatistiksel olarak non-inferior olduğu görülmüştür (Wilcoxon işaretli sıralar testi ile p değeri <0,05).

Address for Correspondence: Krisanat Chuamsaamarkkee Ph.D., Mahidol University Faculty of Medicine Ramathibodi Hospital, Department of Diagnostic and Therapeutic Radiology, Bangkok, Thailand **Phone:** +6622010824 **E-mail:** krisanat.chu@mahidol.ac.th ORCID ID: orcid.org/0000-0002-0362-9125
Received: 01.05.2020 **Accepted:** 28.07.2020

Sonuç: Basitleştirilmiş bir Excel elektronik tablosundan doz değerlendirmesi yapılabilir ve ticari OLINDA/EXM görüntü tabanlı dozimetri yazılımına kıyasla nispeten düşük maliyetlidir.
Anahtar kelimeler: Kırmızı iliğin absorbe ettiği doz, görüntüye dayalı dozimetri, radyoiyot tedavisi, internal dozimetri

Introduction

The red marrow is considered as one of the critical organs in radioiodine treatment (^{131}I-sodium iodide) of differentiated thyroid cancer (DTC). In radioiodine treatment, the absorbed dose to the blood as a surrogate for red marrow is often kept below 2 Gy to avoid hematological toxicity. This safety limit has been defined by blood dosimetry from blood sampling since the original work of Benua et al. (1) in 1962. Such a limit is still widely accepted, even though many new approaches have been introduced to calculate the red marrow absorbed dose such as external whole-body counting using a gamma probe and quantitative imaging using serials of whole-body scans obtained from nuclear medicine imaging modality (2,3,4).

Currently, quantitative imaging is the method of choice due to its non-invasive procedures excluding serial blood collections. Several commercial dosimetry softwares include the function to calculate the time-integrated activity coefficient (TIAC) and absorbed dose in organs using either serial planar whole-body scans or single photon emission computed tomography (SPECT) acquisitions (3,4). However, the image-based commercial dosimetry software is expensive, limiting its use in routine clinical practice. The objectives of this study were to develop a simplified excel spreadsheet for an image-based radioiodine bone marrow dosimetry and to compare the results of this spreadsheet with the commercial OLINDA/EXM image-based dosimetry software.

Materials and Methods

Patient Data Selection

Twenty-nine DTC patients who participated in the routine pretherapeutic dosimetry protocol between May 2017 to March 2019 for radioiodine treatment at the Surin Hospital (Surin Province, Thailand) were included in this retrospective study. Five patients were male and 24 were female. The mean age was 48.8 years (range: 19.0-76.0 years) at the time of the treatment. Ethics Committee Approval was obtained from the Ethical Review Board of the Surin Hospital with the approval number: 12/2562 and date: 9th April 2019.

The inclusion criteria for this routine pretherapeutic dosimetry protocol were DTC patients who had a near-total or total thyroidectomy, with withdrawn thyroid hormone for 4-6 weeks, low iodine diet intake, and serum thyroid-stimulating hormone >30 mIU/L before administration of radioiodine.

Dosimetry and Imaging Protocol

The pretherapeutic dosimetry protocol at the Surin Hospital was performed following European Association of Nuclear Medicine (EANM) standard operational procedures (3). Radioiodine ranging from 74 to 185 MBq was administered to patients. The whole-body data in this protocol were obtained from anterior and posterior conjugate views acquired at 2nd, 6th, 24th, 48th, and 72th hours postadministration. The gamma camera used for imaging was Symbia T16 SPECT/CT (Siemens Medical Solutions USA) and equipped with parallel-hole high energy collimators, using a 10% energy window set at 364 keV. The table speed for the whole-body images was 8 cm/min and the latter were acquired using a 256x1024 matrix. These protocol settings were applied to all patients and time points.

The Commercial OLINDA/EXM Image-based Dosimetry Software

In the pretherapeutic dosimetry protocol, the whole-body calculations were performed using a commercial HERMES OLINDA/EXM image-based dosimetry software (HERMES Medical Solution, Stockholm, Sweden). This software is the OLINDA/EXM version 1.1.

In this commercial software, the whole-body region of interest (ROI) in the anterior image was automatically mirrored and copied to the posterior image. The whole-body ROIs that had been defined in one of the whole-body scans were automatically copied to all other timepoints belonging to the same patient. Examples of image data and whole-body ROI are demonstrated in Figure 1a.

In OLINDA/EXM image-based dosimetry software, the activity in the images is converted from the counts using either standard activity or equipment detection efficiency. In this work, the camera detection efficiency was investigated and used for activity determination for all patients. Then, a bi-exponential function was fitted to the data. Consequently, the whole-body time-activity curve whole-body (TAC_{WB}) was generated. An example of TAC_{WB} is shown in Figure 1b.

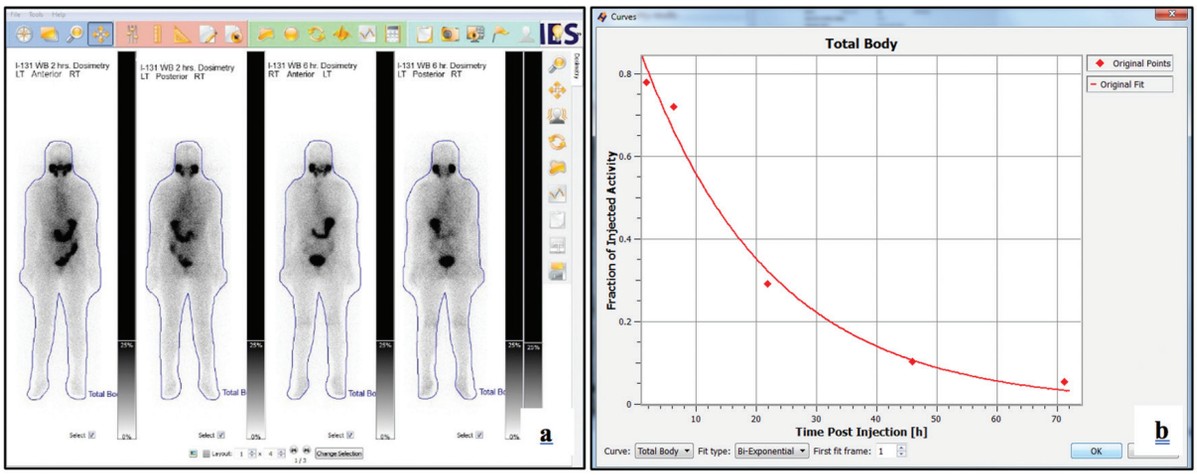

Figure 1. a) Sample screenshot of the image data and whole-body ROI of the commercial OLINDA/EXM image-based dosimetry software. **b)** The bi-exponential fit of the TAC
ROI: Region of interest, TAC: Time-activity curve, OLINDA/EXM: Organ Level Internal Dose Assessmant/Expanential Medelling

The whole-body $TIAC_{WB}$ (formally called residence time) is calculated from the area under TAC_{WB}. The exponential extrapolation with a numerical trapezoidal integration is employed in this OLINDA/EXM image-based dosimetry software. In this software, D_{rm} was calculated in terms of the absorbed dose coefficient (d_{rm}) (mGy/MBq). This commercial software uses the medical internal radiation dose schema and the Cristy and Eckerman (C&E) phantoms (5). In our work, doses were scaled using the patient-specific mass at the time of radioiodine treatment.

A Simplified Excel Spreadsheet

The serial whole-body images of 29 DTC patients were reanalyzed using the vendor-supplied Syngo software (Siemens Medical Solutions, USA) as illustrated in Figure 2a. Data were exported to an Excel spreadsheet (Microsoft Corp., Redmond, WA). For background correction, the average activity in the whole-body background ROIs (BKG_{av}) was subtracted from the average activity in the whole-body ROI (WB_{av}) and multiplied by the number of pixels in the whole-body image (N_{WB}) as illustrated in equation (1).

$$WB_{net} = N_{WB} \times (WB_{av} - BKG_{av}) \quad \text{equation (1)}$$

Then, the whole-body geometric mean (WB_{GM}) was calculated from the whole-body net anterior ($WB_{net(ant)}$) and whole-body net posterior ($WB_{net(post)}$) as shown in equation (2).

$$WB_{GM} = \sqrt{WB_{net(ant)} \times WB_{net(post)}} \quad \text{equation (2)}$$

In the excel spreadsheet, the equipment efficiency was also used to determine the activity similar to the OLINDA/EXM image-based software. Then, the whole-body activity of each time point was computed to the fraction of administered activity (FAA) using a mono-exponential function in MS Excel [as illustrated in equation (3)].

$$FAA(t) = \frac{A(t)}{A_0} = A \times e^{\lambda \times t} \quad \text{equation (3)}$$

Where, FAA(t) is the fraction of administered activity (A_0) as a function of time t and A and λ are fit constants. The $TIAC_{WB}$ (as shown in Figure 2b) in this spreadsheet were calculated by integrating the equation (3) from zero to infinity as shown in the following equation (3, 4).

$$TIAC_{WB} \int_0^{\infty} = FAA(t)dt \quad \text{equation (4)}$$

As recommended in the EANM guideline for bone marrow and whole-body dosimetry in radioiodine therapy for thyroid cancer, the contributors to D_{rm} were the activity in the extracellular fluid (ECF) ($D_{rm \leftarrow ECF}$) and the remainder of the body (RoB) ($D_{rm \leftarrow RoB}$) as illustrated in equation (4,5).

$$Drm = D_{rm \leftarrow ECF} + D_{rm \leftarrow RoB} \quad \text{equation (5)}$$

The contribution from the activity in the ECF is also called the blood method and assumes that the activity distribution in ECF is equal to the activity distribution in the plasma. However, the completed blood method is laborious, invasive, and resource consuming. Many groups have published using this method to avoid blood sampling (2,6,7,8).

In this spreadsheet, the method introduced by Thomas et al. (2) was used to estimate the blood TIAC ($TIAC_{blood}$) assuming that 14% of the $TIAC_{WB}$ can be attributed to blood as shown in equation (6). Thereby, the $D_{rm \leftarrow ECF}$ can be calculated by the activity concentration in blood and the red marrow ECF fraction (RMECFF) as shown in equation (7). The RMECFF was 0.19, based on Sgouros studied using

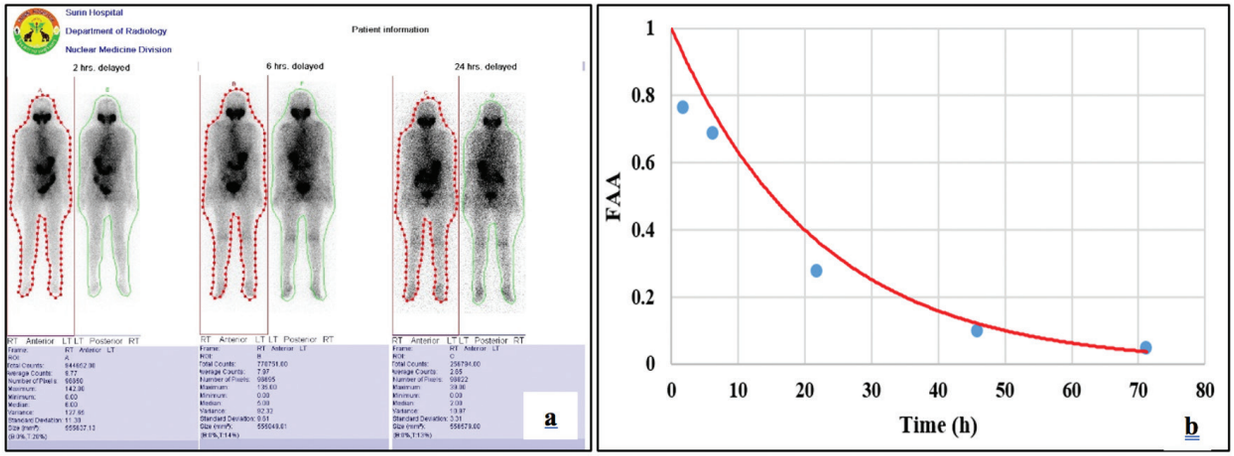

Figure 2. a) The whole-body ROI from the vendor-supplied Syngo software. **b)** The $TIAC_{WB}$ from a simplified eExcel spreadsheet
ROI: Region of interest, $TIAC_{WB}$: Whole-body time-integrated activity coefficient

a theoretical investigation of radiolabeled monoclonal antibodies (9). For $D_{rm\leftarrow ECF}$, the patient-specific bone marrow mass is not necessary as it is canceled out when the S value is scaled (2). For the S value for red marrow to red marrow, the C&E phantoms were also used (10).

$$TIAC_{blood} = 0.14 \times TIAC_{WB} \quad \text{equation (6)}$$

$$D_{rm\leftarrow ECF} = A_0 \times 0.19 \times m_{rm,phantom} \times S_{rm\leftarrow rm,phantom} \quad \text{equation (7)}$$

The remainder of the body TIAC ($TIAC_{RoB}$) can be calculated as the difference between the $TIAC_{WB}$ and the other source organs which is only in this case. in this spreadsheet was calculated by subtracting the $TIAC_{blood}$ from the $TIAC_{WB}$ as shown in equation (8). S value for the remainder of the body to red marrow was taken from the C&E phantoms ($S_{rm\leftarrow RoB,\ phantom}$). In this case, there were only two source organs. The patient-specific S value for the remainder of the body to red marrow ($S_{rm\leftarrow RoB,\ patient}$) was calculated using a linear scaling as recommended in the EANM guideline [illustrated in equation (9)] (4).

$$D_{rm\leftarrow RoB} = [A_0 \times (TIAC_{WB} - TIAC_{blood})] \times S_{rm\leftarrow RoB,\ patient} \quad \text{equation (8)}$$

$$S_{rm\leftarrow RoB,patient} = [S_{rm\leftarrow WB,phantom} \cdot \frac{m_{WB,phantom}}{m_{WB,\ phantom} - m_{RM,\ phantom}} - S_{rm\leftarrow rm,phantom} \cdot \frac{m_{rm,phantom}}{m_{WB,\ phantom} - m_{rm,\ phantom}}] \cdot \frac{m_{WB,phantom}}{m_{WB,\ patient}} \quad \text{equation (9)}$$

Where, $m_{rm,phantom}$, $m_{WB,phantom}$ an $dm_{WB,patient}$ are the red marrow mass, the whole-body mass of the C&E phantoms, and the whole-body mass of the patient respectively (10).

In the same manner, d_{rm} was computed from the D_{rm} normalized by administered activity A_0. The unit of d_{rm} is mGy/Mbq.

Statistical Analysis

SPSS version 20 (IBM Inc., NY, USA) was used for statistical analysis. The $TIAC_{WB}$ and the D_{rm} calculated from the commercial OLINDA/EXM image-based dosimetry software and a simplified excel spreadsheet were expressed as mean ± standard deviation (SD). A comparison of the $TIAC_{WB}$ and the d_{rm} from both methods was statistically assessed using a non-inferiority test based on the paired t-test when normality was assumed or the Wilcoxon signed-rank test for the case of non-normality (11). Pearson's correlation was also used to study the correlation between both methods (12).

Results

This retrospective study included 29 patients who participated in the pretherapeutic dosimetry protocol for radioiodine therapy. In this work, the $TIAC_{WB}$ and the d_{rm} were reanalyzed using a simplified excel spreadsheet. The mean (± SD) and range (minimum-maximum) of the $TIAC_{WB}$ and the d_{rm} are summarized in Table 1. The calculated $TIAC_{WB}$ showed no statistically significant difference between the two methods (p value 0.243 using a two-sided paired t-test because normality was assumed). The Pearson correlation coefficient was 0.851 (p value <0.001) (Figure 3).

The calculated d_{rm} from the commercial OLINDA/EXM image-based dosimetry software was 0.0653±0.0233 mGy/MBq (range: 0.0268 to 0.1280 mGy/MBq). After reanalysis with a simplified excel spreadsheet, the mean (± SD) of the d_{rm} was 0.0798±0.0220 mGy/MBq (range: 0.0356 to 0.1433 mGy/MBq). For D_{rm}, the statistical results showed that the calculated d_{rm} from a simplified excel spreadsheet was statistically non-inferior to that from the commercial

Table 1. The mean (mean ± SD) and range (minimum - maximum) of the $TIAC_{WB}$ in hours and d_{rm} in mGy/MBq calculated from the commercial OLINDA/EXM image-based dosimetry software and a simplified excel spreadsheet

Dosimetric parameter	The commercial OLINDA/EXM image-based dosimetry software		A simplified excel preadsheet	
	Mean ± SD	Range	Mean ± SD	Range
$TIAC_{WB}$ (h)	24.42±8.71	9.61-46.03	23.28±5.00	13.24-31.49
d_{rm} (mGy/MBq)	0.0653±0.0233	0.0268-0.1280	0.0798±0.0220	0.0356-0.1433

SD: Standard deviation, $TIAC_{WB}$: Whole-body time-integrated activity coefficient, d_{rm}: Absorbed dose coefficient, OLINDA/EXM: Organ Level Internal Dose Assessmant/ Expanential Medelling

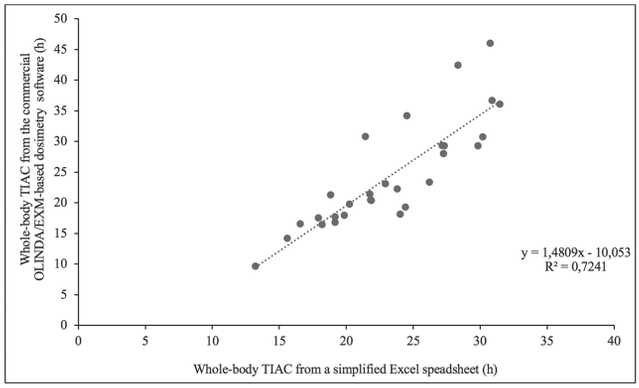

Figure 3. Correlation of the $TIAC_{WB}$ calculated from a simplified Excel excel spreadsheet and the commercial OLINDA/EXM image-based dosimetry software

$TIAC_{WB}$: Whole-body time-integrated activity coefficient

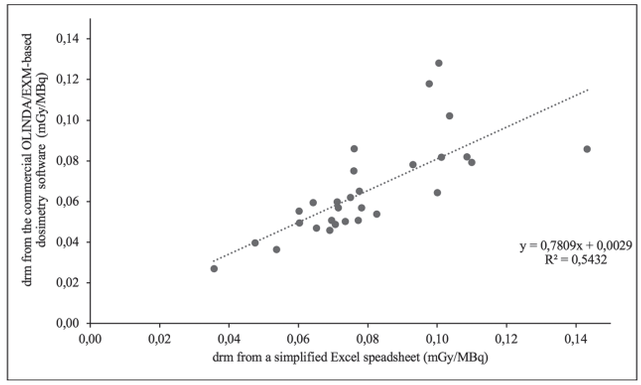

Figure 4. Correlation of the d_{rm} calculated from a simplified Excel excel spreadsheet and the commercial OLINDA/EXM image-based dosimetry software

d_{rm}: Absorbed dose coefficient

OLINDA/EXM image-based dosimetry software with a non-inferiority margin of 0.02 (p value <0.05 using the Wilcoxon signed-rank test because non-normality was assumed). The non-inferiority margin of 0.02 was set based on SD of d_{rm} from the commercial OLINDA/EXM image-based dosimetry software that was used in the pretherapeutic dosimetry protocol. Pearson's correlation coefficient was 0.737 (p value <0.001) as illustrated in Figure 4.

Discussion

Image-based red marrow dosimetry calculation in radioiodine therapy is performed to maximize the radiation dose to remnant thyroid or metastasis CT while considering the patient's safety by minimizing bone marrow toxicity. The primary parameter requested for internal dosimetry is often the TIAC (13). In this study, the calculated from a simplified excel spreadsheet was slightly shorter than that using the commercial OLINDA/EXM image-based dosimetry software. The mean percentage difference in $TIAC_{WB}$ between both methods was 0.41%. Many factors affect TIAC estimation such as counts-to-activity conversion method, ROI delineation, background correction, and method of fit and integration of TAC.

In this study, the counts-to-activity conversion was similar using equipment efficiency for both methods. For ROI delineations, there were drastic differences between the commercial OLINDA/EXM image-based dosimetry software and a simplified excel spreadsheet. As regards illustration, the commercial OLINDA/EXM image-based dosimetry software has an advanced option to draw and automatically copy ROIs from the initial whole-body to all the other images belonging to the same patient. In contrast, the ROI in a simplified Excel spreadsheet was manually drawn using the vendor-supplied software. Many studies have reported that ROI delineation was one of the critical uncertainty factors for dose calculation in nuclear medicine (14,15,16). For the fit and integration method, a simplified excel spreadsheet was used; the mono-exponential fit (also called single exponential function) in MS Excel. The commercial OLINDA/EXM image-based dosimetry software was fitted using a bi-exponential fit function. According to the EANM guideline for pretherapeutic dosimetry in DTC, the bi-exponential fitting is suggested to determine the (3). Many simplified approaches have been developed and illustrate that the simple mono-exponential could be used in routine practice (17,18). However, errors of the mono-exponential might be higher since such a fitting

does not reflect realistic kinetics in the uptake and long-term retention phase of radioiodine kinetics (17). The most desirable next step is to include the bi-exponential fit in our excel spreadsheet to improve the accuracy of TIAC. Comparison of the presented in this work with other publications is tabulated in Table 2.

Table 2. Comparison of the $TIAC_{WB}$ of DTC patients in this study with previous studies

	$TIAC_{WB}$ (h) mean ± SD
Previous studies	
Hänscheid (29) (2006)	24.10±7.80
Willegaignon et al. (25) (2012)	25.77±6.98
Willegaignon et al. (23) (2016)	29.18±18.14
Present study	
A simplified excel spreadsheet The commercial OLINDA/EXM image-based dosimetry software	23.28±5.00 24.42±8.71

$TIAC_{WB}$: Whole-body time-integrated activity coefficient, DTC: Differentiated thyroid cancer, SD: Standard deviation, OLINDA/EXM: Organ Level Internal Dose Assessmant/Expanential Medelling

It was found that most publications reported a large SD in the $TIAC_{WB}$, like our findings. The possible explanations for high SD for $TIAC_{WB}$ in radioiodine treatment might be related to the disease characteristic of ablation in DTC patients such as metastasis, iodine intake/uptake, hormonal level, age of the treated patient.

As previously explained, the d_{rm} is the ratio between the bone marrow absorbed dose and administered activity. In this study, the difference in the d_{rm} from a simplified excel spreadsheet and the commercial OLINDA/EXM image-based dosimetry software was -26.98%. Many factors affect d_{rm}, including the phantom and S factor. In our study, both methods used the C&E phantoms, but different versions. The simplified excel spreadsheet used the C&E phantoms from the study of Stabin et al. (19) in 1995 whereas, the commercial OLINDA/EXM image-based dosimetry software used the newer version from the study of Stabin et al. (5) in 2003. The latter version used the bone marrow specific absorbed fraction from the EGS4 Monte Carlo code.

Statistical comparison of the d_{rm} from both methods was analyzed using a non-inferiority test. Generally, this test is used to assess that a new drug or new treatment is not worse than the main comparator drug or a reference treatment by more than a non-inferiority margin (11,20). In this study, the non-inferiority margin of 0.02 was set. This value was based on the SD of d_{rm} from the commercial OLINDA/EXM image-based dosimetry software and other published works (as illustrated in Table 3). The non-inferiority test showed that a simplified Excel spreadsheet software was no worse than the commercial OLINDA/EXM image-based dosimetry software at the non-inferiority margin.

For comparison, the mean values of d_{rm} calculated from both methods were compared with the values reported by other groups as demonstrated in Table 3.

Table 3. Comparison of the d_{rm} of DTC patients in this study with previous studies

	d_{rm} (mGy/MBq) mean ± SD
Previous studies	
Traino et al. (21) (2007)	0.0739±0.0217
Miranti et al. (22) (2015)	0.0845±0.0385
Willegaignon et al. (23) (2016)	0.0660±0.0550
Alan Selcuk et al. (24) (2018)	0.1079±0.0319
Present study	
A simplified excel spreadsheet	0.0798±0.0220
The commercial OLINDA/EXM image-based dosimetry software	0.0653±0.0233

d_{rm}: Absorbed dose coefficient, DTC: Differentiated thyroid cancer, SD: Standard deviation

In this study, the mean and SD of d_{rm} from the simplified excel spreadsheet was 0.0798±0.0220 mGy/MBq. Traino et al. (21) and Miranti et al. (22) calculated the d_{rm} using the reference data from the RADAR website with an estimated d_{rm} of 0.0739±0.0217 mGy/MBq and 0.0845±0.0385 mGy/MBq, respectively. Willegaignon et al.(23) also computed the d_{rm} from whole-body images using the OLINDA/EXM software with a mean of 0.0660±0.0550 mGy/MBq. Similarly, the d_{rm} calculated by Alan Selcuk et al. (24) using the same software was 0.1079±0.0319 mGy/MBq.

From these results, the reference phantom and S factor value greatly impacted the d_{rm}. This is coherent with many studies and the difference in the dosimetry can be greater than 150% when using different phantoms and S factors (25,26,27,28). Hence, the selection of phantom is an important factor in the dosimetry calculation. Although the d_{rm} results showed some differences between both the software, the clinical outcome is still difficult to prove at this stage.

Study Limitations

The small number of patients and the heterogeneity of the stages of the disease (local or distant metastasis) in the patient group might have biased the outcome of this study.

Conclusion

The $TIAC_{WB}$ calculated from a simplified excel spreadsheet was not statistically different from that of the software. The calculated d_{rm} using the simplified excel was non-inferior to that calculated by the software with an acceptable margin.

It can be concluded that a simplified excel spreadsheet can be used to calculate the d_{rm} in radioiodine therapy of DTC patients. The dose assessment using this method is feasible and relatively low cost compared to the commercial OLINDA/EXM image-based dosimetry software. Hence, the simplified Excel spreadsheet should increase the number of dosimetry studies in low or middle-income countries, though it requires further validation with more patients. Also, a method for improving TAC integration and the updated phantom for S-factor should be further considered.

Ethics

Ethics Committee Approval: Ethics Committee Approval was obtained from the Ethical Review Board of the Surin Hospital with the approval number: 12/2562 and date: 9th April 2019.

Informed Consent: This retrospective study represents no more than minimal risk to subjects and will not adversely affect their rights and welfare. Due to the impracticality of contacting those individuals no longer in follow-up at Surin Hospital. Hence, the authors are requesting waiver of consent from the Ethical Review Board.

Peer-review: Externally peer-reviewed.

Authorship Contributions

Surgical and Medical Practices: K.R., Concept: K.C., Design: K.C., P.C., Data Collection or Processing: R.S., Analysis or Interpretation: R.S., K.R., Literature Search: R.S., P.C.,

Writing: K.C., P.C.

Conflict of Interest: No conflict of interest was declared by the authors.

Financial Disclosure: The authors declared that this study has received no financial support.

References

1. Benua RS, Cicale NR, Sonenberg M, Rawson RW. The relation of radioiodine dosimetry to results and complications in the treatment of metastatic thyroid cancer. Am J Roentgenol Radium Ther Nucl Med 1962;87:171-182.
2. Thomas SR, Samaratunga RC, Sperling M, Maxon HR, 3rd. Predictive estimate of blood dose from external counting data preceding radioiodine therapy for thyroid cancer. Nucl Med Biol 1993;20:157-162.
3. Lassmann M, Hanscheid H, Chiesa C, Hindorf C, Flux G, Luster M, EANM Dosimetry Committee. EANM Dosimetry Committee series on standard operational procedures for pre-therapeutic dosimetry I: blood and bone marrow dosimetry in differentiated thyroid cancer therapy. Eur J Nucl Med Mol Imaging 2008;35:1405-1412.
4. Hindorf C, Glatting G, Chiesa C, Linden O, Flux G, Committee ED. EANM Dosimetry Committee guidelines for bone marrow and whole-body dosimetry. Eur J Nucl Med Mol Imaging 2010;37:1238-1250.
5. Stabin MG, Siegel JA. Physical models and dose factors for use in internal dose assessment. Health Phys 2003;85:294-310.
6. Hanscheid H, Lassmann M, Luster M, Kloos RT, Reiners C. Blood dosimetry from a single measurement of the whole body radioiodine retention in patients with differentiated thyroid carcinoma. Endocr Relat Cancer 2009;16:1283-1289.
7. Sisson JC, Shulkin BL, Lawson S. Increasing efficacy and safety of treatments of patients with well-differentiated thyroid carcinoma by measuring body retentions of 131I. J Nucl Med 2003;44:898-903.
8. Traino AC, Di Martino F, Boni G, Mariani G, Lazzeri M. A minimally invasive method to evaluate 131I kinetics in blood. Radiat Prot Dosimetry 2004;109:249-252.
9. Sgouros G. Bone marrow dosimetry for radioimmunotherapy: theoretical considerations. J Nucl Med 1993;34:689-694.
10. Stabin MG, Sparks RB, Crowe E. OLINDA/EXM: the second-generation personal computer software for internal dose assessment in nuclear medicine. J Nucl Med 2005;46:1023-1027.
11. NCSS. Paired T-Test for Non-Inferiority. In: NCSS, editor. Utah K.
12. Evans JD. Straightforward statistics for the behavioral sciences. Pacific Grove: Brooks/Cole Pub. Co, 1996.
13. Bolch WE, Eckerman KF, Sgouros G, Thomas SR. MIRD pamphlet No. 21: a generalized schema for radiopharmaceutical dosimetry–standardization of nomenclature. J Nucl Med 2009;50:477-484.
14. Gear JI, Cox MG, Gustafsson J, Gleisner KS, Murray I, Glatting G, Konijnenberg M, Flux GD. EANM practical guidance on uncertainty analysis for molecular radiotherapy absorbed dose calculations. European Journal of Nuclear Medicine and Molecular Imaging. 2018;45:2456-2474.
15. Götz TI, Schmidkonz C, Lang EW, Maier A, Kuwert T, Ritt P. Factors affecting accuracy of S values and determination of time-integrated activity in clinical Lu-177 dosimetry. Ann Nucl Med 2019;33:521-531.
16. Pereira JM, Stabin MG, Lima FR, Guimaraes MI, Forrester JW. Image quantification for radiation dose calculations–limitations and uncertainties. Health Phys 2010;99:688-701.
17. Hermanska J, Karny M, Zimak J, Jirsa L, Samal M, Vlcek P. Improved prediction of therapeutic absorbed doses of radioiodine in the treatment of thyroid carcinoma. J Nucl Med 2001;42:1084-1090.
18. Jentzen W, Bockisch A, Ruhlmann M. Assessment of Simplified Blood Dose Protocols for the Estimation of the Maximum Tolerable Activity in Thyroid Cancer Patients Undergoing Radioiodine Therapy Using 124I. J Nucl Med 2015;56:832-838.
19. Stabin MG, Watson, EE, Cristy M, Ryman JC, Eckerman KF, Davis JL, Marshall D, Gehlen MK. Mathematical models and specific absorbed fractions of photon energy in the nonpregnant adult female and at the end of each trimester of pregnancy. 1995.

20. NCSS. Two Correlated Proportions Non-Inferiority, Superiority, and Equivalence Tests. In: NCSS, editor. USA: Utah K,.
21. Traino AC, Ferrari M, Cremonesi M, Stabin MG. Influence of total-body mass on the scaling of S-factors for patient-specific, blood-based red-marrow dosimetry. Phys Med Biol 2007;5231-5248.
22. Miranti A, Giostra A, Richetta E, Gino E, Pellerito RE, Stasi M. Comparison of mathematical models for red marrow and blood absorbed dose estimation in the radioiodine treatment of advanced differentiated thyroid carcinoma. Phys Med Biol 2015;60:1141-1157.
23. Willegaignon J, Pelissoni RA, Lima BC, Sapienza MT, Coura-Filho GB, Queiroz MA, Buchpiguel CA. Estimating (131)I biokinetics and radiation doses to the red marrow and whole body in thyroid cancer patients: probe detection versus image quantification. Radiol Bras 2016;49:150-157.
24. Alan Selcuk N, Toklu T, Beykan S, Karaaslan SI. Evaluation of the dosimetry approaches in ablation treatment of thyroid cancer. J Appl Clin Med Phys 2018;19:134-140.
25. Willegaignon J, Sapienza MT, Buchpiguel CA. Comparison of different dosimetric methods for red marrow absorbed dose calculation in thyroid cancer therapy. Radiat Prot Dosimetry 2012;149:138-146.
26. Josefsson A, Hobbs RF, Ranka S, Schwarz BC, Plyku D, Willegaignon de Amorim de Carvalho J, et al. Comparative Dosimetry for (68) Ga-DOTATATE: Impact of Using Updated ICRP Phantoms, S Values, and Tissue-Weighting Factors. Journal of nuclear medicine : official publication, Soc Nucl Med 2018;59:1281-1288.
27. Lamart S, Bouville A, Simon SL, Eckerman KF, Melo D, Lee C. Comparison of internal dosimetry factors for three classes of adult computational phantoms with emphasis on I-131 in the thyroid. Physics in medicine and biology. 2011;56:7317-7335.
28. Andersson M, Johansson L, Minarik D, Leide-Svegborn S, Mattsson S. Effective dose to adult patients from 338 radiopharmaceuticals estimated using ICRP biokinetic data, ICRP/ICRU computational reference phantoms and ICRP 2007 tissue weighting factors. EJNMMI physics. 2014;1:9.
29. Hänscheid H, Lassmann M, Luster M, Thomas SR, Pacini F, Ceccarelli C, Ladenson PW, Wahl RL, Schlumberger M, Ricard M, Driedger A, Kloos T, Sherman AI, Haugen BR, Carriere V, Corone C, Reiners C. Iodine biokinetics and dosimetry in radioiodine therapy of thyroid cancer: procedures and results of a prospective international controlled study of ablation after rhTSH or hormone withdrawal. J Nucl Med 2006;47:648-654.

Interesting Image
Mol Imaging Radionucl Ther 2020;29:132-134 DOI:10.4274/mirt.galenos.2019.75437

Mickey Mouse Sign on Bone Scan in the Monostotic Form of Paget's Disease Mimicking Osseous Metastasis

Metastazı Taklit Eden Monostotik Tip Paget Hastalığı'nda Mickey Mouse İşareti

Selin Kesim, Halil Turgut Turoğlu, Salih Özgüven, Tunç Öneş, Tanju Yusuf Erdil
Marmara University Training and Research Hospital, Clinic of Nuclear Medicine, İstanbul, Turkey

Abstract

Paget's disease is a chronic benign bone disease characterized by excessive and abnormal bone remodeling. Monostotic Paget's disease accounts for only 20% of the cases, and the monostotic form involving the vertebra with the Mickey Mouse sign is very rare. Herein, we report a case of suspected bony metastasis in the second lumbar vertebra that was diagnosed as Paget's disease because of the Mickey Mouse sign on bone scintigraphy, and the diagnosis was confirmed by biopsy. Therefore, bone scintigraphy may provide a positive contribution to the diagnosis, and may help to avoid unnecessary biopsy in cases with specific signs and patterns.

Keywords: Paget's disease, monostotic Paget's disease, spine, Mickey Mouse sign, technetium 99m-methylene diphosphonate bone scintigraphy, SPECT/CT

Öz

Paget, aşırı ve anormal kemik yapımı ve yıkımı ile karakterize kronik, iyi huylu bir kemik hastalığıdır. Monostotik Paget hastalığı, sadece olguların %20'sini oluşturmakla kalmaz; Mickey Mouse bulgusu olan, vertebra tutulumu ile giden monostotik formu daha da nadirdir. Sunduğumuz olguda, ikinci lumbar vertebrada metastaz şüphesi ile araştırılan hastada; kemik sintigrafisinde Mickey Mouse işareti görülmesi üzerine Paget hastalığı tanısı kondu ve tanı biyopsiyle doğrulandı. Bu olguda görülmektedir ki; kemik sintigrafisi tanıya olumlu katkıda bulunur ve belirli belirti ve paternler görülmesi sayesinde gereksiz biyopsileri önleyebilir.

Anahtar kelimeler: Paget hastalığı, monostotik Paget hastalığı, vertebra, Mickey Mouse işareti, teknesyum 99m-metilen difosfonat kemik sintigrafisi, SPECT/BT

Address for Correspondence: Selin Kesim MD, Marmara University Training and Research Hospital, Clinic of Nuclear Medicine, İstanbul, Turkey
Phone: +90 216 396 86 48 **E-mail:** selinkesim@yandex.com ORCID ID: orcid.org/0000-0002-6164-9781
Received: 05.09.2019 **Accepted:** 22.11.2019

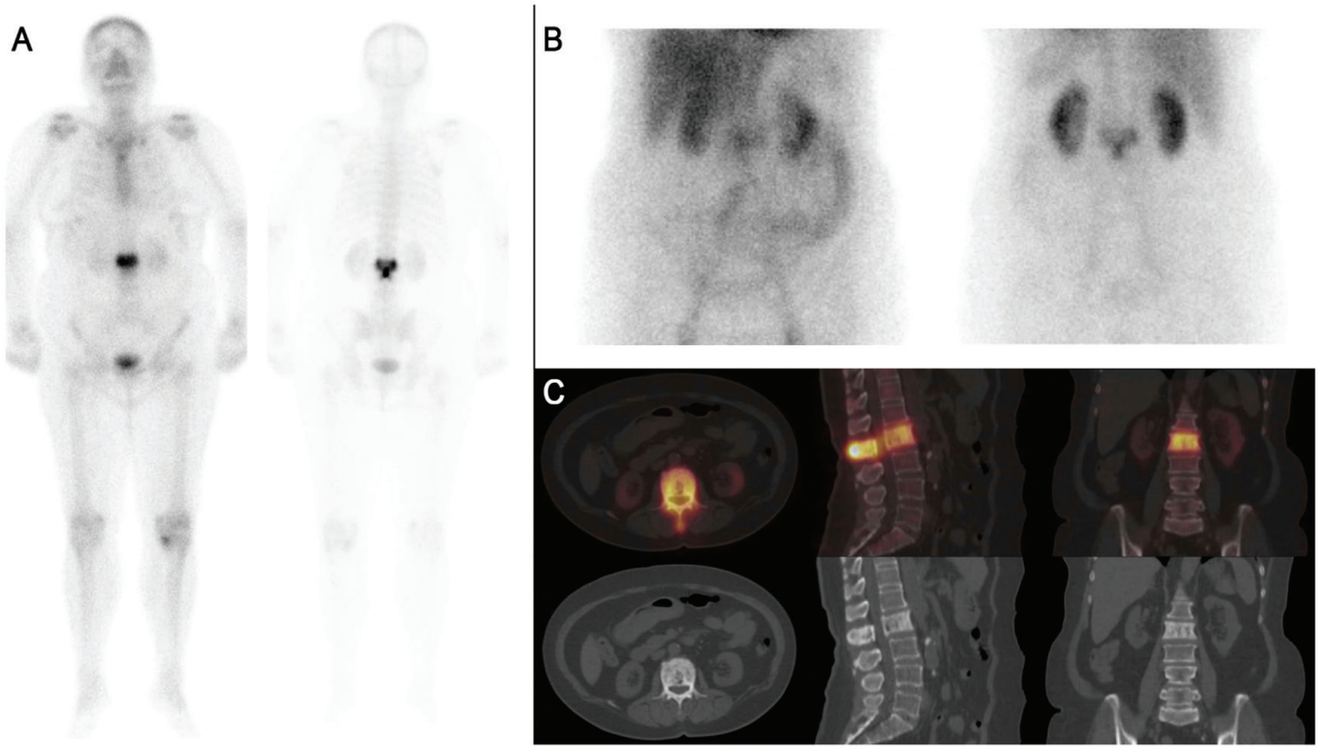

Figure 1. A 62-year-old woman who presented with a two-year history of low back pain was referred for bone scintigraphy. Technetium 99m-methylene diphosphonate [Tc-99m methyl diphosphonate (MDP)] whole body bone scan revealed an intensely increased uptake throughout the whole second lumbar vertebra (L-2), involving the body, posterior elements, and spinous process (A). The simultaneously performed three-phase bone scintigraphy demonstrated increased blood flow and local hyperemia on the respective dynamic blood flow and static blood pool images that accompanied the increased uptake involving the L-2 vertebra (B). The single photon emission computerized tomography/computed tomography (SPECT/CT) hybrid imaging revealed vertebral expansion with diffuse sclerosis involving the body and posterior vertebral arch of the second lumbar vertebra, correlating with the diffuse and intense Tc-99m MDP uptake in the entire vertebra (C).

Paget's disease of bone (PD), which is a chronic benign bone disease characterized by excessive and abnormal bone remodeling, has three phases: the early lytic phase, the second mixed phase, and the final sclerotic phase. The pelvis is the most commonly affected bone, followed by the spine, skull, femur, scapula, tibia, and humerus. Pagetic lesions are commonly (approximately 70-80% of the cases) multiple (polyostotic) lesions (1).

Bone scintigraphy is useful not only to survey the entire skeleton for PD, but also to screen for complications like fracture and malignant transformation, and to monitor the response to therapy. The monostotic form of PD, as in this case, is not common and may lead to a misdiagnosis with a variety of metabolic and neoplastic diseases (2). Vertebral neoplasia (including metastases) may involve both the vertebral body and partially the posterior vertebral arch. However, the spinous process is spared in most of these cases.

Multimodality imaging using s SPECT/CT integrates different techniques to make a correct diagnosis, and avoids unnecessary biopsy. The advantages of bone SPECT/CT imaging are as follows: it may be performed on the same day after the bone scan and it provides anatomical detail and morphological information (3,4,5).

The "Mickey Mouse" or "Mouse Face" sign, which typically shows an upside-down triangle consisting of three foci of intense radiopharmaceutical uptake, and corresponding to the involvement of the pedicles and spinous process, is a specific and rare pattern of Paget's disease.

This sign was originally described by Van Heerden (6). Subsequently, Kim et al. (7) reported this "Mouse Face" appearance of the vertebrae as a specific finding of bone PD. Additionally, Rotés-Sala et al. (8) described the "clover sign," where the vertebral pedicles and spinous process are affected.

The recognition of typical patterns like the "Mickey Mouse sign" in this case, together with the increased blood flow and hyperemia on the three-phase bone scintigraphy and using the multimodality imaging (SPECT/CT in our case) to demonstrate the accompanying vertebral expansion, and sclerosis increases the specificity and diagnostic accuracy of bone scan in the identification of PD

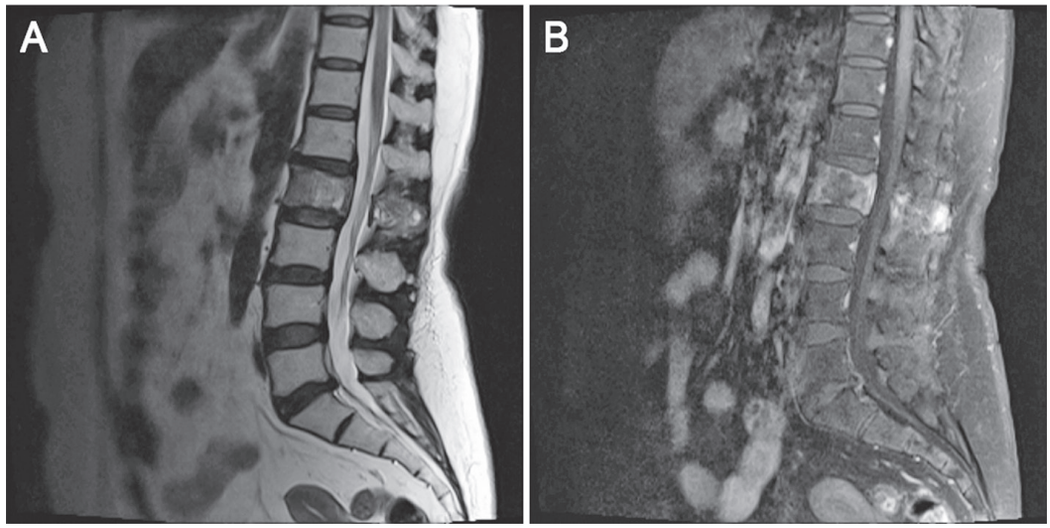

Figure 2. T2-weighted lumbar magnetic resonance imaging (MRI) images depicted diffuse heterogeneous density changes (A) and contrast-enhanced T1-weighted MRI images showed contrast enhancement involving the body of the second lumbar vertebra that was extending to the posterior elements, and reported as suspicion for osseous metastasis (B)

Ethics

Informed Consent: We have obtained all appropriate patient consent forms. In the form the patient has given her consent for her images and other clinical information to be reported in the journal.

Peer-review: Externally peer-reviewed.

Authorship Contributions

Surgical and Medical Practices: S.K., Concept: H.T.T., S.Ö., Design: T.Ö., T.Y.E., Data Collection or Processing: S.K., Analysis or Interpretation: H.T.T., Literature Search: H.T.T., Writing: S.K., H.T.T.

Conflict of Interest: No conflict of interest was declared by the authors.

Financial Disclosure: The authors declared that this study received no financial support.

References

1. Dohan A, Parlier-Cuau C, Kaci R, Touraine S, Bousson V, Larédo JD. Vertebral involvement in Paget's disease: morphological classification of CT and MR appearances. Joint Bone Spine 2015;82:18-24.
2. Senthil V, Balaji S. Monostotic Paget Disease of the Lumbar Vertebrae: A Pathological Mimicker. Neurospine 2018;15:182-186.
3. Whitehouse RW, Davies AM. Paget's disease of bone. Semin Musculoskelet Radiol 2002;6:313-322.
4. Scutellari PN, Giorgi A, De Sario V, Campanati P. Correlation of multimodality imaging in Paget's disease of bone. Radiol Med 2005;110:603-615.
5. Farid K, Caillat-Vigneron N. SPECT-CT improves the identification of Paget's disease of bone. Joint Bone Spine 2010;77:370-371.
6. Van Heerden BB. Mickey Mouse sign in Paget's disease. J Nucl Med 1994;35:924-925.
7. Kim CK, Estrada WN, Lorberboym M, Pandit N, Religioso DG, Alavi A. The "mouse face" appearance of the vertebrae in Paget's disease. Clin Nucl Med 1997;22:104-108.
8. Rotés-Sala D, Monfort J, Solano A, Miralles E, Vila J, Carbonell J. The clover and heart signs in vertebral scintigraphic images are highly specific of Paget's disease of bone. Bone 2004;34:605-608.

Interesting Image
Mol Imaging Radionucl Ther 2020;29:135-138 DOI:10.4274/mirt.galenos.2020.50455

Comparative Findings Between ^{68}Ga-PSMA and ^{18}F-FDG PET/CT for Hepatocellular Carcinoma

Hepatoselüler Karsinomda ^{68}Ga-PSMA ve ^{18}F-FDG PET/BT ile Karşılaştırmalı Bulgular

Seval Erhamamcı[1], Nesrin Aslan[2]

[1]*Başkent University Faculty of Medicine, Ankara; Başkent University İstanbul Hospital, Department of Nuclear Medicine, İstanbul, Turkey*
[2]*Neolife Medical Center, Clinic of Nuclear Medicine, İstanbul, Turkey*

Abstract

We have reported here the case of a 69-year-old man who presented with spinal cord compression due to bone metastases as the first manifestation of hepatocellular carcinoma (HCC). For the initial staging, the patient underwent ^{18}F-fluorodeoxyglucose (FDG) positron emission tomography/computerized tomography (PET/CT) imaging, which demonstrated mild ^{18}F-FDG uptake in the multiple expansile osteolytic bone lesions, but no remarkable atypical ^{18}F-FDG uptake in the liver lesion on low-doses CT. An additional PET/CT scan was performed to evaluate the prostate-specific membrane antigen (PSMA) expression, which has recently been reported to be a potential biological marker in a variety of tumors including HCC. High PSMA uptake was recorded in both the metastatic bone lesions and the primary liver lesion/tumor by the ^{68}Ga-PSMA PET/CT.

Keywords: Hepatocellular carcinoma, bone metastases, PET/CT, ^{68}Ga-PSMA, ^{18}F-FDG

Öz

Hepatoselüler karsinomun (HSK) ilk belirtisi olarak, kemik metastazının neden olduğu spinal kord kompresyonu ile başvuran 69 yaşında bir erkek hastayı tanımladık. Başlangıç evreleme için, hastaya ^{18}F-florodeoksiglukoz (FDG) pozitron emisyon tomografisi/bilgisayarlı tomografi (PET/BT) görüntüleme yapıldı. Görüntüleme çok sayıda ekspansil osteolitik kemik lezyonlarında hafif ^{18}F-FDG tutulumu gösterdi ve düşük doz BT'deki karaciğer lezyonunda kayda değer atipik ^{18}F-FDG tutulumu göstermedi. HSK'da dahil olmak üzere çeşitli tümörlerde potansiyel bir biyolojik marker olduğu bildirilen prostat spesifik membran antijen (PSMA) ekspresyonunu değerlendirmek için ek bir PET/BT görüntüleme yapıldı. Hem metastatik kemik lezyonlarında hem de primer karaciğer lezyonunda/tümöründe yüksek PSMA tutulumu ^{68}Ga-PSMA PET/BT ile saptandı.

Anahtar kelimeler: Hepatoselüler karsinom, kemik metastazı, PET/BT, ^{68}Ga-PSMA, ^{18}F-FDG

Address for Correspondence: Seval Erhamamcı MD, Baskent University Faculty of Medicine, Ankara; Baskent University İstanbul Hospital, Department of Nuclear Medicine, İstanbul, Turkey **Phone:** +90 216 554 15 00 **E-mail:** sevaler@yahoo.com ORCID ID: orcid.org/0000-0001-5016-4650
Received: 26.04.2020 **Accepted:** 29.06.2020

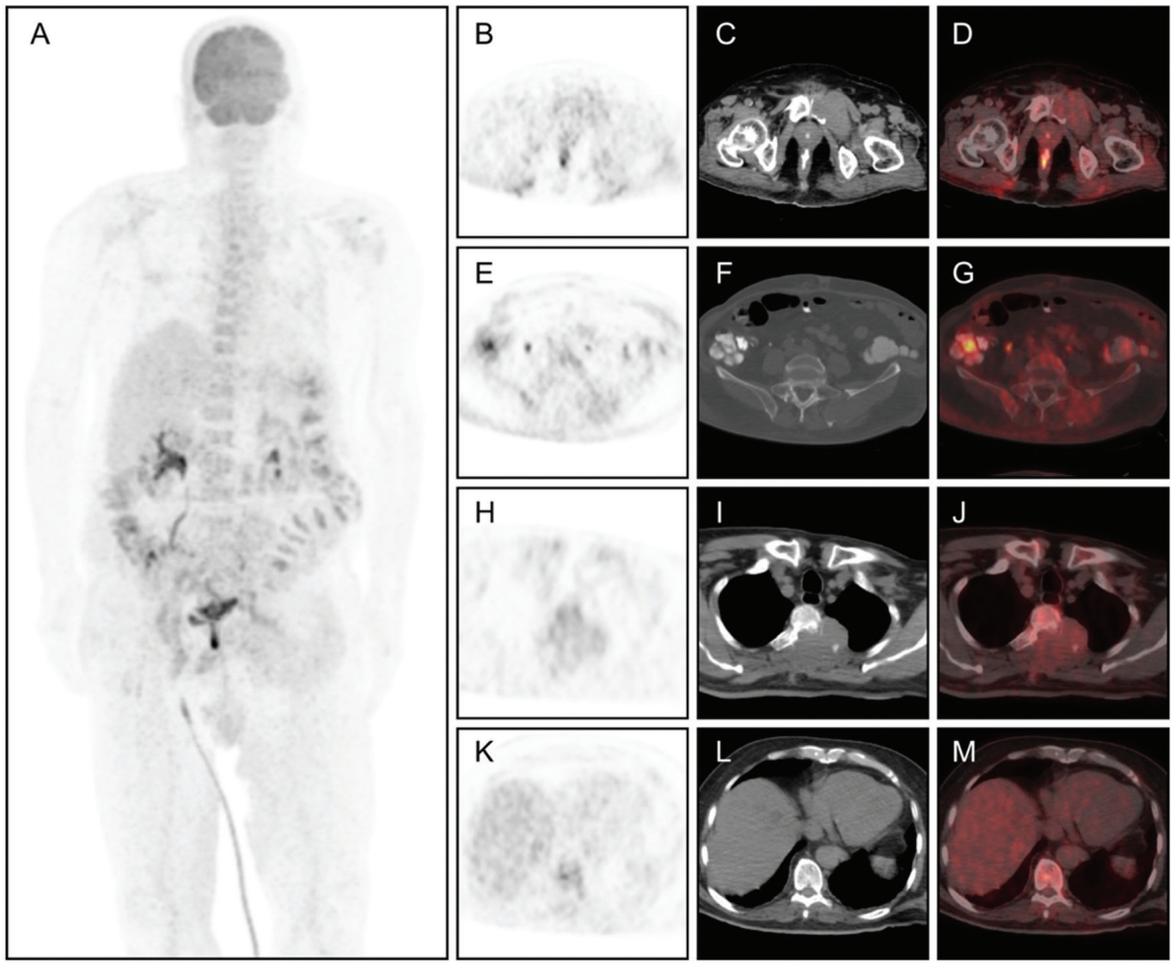

Figure 1. The case patient was a 69-year-old man who presented with the complaint of back pain. His magnetic resonance imaging revealed multiple metastatic lesions of the thoracic vertebral with spinal cord compression and bilateral iliac bones. Excisional biopsy of the T2-3 vertebral lesion due to spinal cord compression was also performed. Histopathological examination demonstrated metastatic malign tumor, which was consistent with the signs of hepatocellular carcinoma (HCC) metastases. The patient accordingly underwent ^{18}F- fluorodeoxyglucose (FDG) positron emission tomography/computerized tomography (PET/CT) imaging for initial staging. The scan MIP **(A)**, transaxial PET **(B, E, H, K), CT (C, F, I, L)**, and fused **(D, G, J, M)** images revealed mild uptake [maximum standardized uptake value (SUV_{max})= 4.8] in the multiple osteolytic bone lesions in the thoracal vertebra, iliac bones, and sacroiliac joints, most of which also showed remarkable soft tissue components. On the other hand, no significant atypical uptake was noted in the primary liver tumor in the corresponding low-dose CT

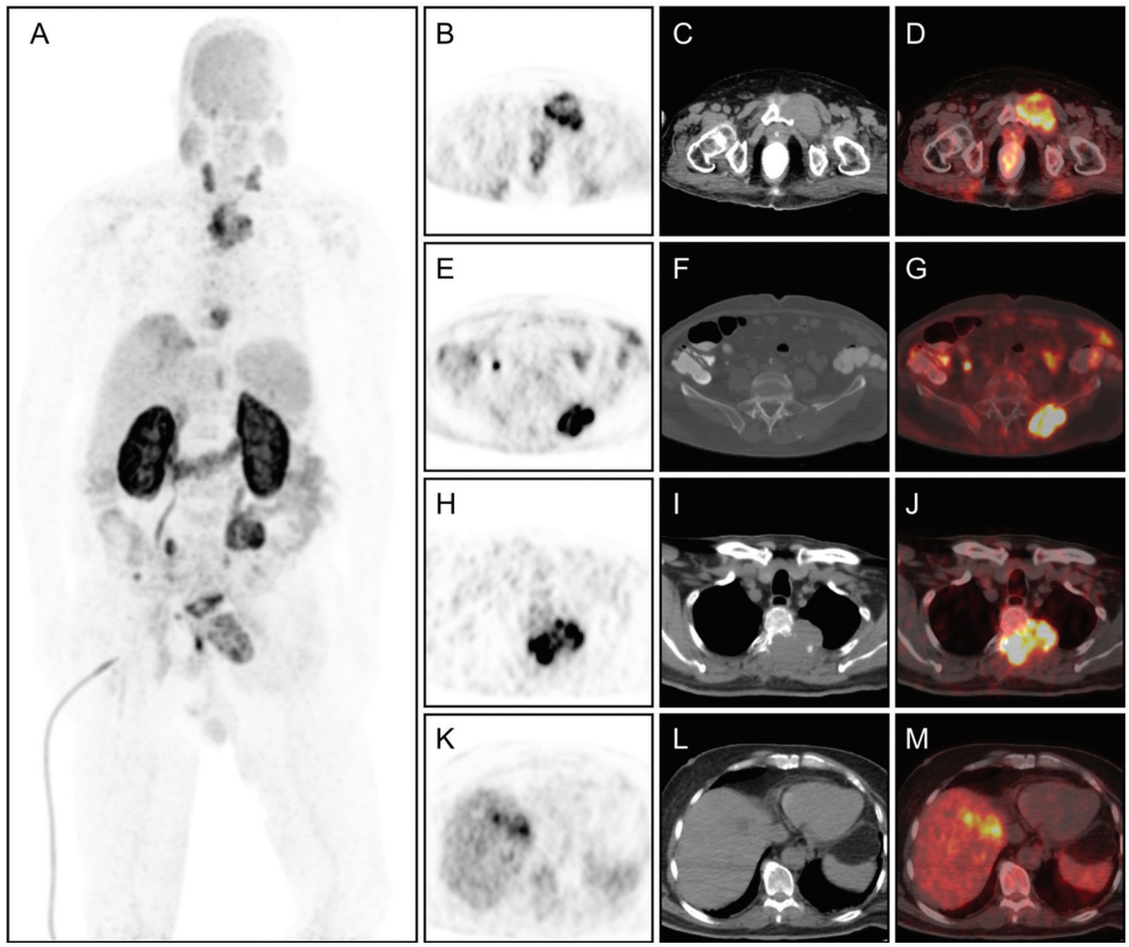

Figure 2. As an alternative PET/CT imaging, ^{68}Ga-prostate-specific membrane antigen (PSMA) PET/CT was performed the same day. Corresponding to the lesions in ^{18}F-FDG PET, ^{68}Ga-PSMA PET/CT MIP **(A)**, transaxial PET **(B, E, H, K),** CT **(C, F, I, L)**, and fused **(D, G, J, M)** images demonstrated high PSMA expression in the metastatic bone lesions (SUV_{max}=23.9) and in the primary liver tumor (SUV_{max}=12.1). No other findings showed metastatic disease elsewhere in the body.

PET/CT imaging with ^{18}F-FDG has low diagnostic accuracy in assessing HCC patients because of its low metabolism (1). ^{68}Ga-PSMA PET/CT is a new diagnostic technique to image recurrent prostate cancer (2). However, increased PSMA expression has been reported for different non-prostate malignancies, including HCC (3,4,5,6,7,8). There are only a few published documents on the merits of PSMA-PET for HCC (3,4,5,6,7,8). In fact, a few case reports and only 2 studies involving a small sample size has been reported in the recent past. In one of these studies, ^{68}Ga-PSMA was reported to be superior relative to ^{18}F-FDG for imaging HCC patients (7). However, in another study on advanced HCC patients, the PSMA expression was detected by ^{68}Ga-PSMA PET, but it was not superior to that by ^{18}F-FDG PET (8). In the current case, ^{68}Ga-PSMA uptake was extremely high as compared to ^{18}F-FDG uptake for bone metastases, and without ^{18}F-FDG uptake in the primary tumor. Therefore, it is suggested that PET imaging with ^{68}Ga-PSMA is helpful in HCC patients with low FDG affinity. Moreover, we believe that the existence of PSMA expression may act as a guide for radioligand therapy targeting PSMA in the future

Ethics

Informed Consent: Informed consent was taken.

Peer-review: Externally and internally peer-reviewed.

Authorship Contributions

Concept: S.E., Design: S.E., Data Collection or Processing: S.E., N.A., Analysis or Interpretation: S.E., N.A., Literature Search: S.E., Writing: S.E.

Conflict of Interest: No conflict of interest was declared by the authors.

Financial Disclosure: The authors declared that this study received no financial support.

References

1. Sacks A, Peller PJ, Surasi DS, Chatburn L, Mercier G, Subramaniam RM. Value of PET/CT in the management of primary hepatobiliary tumors, part 2. AJR Am J Roentgenol 2011;197:260-265.
2. Afshar-Oromieh A, Avtzi E, Giesel FL, Holland-Letz T, Linhart HG, Eder M, Eisenhut M, Boxler S, Hadaschik BA, Kratochwill C, Weichert W, Kopka K, Debus J, Haberkorn U. The diagnostic value of PET/CT imaging with the (68)Ga-labelled PSMA ligand HBED-CC in the diagnosis of recurrent prostate cancer. Eur J Nucl Med Mol Imaging 2015;42:197-209.
3. Erhamamci S, Aslan N. Primary Hepatocellular Carcinoma With Intense 68Ga-PSMA Uptake But Slight 18F-FDG Uptake on PET/CT Imaging Clin Nucl Med 2020; 45:e176-e177.
4. Perez PM, Flavell RR, Kelley RK, Umetsu S, Behr SC. Heterogeneous Uptake of 18F-FDG and 68Ga-PSMA-11 in Hepatocellular Carcinoma. Clin Nucl Med 2019;44:e133-e135.
5. Taneja S, Taneja R, Kashyap V, Jha A, Jena A. 68Ga-PSMA Uptake in Hepatocellular Carcinoma. Clin Nucl Med 2017;42:e69-e70.
6. Sasikumar A, Joy A, Nanabala R, Pillai MRA, Thomas B, Vikraman KR. 68Ga-PSMA PET/CT imaging in primary hepatocellular carcinoma. Eur J Nucl Med Mol Imaging 2016;43:795-796.
7. Kesler M, Levine C, Hershkovitz D, Mishani E, Menachem Y, Lerman H, Zohar Y, Shibolet O, Even-Sapir E. 68Ga-labeled prostate-specific membrane antigen is a novel PET/CT tracer for imaging of hepatocellular carcinoma: a prospective pilot study. J Nucl Med 2019;60:185-191.
8. Kuyumcu S, Has-Simsek D, Iliaz R, Sanli Y, Buyukkaya F, Akyuz F, Turkmen C. Evidence of Prostate-Specific Membrane Antigen Expression in Hepatocellular Carcinoma Using 68Ga-PSMA PET/CT. Clin Nucl Med 2019;44:702-706.

Interesting Image
Mol Imaging Radionucl Ther 2020;29:139-142 DOI:10.4274/mirt.galenos.2020.76059

Unforeseen COVID-19 on Oncologic Bone Scan with SPECT/CT in a High Prevalence Area

COVID-19'un Yaygın Görüldüğü Bir Bölgede SPECT/BT ile Onkolojik Kemik Taramasında Beklenmedik Şekilde COVID-19 Bulguları

Sana Munir Gill, Aamna Hassan, Humayun Bashir
Shaukat Khanum Memorial Cancer Hospital and Research Center, Department of Nuclear Medicine, Lahore, Pakistan

Abstract

A 65-year-old woman with known diabetes and hypertension underwent a technetium methylene diphosphonate (Tc-99m MDP) bone scan with single photon emission computed tomography/computed tomography (SPECT/CT) for shoulder pain. She was initially treated for breast cancer and later for hepatocellular carcinoma. SPECT/CT showed MDP nonavid and scattered pulmonary ground-glass opacities bilaterally along with rounded nodular densities. Another 56-year-old patient who was newly diagnosed with right breast invasive ductal carcinoma underwent a bone scan with SPECT/CT, which revealed bilateral pulmonary infiltrates. Both patients later tested positive for Coronavirus Disease-2019 (COVID-19). Therefore, nuclear physicians should be watchful of findings related to COVID-19 on SPECT/CT thorax as this is becoming the new normal.

Keywords: Bone scan, single photon emission computed tomography/computed tomography, SARS-CoV-2, COVID-19

Öz

Altmış beş yaşında, diyabetik ve hipertansif olduğu bilinen kadın hastaya omuz ağrısı için tek foton emisyonlu bilgisayarlı tomografi/bilgisayarlı tomografi (SPECT/BT) ile teknesyum metilen difosfonat (Tc-99m MDP) kemik taraması yapıldı. Hasta başlangıçta meme kanseri ve daha sonra hepatosellüler karsinom tedavisi görmüştü. SPECT/BT; MDP tutmayan, iki yanlı, dağınık pulmoner buzlu cam opasiteleri ve yuvarlak nodüler dansiteler gösterdi. Başka bir 56 yaşında yeni teşhis edilmiş sağ memede invaziv duktal karsinomu olan hastada, SPECT/BT ile kemik taraması bilateral pulmoner infiltrasyonları ortaya çıkardı. Bu hastaların her ikisinde de daha sonra Koronavirüs Hastalığı-2019 (COVID-19) testi pozitif saptandı. Bu nedenle, nükleer tıp hekimleri SPECT/BT'de COVID-19'un toraks bulgularına dikkat etmelidir çünkü bu onlar için yeni normal haline gelmiştir.

Anahtar kelimeler: Kemik taraması, tek foton emisyonlu bilgisayarlı tomografi/bilgisayarlı tomografi, SARS-CoV-2, COVID-19

Address for Correspondence: Aamna Hassan MD, Shaukat Khanum Memorial Cancer Hospital and Research Center, Department of Nuclear Medicine, Lahore, Pakistan **Phone:** +92 42 35905000 **E-mail:** aamnah@skm.org.pk ORCID ID: orcid.org/0000-0003-0026-0729
Received: 30.06.2020 **Accepted:** 23.08.2020

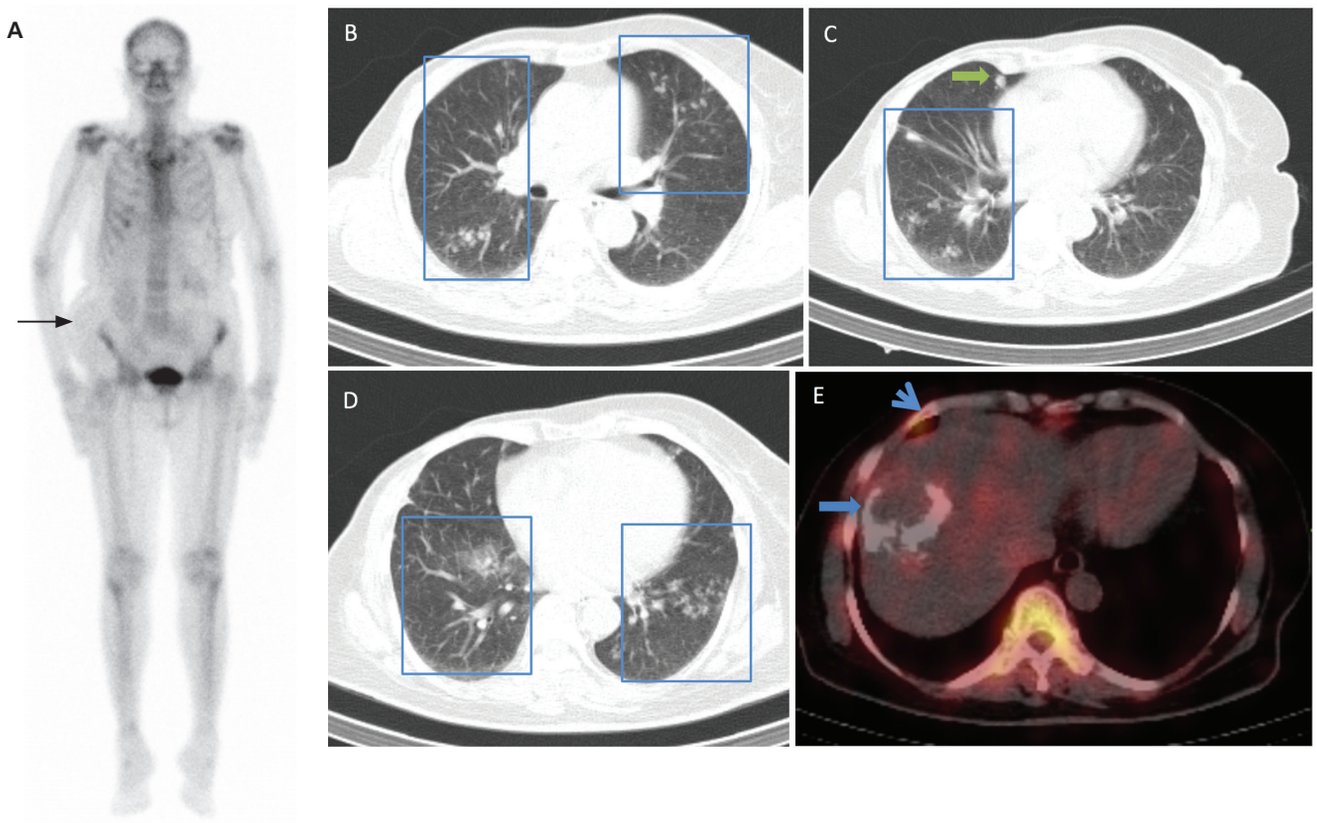

Figure 1A, B, C, D, E, F, G. No evidence of osteoblastic metastases was seen on the whole-body planar bone scintigraphy anterior image (A) of a 65-year-old woman who had previously undergone modified radical mastectomy and chemotherapy for breast cancer. Spigelian hernia was noted on the right side of the abdomen (black arrow). Some heterogeneity was visible in the sacroiliac joints, which is likely to be degenerative in nature. No abnormal uptake was observed in the right shoulder. The uptake in the right anterior costochondral junction corresponded to an arthritic change on single photon emission computed tomography/computed tomography (SPECT/CT) (F: blue arrow head). Axial images of low-dose CT of correlative SPECT/CT (B, C, D) showed scattered and predominantly peripheral ground-glass opacities (GGO) in both lungs (blue box) and a couple of scattered rounded nodular densities (green arrow). Fused SPECT/CT image (E) revealed a calcified site of prior transarterial chemoembolization which was performed for treating second primary hepatocellular carcinoma (blue arrow).

In the coronal CT (F) and fuzed SPECT/CT (G) images of another 56-year-old patient, pulmonary infiltrates were observed in the bilateral upper lung lobes (red arrows); the largest consolidative area was in the right upper lobe. The scan was acquired as part of the staging workup related to breast carcinoma.

Detailed history of the patients revealed the absence of coughing, shortness of breath, fever, myalgia, diarrhea, or vomiting. Besides, there was no history of contact with a suspected or confirmed case of severe acute respiratory syndrome-coronavirus-2 (SARS-CoV-2). Objectively, they were afebrile and normotensive; oxygen saturation was 98% on room air.

In view of the current Coronavirus Disease-2019 (COVID-19) pandemic, suspicion of the disease was raised despite the negative history owing to preexisting comorbidities, GGO, and pulmonary infiltrates on SPECT/CT. One study established that up to 97% of the confirmed COVID-19 patients exhibited GGO on CT irrespective of the severity of the disease (1). Therefore, the patients' nasopharyngeal swabs were subjected to reverse transcriptase-polymerase chain reaction (RT-PCR), which turned out to be positive for SARS-CoV-2 infection 24 hours later. Hence, the patients were advised self-isolation, and they continued to be asymptomatic.

COVID-19 is a rapidly emerging disease with over 9,373,719 patients affected worldwide (2) and continues to be a public health challenge. Ever since the initial cases were reported in December 2019 (3), there have been variable presentations with poor prognosis in certain age groups. Thus, a high

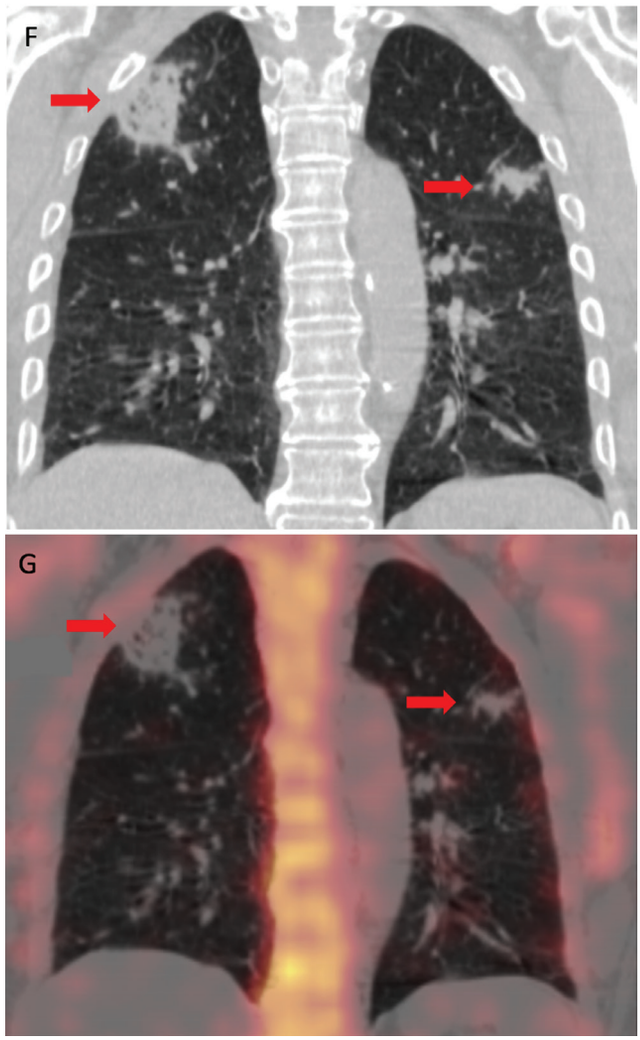

index of suspicion is required for its diagnosis, especially in asymptomatic patients. To curtail the spread of the pandemic, early recognition and isolation of the affected people are of paramount importance. In such a scenario, hybrid imaging is playing a central role in flagging potential COVID-19 patients with incidental lung findings on positron emission tomography/CT (PET/CT) and SPECT/CT. The benefit of PET/CT has been documented in literature (4,5). However, there have been only a few reported incidental cases on SPECT/CT (6). In the constantly changing situation in our country that has a current tally of 188,925 (7) confirmed COVID-19 cases, most of the patients are asymptomatic. Hence, there is a high chance of these patients getting missed out on hybrid imaging performed for other unrelated causes. Therefore, nuclear medicine physicians should be aware of the COVID-19 related findings on thorax CT and inform the referring clinician if suspicious GGO are detected (8). Although RT-PCR is currently considered the gold standard for the diagnosis of the disease, some studies have highlighted the importance of combining the results with imaging, laboratory, and clinical findings. This approach is essential since many patients present with either nil or variable symptoms and might have a negative RT-PCR test (9)

Ethics

Informed Consent: Institutional review board did not mandate informed consent.

Peer-review: Externally and internally peer-reviewed.

Authorship Contributions

Concept: A.H., H.B., Literature Search: S.M.G., Writing: S.M.G.

Conflict of Interest: No conflict of interest was declared by the authors.

Financial Disclosure: The authors declared that this study received no financial support.

References

1. Li K, Wu J, Wu F, Wu, F, Guo D, Chen L, Fang Z, Li C. The Clinical and Chest CT Features Associated with Severe and Critical COVID-19 Pneumonia. Invest Radiol 2020;55:327-331.

2. https://www.worldometers.info/coronavirus/ Last accessed on 24-6-20.
3. Zhu N, Zhang D, Wang W, Li X, Yang B, Song J, Zhao X, Huang B, Shi W, Lu R, Niu P, Zhan F, Ma X, Wang D, Xu W, Wu G, Gao GF, Tan W, China Novel Coronavirus Investigating and Research Team. A Novel Coronavirus from Patients with Pneumonia in China, 2019. N Engl J Med 2020;382:727-733.
4. Qin C, Liu F, Yen TC, Lan X. 18F-FDG PET/CT findings of COVID-19: a series of four highly suspected cases. Eur J Nucl Med Mol Imaging 2020;47:1281-1286.
5. Albano D, Bertagna F, Bertoli M, Bosio G, Lucchini S, Motta F, Panarotto MB, Peli A, Camoni L, Bengel FM, Giubbini R. Incidental Findings Suggestive of COVID-19 in Asymptomatic Patients Undergoing Nuclear Medicine Procedures in a High-Prevalence Region. J Nucl Med 2020;61:632-636.
6. Hindle-Katel W, Oen-Hsiao J, Lussnig E, Miller EJ. Incidental finding of COVID-19 pulmonary infiltrates on SPECT/CT attenuation correction CT [published online ahead of print, 2020 May 11]. J Nucl Cardiol 2020;1-2.
7. http://covid.gov.pk/ Last accessed on 24-6-20
8. Ayan A, Kıraç FS. Guide for Nuclear Medicine Applications During the COVID-19 Outbreak. Mol Imaging Radionucl Ther 2020;29:49-58.
9. Xie X, Zhong Z, Zhao W, Zheng C, Wang F, Liu J. Chest CT for Typical 2019-nCoV Pneumonia: Relationship to Negative RT-PCR Testing [published online ahead of print, Radiology 2020;200343.

Letter to the Editor
Mol Imaging Radionucl Ther 2020;29:143-144 DOI:10.4274/mirt.galenos.2020.52244

Lung Perfusion Imaging with Technetium-99m Macroaggregated Albumin should be Combined with Contrast-enhanced Echocardiography for the Diagnosis of Hepatopulmonary Syndrome

Hepatopulmoner Sendrom Tanısı için Teknesyum-99m Makroagregasyonlu Albümin ile Akciğer Perfüzyon Görüntülemesi Kontrastlı Ekokardiyografi ile Birleştirilmelidir

Georgios Meristoudis[1], Georgia Keramida[2], Ioannis Ilias[3]

[1]*Hippokration General Hospital, Clinic of Nuclear Medicine, Thessaloniki, Greece*
[2]*Royal Brompton and Harefield, NHS Foundation Trust, Department of Nuclear Medicine, London, United Kingdom*
[3]*Elena Venizelou General Hospital, Clinic Endocrine Unit, Athens, Greece*

Keywords: Hepatopulmonary syndrome, technetium-99m macroaggregated albumin, lung perfusion scintigraphy, right-to-left shunt, contrast-enhanced echocardiography

Anahtar kelimeler: Hepatopulmoner sendrom, teknesyum-99m makroagregasyonlu albümin, akciğer perfüzyon sintigrafisi, sağdan sola şant, kontrastlı ekokardiyografi

Dear Editor,

We have read with great interest the recent article by Alipour et al. (1) regarding the diagnosis of hepatopulmonary syndrome (HPS) with right-to-left (R-L) shunt in cirrhotic patients using the technetium-99m macroaggregated albumin (Tc-99m MAA) lung perfusion scintigraphy (LPS). The authors have found that LPS was more sensitive than contrast-enhanced echocardiography (CEE) for detecting intrapulmonary vascular dilatations (IPVDs) and concluded that Tc-99m MAA LPS can be used complementarily with other diagnostic methods in the assessment of HPS (1). However, we have some concerns regarding this work. The authors appraised the shunt fraction (SF) by using the formula SF=(geometric mean of brain counts)/(geometric mean of brain counts+geometric mean of lung counts), without dividing the geometric mean of brain counts by 0.13, although the brain is presumed to receive 13% of the cardiac output (2). Moreover, both LPS and CEE procedures were not described in sufficient detail.

Apart from the patients' characteristics, the diagnostic accuracy of LPS for identifying IPVDs can be affected by procedures and protocols. It should be noted that quantification with a technique that uses only brain uptake underestimates SF (2). In a recent prospective study, Zhao et al. (2) compared the whole-body uptake and brain uptake techniques for calculating R-L shunt in 69 patients who received Tc-99m MAA in an upright position to maximize the degree of R-L shunt. The study demonstrated that the whole-body uptake technique has a higher diagnostic accuracy than the brain uptake (74% versus 59%, respectively) for detecting IPVDs in HPS (2). Furthermore, to the best of our knowledge, in all studies

Address for Correspondence: Georgios Meristoudis MD, Hippokration General Hospital, Clinic of Nuclear Medicine, Thessaloniki, Greece
Phone: +30 231 331 2090 **E-mail:** meristoudis@yahoo.gr ORCID ID: orcid.org/0000-0002-0382-6962
Received: 18.08.2020 **Accepted:** 20.08.2020

assessing patients with HPS, the diagnosis of IPVDs was based only on strict numerical values as expressed by the quantitative analysis, and no qualitative assessment of LPS was made. In a retrospective cohort study, 126 patients with a clinical suspicion of intracardiac R-L shunt underwent LPS (3). A visual scan interpretation demonstrated that the absence of brain parenchymal accumulation of Tc-99m MAA in a static image excluded the R-L shunt, and the specificity of a positive result was 100% (3). Quantitative brain imaging is characterized by a very high specificity and is extremely useful in patients with HPS and concomitant pulmonary diseases (30% of cases), severe and very severe HPS according to the arterial blood-gas analysis (PaO_2 <60 mmHg), and nondiagnostic CEE (approximately 7%) (2,4,5). Alternatively, although CEE is deemed as a sensitive screening test, it lacks specificity, as many cirrhotic patients with positive results on CEE have normal arterial blood-gas analysis and thus, by definition, have no HPS (4). Thus, differences in sensitivity and specificity for CEE and LPS show that these modalities should be combined to get the most of their characteristics for assessing HPS. Additionally, we should bear in mind that both LPS and transthoracic CEE cannot distinguish IPVDs from other anatomical intrapulmonary shunts, such as pulmonary arteriovenous malformations or intracardiac shunts (5). A standardized and optimized Tc-99m MAA LPS protocol, implementing methods of both quantitative and qualitative evaluations and interpretations, is essential for improving the diagnostic accuracy of HPS.

Ethics

Peer-review: Internally peer-reviewed.

Authorship Contributions

Concept: G.M., G.K., I.I., Design: G.M., G.K., I.I., Data Collection or Processing: G.M., G.K., I.I., Analysis or Interpretation: G.M., G.K., I.I., Literature Search: G.M., G.K., I.I., Writing: G.M., G.K., I.I.

Conflict of Interest: No conflict of interest was declared by the authors.

Financial Disclosure: The authors declared that this study received no financial support.

References

1. Alipour Z, Armin A, Mohamadi S, Tabib SM, Azizmohammadi Z, Gholamrezanezhad A, Assadi M. Hepatopulmonary Syndrome with Right-to-left Shunt in Cirrhotic Patients Using Macro-Aggregated Albumin Lung Perfusion Scan: Comparison with Contrast Echocardiography and Association with Clinical Data. Mol Imaging Radionucl Ther 2020;29:1-6.
2. Zhao H, Tsauo J, Zhang XW, Ma HY, Weng NN, Tang GS, Li X. Technetium-99m-labeled macroaggregated albumin lung perfusion scan for diagnosis of hepatopulmonary syndrome: A prospective study comparing brain uptake and whole-body uptake. World J Gastroenterol 2020;26:1088-1097.
3. Graves MW, Kiratli PO, Mozley D, Palevsky H, Zukerberg B, Alavi A. Scintigraphic diagnosis of a right to left shunt in end-stage lung disease. Respir Med 2003;97:549-554.
4. Rodríguez-Roisin R, Krowka MJ, Hervé P, Fallon MB; ERS Task Force Pulmonary-Hepatic Vascular Disorders (PHD) Scientific Committee. Pulmonary-Hepatic vascular Disorders (PHD). Eur Respir J 2004;24:861-880.
5. Angeli P, Bernardi M, Villanueva C, Francoz C, Mookerjee RP, Trebicka J, Krag A, Laleman W, Gines P. EASL Clinical Practice Guidelines for the management of patients with decompensated cirrhosis. J Hepatol 2018;69:406-460.

2020 Referee Index - 2020 Hakem Dizini

Bilal Kovan
Bilge Volkan Salancı
Billur Çalışkan
Bircan Sönmez
Bülent Turgut
Dragana Sobic Saranovic
Emel Ceylan Günay
Emre Entok
Fatma Suna Kıraç
Fikriye Gül Gümüşer
Funda Üstün
Georgios Spyridon Limouris
Gonca G. Bural
Gözde Dağlıöz Görür
Gülay Durmuş Altun
Gülin Vural Uçmak
Hakan Demir
Hülya Yalçın
İlknur Ak Sivrikoz
İnanç Karapolat
Leyla Poyraz
Lorenzo Biassoni
Mahmut Yüksel
Mehmet Reyhan
Meliha Korkmaz
Meral Değer
Meryem Kaya
Mine Araz
Murat Fani Bozkurt
Mustafa Demir
Mustafa Yıldız
Nilüfer Yıldırım
Nurhan Ergül
Olga Yaylalı
Özgür Ömür
Pınar Pelin Özcan Kara
Sait M. Sağer
Salih Özgüven
Salih Sinan Gültekin
Semra Dönmez
Semra Özdemir
Seval Erhamamcı
Sevin Coşar Ayaz
Seyhan Karaçavus
Ülkem Yararbaş
Ümit Özgür Akdemir
Zehra Özcan
Zeynep Burak

2020 Author Index - 2020 Yazar Dizini

Aamna Hassan....139
Abbas Armin....1
Ahmet Öz....112
Ali Gholamrezanezhad....1
Aslı Ayan....49
Aydan Akdeniz....85
Burak Ayca....112
Cihan Gündoğan....25, 112
Çiğdem Şen....25
Çiğdem Soydal....79
Daniel Novakovic....72
David Joffe....72
Derya Çayır....33
Ekrem Çakar....17
Emine Elif Özkan....98
Erhan Ayan....105
Erman Çakal....33
Esra Arslan....17, 25
Esra Kaytan Sağlam....65
F. Suna Kıraç....49
Farida Bentayeb....118
Fatma Fulya Köybaşıoğlu....33
Faustino Bonutti....118
Funda Ustun....41
Georgia Keramida....143
Georgios Meristoudis....143
Göksel Alçın....65
Gregory Falk....72
Gregory L. Falk....7
Gülçin Yeğen....65
Güngör Utkan....79
Halil Turgut Turoğlu....132
Hans Van der Wall....7, 72
Harun Karabacak....33
Hicham Asmi....118
Humayun Bashir....139
Ioannis Ilias....143
John Beattie....7, 72
John Dennis Ehrhardt....88
Kaan Esen....37
Karl Baumgart....7, 72
Kemal Ünal....82
Kenan Turgutalp....37
Krisana Roysri....124
Krisanat Chuamsaamarkkee....124
Leticia Burton....7, 72
Luca Filippi....45
Majid Assadi....1
Mehmet Erdoğan....98
Mehmet Yaldız....85
Mina Ouahman....118
Mine Araz....33, 79
Mustafa Yıldız....98
Nahide Gökçora....82
Nesrin Aslan....135
Nevra Dursun....17, 25
Onur Üstün....59
Osman Güven....59
Özlem Özdemir Candan....112
Pelin Özcan Kara....85
Pınar Akkuş....79
Pınar Pelin Özcan....37, 105
Putthiporn Charoenphun....124
Rabia Bozdoğan Arpacı....105
Rachid Errifai....118
Rangsee Songprakhon....124
Rıza Umar Gürsu....17
Salih Özgüven....132
Sana Munir Gill....139
Sanae Douama....118
Savaş Karyağar....59
Scott Simpson....7
Sefa Alperen Öztürk....98
Selda Yılmaz Tatar....25
Selin Kesim....132
Seval Erhamamcı....135
Sevda Sağlampınar Karyağar....59
Sevim Süreyya Şengül....98
Seyed Masoud Tabib....1
Seza Güleç....88
Sudabeh Mohamadi....1
Süleyman Çağan Efe....112

2020 Author Index - 2020 Yazar Dizini

Tamer Aksoy 17, 25
Tanju Yusuf Erdil 132
Tevfik Fikret Çermik 17, 25, 65, 112
Tuğba Kara 37
Tunç Öneş 132
Ulku Korkmaz 41
Yasemin Şanlı 65
Yasin Yüksel 112
Yavuz Atar 59
Yavuz Uyar 59
Youssef Bouzekraoui 118
Zahra Azizmohammadi 1
Zehra Pınar Koç 37, 85, 105
Zeynab Alipour 1

2020 Author Index - 2020 Yazar Dizini

^{18}F-choline/^{18}F-kolin 45

^{18}F-FDG PET/CT/^{18}F-FDG PET/BT 65

^{18}F-FDG positron emission tomography/computed tomography/^{18}F-FDG pozitron emisyon tomografi/bilgisayarlı tomografi 37

^{18}F-FDG/^{18}F-FDG 105, 135

^{18}F-fluoro-deoxy-glucose positron emission tomography/computerized tomography (^{18}F-FDG PET/CT)/^{18}F-floro-2-deoksi-glukoz pozitron emisyon tomografi/bilgisayarlı tomografi (^{18}F-FDG PET/BT) 17

^{18}F-fluorodeoxyglucose positron emission tomography/^{18}F-fluorodeoksiglukoz positron emisyon tomografisi 79

^{18}F-fluorodeoxyglucose positron emission tomography/computed tomography (^{18}F-FDG PET/CT)/^{18}F-florodeoksiglukoz pozitron emisyon tomografisi/bilgisayarlı tomografi (^{18}F-FDG PET/BT) 25

^{68}Ga-PSMA/^{68}Ga-PSMA 135

Abdominal mass/Abdominal kitle 37

Adenocarcinomas/Adenokarsinomlar 25

Allergic/Alerjik 72

Amyloidosis/Amiloidoz 37

Anterior mediastinum/Anterior mediasten 105

Bicalutamide/Bicalutamide 82

Bone metastases/Kemik metastazı 135

Bone scan/Kemik sintigrafisi 82

Bone scan/Kemik taraması 139

Brachial plexopathy/Brakial pleksopati 79

Brain/Beyin 41

C-reactive protein/albumin ratio/C-reaktif protein/albümin oranı 112

Cervical lymph node/Servikal lenf nodu 59

Cirrhosis/Siroz 1

Colorectal cancer/Kolorektal kanser 17

Contrast echocardiography/Kontrast ekokardiyografisi ... 1

Contrastenhanced echocardiography/Kontrastlı ekokardiyografi 143

Coronavirus/Koronavirüs 49

COVID-19 outbreak/COVID-19 salgını 49

COVID-19/COVID-19 139

Disinfection/Dezenfeksiyon 49

FDG/FDG 85

Fungal/Mantar 72

Ga-67 imaging/Ga-67 görüntüleme 118

Ga-68 PSMA PET/CT/Ga-68 PSMA PET/BT 98

Gastric cancer/Mide kanseri 25

Gastroesophageal reflux disease/Gastroözofageal reflü hastalığı 7

Genomics/Genomik 88

Gynecomastia/Jinekomasti 82

Henry Beierwaltes/Henry Beierwaltes 88

Hepatocellular carcinoma/Hepatosellüler karsinom 45, 135

Hepatopulmonary syndrome/Hepatopulmoner sendrom ... 1,143

Image-based dosimetry/Görüntüye dayalı dozimetri 124

Impedance/Empedans 7

Infection protection rules/Enfeksiyondan korunma kuralları 49

Internal dosimetry/İnternal dozimetri 124

Irving Ariel/Irving Ariel 88

KRAS mutation/KRAS mutasyonu 17

Laryngopharyngeal reflux/Larengofarengeal reflü 7

Larynx cancer/Larenks kanseri 59

Lung perfusion scintigraphy/Akciğer perfüzyon sintigrafisi ... 143

Lymphoma/Lymphoma 85

Macro-aggregated albumin lung perfusion scan/Makroagregat albümin akciğer perfüzyon sintigrafisi 1

Manometry/Manometri 7

Mass/Kitle 105

Metabolic activity/Metabolik aktivite 59

Metastasis/Metastaz 41

Metastatic breast cancer/Metastatik meme kanseri 79

Mickey Mouse sign/Mickey Mouse işareti 132

Monostotic Paget's disease/Monostotik Paget hastalığı ... 132

Myocardial perfusion scintigraphy/Miyokard perfüzyon sintigrafisi 112

NaF/NaF 41

Nuclear medicine staff/Nükleer tıp personeli 49

Nuclear oncology/Nükleer onkoloji 88

Oligometastasis/Oligometastaz 98

Paget's disease/Paget hastalığı 132

Parathyroid adenoma/Paratiroid adenomu 33

Parathyroid gland/Paratiroid bezi 33

Penetration/Penetrasyon 118

2020 Author Index - 2020 Yazar Dizini

PET/CT/PET/BT 85, 105, 135
PET/PET 41
pH/pH 7
Pneumonia/Pnömoni 72
Positron emission tomography/computed tomography/ Pozitron emisyon tomografisi/bilgisayarlı tomografi 45, 59
Positron emission tomography/computerized tomography/ Pozitron emisyon tomografi/bilgisayarlı tomografi 49
Primary photons (original)/Primer fotonlar (orijinal) 118
Prognosis/Prognoz 17, 65
Prostate cancer/Prostat kanseri 82, 98
Pulmonary aspiration/Pulmoner aspirasyon 7
Radioactive iodine/Radyoaktif iyot 88
Radioiodine therapy/Radyoiyot tedavisi 124
Rectal adenocarcinoma/Rektum kanseri 65
Red marrow absorbed dose/Kırmızı iliğin absorbe ettiği doz 124
Reflux/Reflü 7, 72
Rhinosinusitis/Rinosinüzi 72
Right-to-left shunt/Sağdan sola şant 143
Samuel Seidlin/Samuel Seidlin 88
SARS-CoV-2/SARS-CoV-2 139
Saul Hertz/Saul Hertz 88
Scatter/Saçılma 118
Scintigraphy/Sintigrafi 7, 72
Sensitivity/Duyarlılık 118
SIMIND/SIMIND 118
Single photon emission computed tomography/computed tomography/Tek foton emisyonlu bilgisayarlı tomografi/ bilgisayarlı tomografi 139
Single photon emission computed tomography/Tek foton emisyonlu bilgisayarlı tomografi 33
SPECT/CT/SPECT/BT 132
Spine/Vertebra 132
Stable coronary artery disease/Kararlı koroner arter hastalığı 112
Staging/Evreleme 65
Superscan/Supersken 85
SUV_{max}/SUV_{maks} 65, 98
Tc-99m sestamibi/Tc-99m sestamibi 33
Technetium 99m-methylene diphosphonate bone scintigraphy/Teknesyum 99m-metilen difosfonat kemik sintigrafisi 132
Technetium-99m macroaggregated albümin/Teknesyum-99m makroagregasyonlu albümin 143
Thalassemia/Talasem 45
Theranostics/Teranostik 88
Thyroid cancer/Tiroid kanseri 88